Optical Absorption Spectroscopy for Gas Analysis in Biomass Gasification

Grosch, Helge

Publication date:
2014

Document Version
Publisher's PDF, also known as Version of record

Optical Absorption Spectroscopy for Gas Analysis in Biomass Gasification

Optisk absorptionsspektroskopi til gasmåling i biomasseforgasning

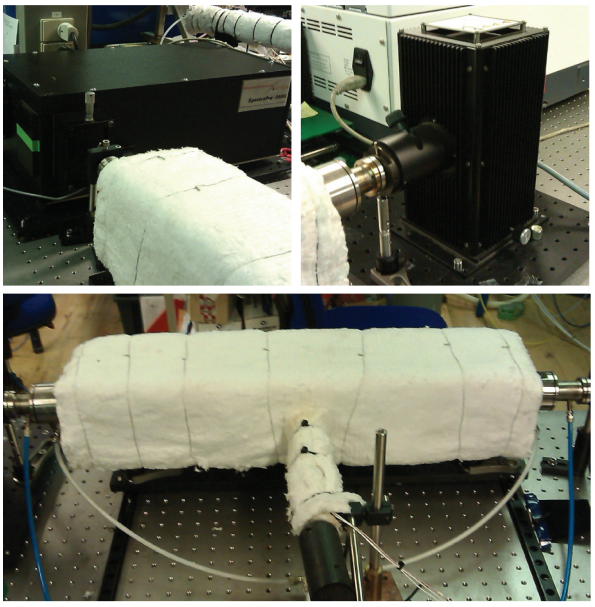

Helge Grosch
PhD thesis
November 2014

DTU Chemical Engineering
Department of Chemical and Biochemical Engineering

Optical Absorption Spectroscopy for Gas Analysis in Biomass Gasification

Helge Grosch
Ph.D. Thesis
November 2014

DTU Chemical Engineering
Department of Chemical and Biochemical Engineering

Address: Centre of Combustion and Harmful Emission Control
Department of Chemical and
Biochemical Engineering
Technical University of Denmark
Søltofts Plads, Building 229
DK-2800 Kgs. Lyngby
Denmark
Phone: +45 4525 2800
Fax: +45 4525 4588
Web: www.chec.kt.dtu.dk

Print: J&R Frydenberg A/S
København
May 2015

ISBN: 978-87-93054-71-4

Abstract

Biomass gasification as a source of heat, power and chemical feedstock needs monitoring of the gas species to improve the performance and gas quality, deepen the understanding of the process and to be able to control the emission of hazardous compounds. Major species, like H_2, CO and CO_2, can already be determined with sufficient precision. However, minor species, like organic, aromatic, sulfur- and nitrogen-containing compounds, still cause problems in down-stream equipment and are harmful for health and environment. As a result, many different approaches for applications have been proposed to evaluate the concentration of the mentioned compounds. However, continuous measurements of different species directly in the gas (in-situ) and at the same time are scarce. In this work, the basis of optical in-situ analysis with ultraviolet and infrared spectroscopy was build to determine the concentration of the most important gas species of the low-temperature circulating fluidized bed gasifier. At first, a special gas cell, the hot gas flow cell (HGC), was build up and verified. In this custom-made gas cell, the optical properties, the so-called absorption cross-sections, of the most important sulfur and aromatic compounds were determined in laboratory experiments. By means of the laboratory results and spectroscopic databases, the concentrations of the major gas species and the aromatic compounds phenol and naphthalene were determined in extraction and in-situ measurements.

Resume

Forgasning af biomasse er en bæredygtigt kilde til produktion af varme, el og kemiske råstoffer. Forgasningsgassens hovedkomponenter, såsom H_2, CO, CO_2 og CH_4, kan måles med den fornødne præcision. Det kniber til gengæld med at måle sporgasserne, såsom organiske, aromatiske, svovl- og kvælstofholdige komponenter, som dels kan volde problemer i de systemer der aftager forgasningsgassen og dels være skadelige for helbred og miljøet. I dette arbejde er der udviklet en optisk metode til direkte kontinuert in-situ måling af gassammensætningen i den varme gas vha. ultraviolet (UV) og infrarød (IR) spektroskopi. Forsøgsmålinger er gennemført med godt resultat direkte i procesgas fra en lavtemperatur biomasseforgasser, hvilket er et gennembrud indenfor området. Målingerne er særdeles vanskelige pga. en kompleks gassammensætning og et højt indhold af tjærestoffer som kan kondensere ud i måleudstyr og giver anledning til komplekse spektre. Bestemmelse af gassammensætningen ud fra de målte spektre kræver således et detaljeret kendskab til de enkelte stoffers optiske egenskaber ved det aktuelle temperaturniveau i processen. Det er derfor designet og indkørt en ny særlig gascelle i kvarts til udmåling af de såkaldte absorptions-tværsnit for de mest vigtige svovl og aromatiske stoffer i såvel UV og IR området for temperaturer op til 525°C. Ud fra disse laboratorieresultater og ved brug spektroskopiske gasdatabaser er koncentration af gas komponenter og indhold af aromatiske forbindelser, fenol og naftalin, målt ved såvel en ekstraktiv og optisk in-situ metode på en forgasser.

Preface

This thesis was prepared at the department of Chemical and Biochemical Engineering at the Technical University of Denmark in fulfilment of the requirements for acquiring a PhD in Chemical Engineering.

The thesis deals with the quantification of gaseous species in biomass gasification. In particular, the two major tars, phenol and naphthalene, are investigated in the real product gas of the low temperature circulating fluidized bed gasifier (LT-CFB) at DTU Risø Campus.

The thesis consists of three major publications and the report at hand. The three publications build the basis for the measurements at the gasifier, which are described in this report.

København, 30-November-2014

Helge Grosch

Contents

Chapter 1

Introduction

1.1 Biomass Gasification

Biomass has always played an important role as a source of energy and chemical products, e.g. chars, tars and biofuels [1, 2]. Due to the interest in lowering the amount of fossil fuels, the advantages of this renewable source have been investigated more deeply and new and enhanced methods of biomass utilization have been introduced in the recent years.

One of the methods is biomass gasification. In the gasifier, a heterogeneous fuel, e.g., wood, straw but also sludge and waste [3, 4, 5, 6], is converted to the so called product gas. This gas consists mainly of H_2, CO, CO_2 and CH_4. As minor or trace gases, the product gas also may contain sulfur species, nitrogen species, organic species (e.g., aromatic species, PAH and higher tars), highly reactive gases (e.g., HCl) and others that can be considered as pollutants of the product gas. The production of these pollutants, and hence their concentration, strongly depends on the fuel, the gasifier type and the gasifier settings [7]. Depending on the application, their presence can be a major problem for further utilization of the product gas.

The product gas can and has been used in a wide variety of applications. It can be directly used in combined heat and power units (CHP) [2, 8, 9] by co-

firing with other fuels or direct combustion. In addition, the product gas can be cleaned and upgraded for use as biofuels or chemical feedstock [10]. The application depends largely on the concentration of the pollutants, that is the gas quality. For example, many gas cleaning methods are prone to fouling and destruction by one of the mentioned species [11, 12].

Therefore, it is of interest to monitor the species in question at an early stage to find possible improvements to the process, both by technical settings and fitting fuels, with the purpose of reducing the production of species harmful to the environment and further utilization.

1.2 Quantification of Gas Species

The major gas components seem to be a minor problem and can be determined with sufficient accuracy also by optical methods [13]. There are even optical in-situ methods [14, 15, 16, 17] available. However, there is a lack of knowledge on the production of the minor species. This is connected tightly to the wide variety of species that fall under this very loose definition.

The sulfur containing species, like hydrogen sulfide (H_2S), carbon disulfide (CS_2), carbonyl sulfide (OCS), mercaptanes/thiols (gases with an -S-H group) and aromatic species like thiophenes, already have a huge variety of compounds present in a product gas [18, 19, 20, 21, 22]. Even a small concentration can harm the equipment of applications [23] and influence the abilities and lifetime of potential gas cleaning systems dramatically. For instance, catalysts reforming tar components can have problems with a sulfur species that inactivate the catalyst and reduce their lifetime significantly [24, 25]. In addition, these compounds are known for their noxious effects and harmful impact on the environment [26].

The same discussion gets even more difficult, if another set of compounds, e.g., specific organic compounds, is taken into account. Within the group of aromatic compounds as a specific set of organics, exist the so-called BTX (from Benzene, Toluene and Xylenes), the phenols (phenol and other aromatic compounds containing at least one -OH group) and the PAHs (*P*oly *A*romatic *H*ydrocarbons). These different classes of aromatic species can also be called lighter tars. However, higher tars exist as well. With up to 90% of the weight of the total tars, they make up a substantial part of the overall tars.

Chapter 2

Scope of the Thesis

The scope of this thesis is to provide the basic tools to analyse different gas species online and in-situ in a real product gas of biomass gasification. For that purpose, the optical diagnostic methods of UV and IR spectroscopy are used. The obtained results of the in-situ measurements are to be compare to online measurements of the same methods obtained through gas extraction, as well as traditional sampling and subsequent GC-MS analyses.

The centerpiece of this thesis is the determination of the temperature dependent UV absorption cross-sections of important gasification products in laboratory experiments and their use for the evaluation of gas concentrations in a real product gas.

To do so, it is necessary to build up a gas cell that can handle corrosive and sticky gases in a laboratory environment. The cell is validated for its accuracy at temperatures up to 525°C (article 1 [27]). Afterwards, a list of important gases needs to be investigated on the temperature dependency of their absorption cross-sections (article 2 [28] and 3 [29]), and in a third step, some of the gases should be quantified in the product gas of the LT-CFB at DTU Risø Campus (described in this PhD Report). Accordingly, the thesis consists of the three articles and this PhD report.

2.1 Article 1: The Hot Gas Flow Cell for Optical Measurements on Reactive Gases

Two problems can be identified for tradition gas cell designs: The optical windows are first of all in contact with the corrosive or sticky gas mixtures and second of all, they are heated. This often causes changes in the optical properties of the window due to deposition, corrosion and temperature and therefore changes the results of the measurements. This article proposes a special design for a hot gas flow cell (HGC), using so-called flow windows. These make it possible to keep the optical windows cool and in contact with inactive nitrogen, but still keeping a defined path length. In addition, the windows are replaceable depending on the application and thus, measurements between 190 - 20000 nm are possible. The new design is tested and validated in its performance in regard to temperatures up to 525°C, path length and stability of the flow windows with great success. Afterwards, a novel set of high resolution SO_2 absorption cross-sections in the UV range is presented for temperatures up to 500°C.

The HGC can be used for all gases that might interfere with the optical properties of a solid optical window. The setup even allows the production of certain compounds in a mixing/chemical reaction chamber. This was already proven by the measurements of the absorption cross-sections of SO_3. Due to the replacable nature of the optical windows, other wavelengths below and above the mentioned region can in principle be achieved.

2.2 Article 2: Temperature Dependent Absorption Cross-Section of Sulfur Compounds up to 500°C

In the second article, the temperature dependency of the UV absorption cross-sections of H_2S, CS_2 and OCS were measured in the HGC up to a temperature of 500°C. These gases were chosen, because they are considered to be the most important sulfur species in biomass gasification. The temperatures were room temperature, 150°C, 300°C and 500°C. Room temperature was necessary to verify the absorption cross-sections by comparison to already published data; 150°C was the standard temperature of the UV and IR measurements in the online gas extraction system; 300°C was the temperature of the product gas after the particle filter at the LT-CFB in Risø, and 500°C was the temperature of the product gas before the particle filter at the LT-CFB. The gases used in the laboratory experiments were ready-made mixtures of nitrogen and the

compound in question. These gas mixtures could be further diluted to achieve different concentrations. Thus, all structures in the wavelength range between 200 nm and 380 nm could be resolved with sufficient signal-to-noise ratio. The major result were fully resolved absorption cross-sections of H_2S, CS_2 and OCS at around 20°C, 150°C, 300°C and 500°C.

While the obtained absorption cross-sections targeted mainly the products of biomass gasification, they can also be used for different applications like other high temperature processes (e.g. combustion), atmospheric research and others.

2.3 Article 3: Temperature Dependent Absorption Cross-Section of Phenol and Naphthalene up to 500°C

The third article has a similar scope as the second one, but focusing on the most important aromatic compounds produced by the LT-CFB in Risø: phenol and naphthalene. Their importance was verified by previous gas chromatographic measurements from gas samples. With the same reasoning, the chosen temperatures were the same as in the previous article: room temperature, 150°C, 300°C and 500°C. However, no ready-made gas mixtures could be used, because phenol and naphthalene are solid crystals at room temperature. Thus, the gas mixtures were produced by enriching a flow of nitrogen with the aromatic in a glass tube with molten crystals. Again, additional dilution was achieved by adding a constant flow of N_2. The optical absorption spectra of the species were measured in the HGC in the UV range of 195 nm and 380 nm. In this method, the concentration of the aromatic in nitrogen was unknown. However, the concentration is an essential part in the calculation of the absorption cross-sections from the measured absorption spectra. Thus, it was necessary to sample the aromatic compound after the HGC. This was done with the Petersen column, a device in which a solvent (here acetone) is used to extract the aromatic compound. Afterwards, the concentration of the aromatic in the acetone was analyzed with GC-MS and the mean concentration of aromatic in nitrogen during the sampling time could be calculated. The major results of this article were temperature dependent absorption cross-sections for phenol and naphthalene at around 20°C, 150°C, 300°C and 500°C.

Similar as in the second article, the results were obtained to quantify these gases in biomass gasification. Especially high temperature processes, but also atmospheric research can benefit from these results.

2.4 PhD Report

With the three articles as background, the report focuses on the application of some of their results to the product gas of the LT-CFB at DTU Risø Campus. In particular, the quantification of phenol and naphthalene and the challenges of this approach will be the main output of this report. Since first measurements determined, a minor role of the mentioned sulfur species under the given circumstances (gasifier type and setting, fuel) and the application, they were not investigated. In addition, the results from the IR spectroscopy for the major gas species and its possibilities in quantifying trace gases are presented.

At first, an overview on the state of the art in quantification of tar components with a special focus on online techniques will be given and the principles of the LT-CFB will be described. Afterwards, the methods and the setup at the gasifier will be described in detail, before the results and their discussion takes place. In the end a conclusion and an outlook on possible future works will be given.

Chapter 3

State of the Art

3.1 Overview of the Offline Methods for Tar Quantification

There are numerous offline tar analysis methods available. Mainly, wet chemical methods are used. There, a sample of the product gas is taken by extraction and further analyzed in a laboratory. The sampling is done by extracting a small part of the product gas through a solvent. Afterwards, the samples are analyzed by different methods. For tars, often gas and liquid chromatographic methods are coupled with a detector, e.g., gas chromatography/mass spectrometry (GC/MS), gas chromatography/flame ionizing detector (GC/FID) or high performance liquid chromatography (HPLC). In general, wet chemical techniques are quite precise in the analysis of the sample and especially chromatographic methods can detect a wide range of compounds. However, all of these approaches are time and resource consuming and thus, expensive. In addition, they are prone to errors due to mistakes in sampling, sample handling and interpretation of the results. To reduce the greatest errors and to unify the approach in sampling, the tar protocol as standard has been issued [30]. However, other sampling methods have their advantages as well and are successfully used, e.g. the Peterson column [31, 32, 33].

In 1997, Brage et al. [34] from the KTH in Stockholm have introduced a new

sampling technique, the so-called solid-phase adsorption (SPA) method. In this method, a small amount of the product gas is extracted and condensed at room temperature on an amino phase adsorbent. Afterwards, the samples are desorbed and analyzed with common chromatographic methods. The use of this method reduces the sampling time dramatically and due to its defined application, the results are less ambiguous. However, the samples need to be transported to Stockholm where they are analyzed. The tars that can be covered with this method are the same as in wet chemical approaches. The influence of adsorption an desorption effects on the organic compounds is unknown.

In case of tar analysis, the technical limits of the chromatographic methods, like the characteristics of the column or the abilities of the detector, limit the analyses. While it is possible to investigate the "lighter tars", also called GC-tars, it is impossible to separate heavy tars. To measure the overall tars, it is common to use gravimetric methods. Here, the weight of the overall tars sampled is measured by evaporating the solvent and measuring the weight of the remaining organic compounds. Since this method also covers the tars unable to seperate with a chromatographic method, they are often called gravimetric tars.

3.2 Overview of the Online Methods for Tar Quantification

In addition to the already named offline methods, there are many different methods that can analyze the tar contant in the gas composition online.

Before they are named and explained, the principles of online methods should be discussed in general: Online means, that a small part of the product gas is extracted from the product gas and analyzed on site. Like this, no sample preparation or analysis in a laboratory is needed. A good general overview of the available online techniques has been given by Monkhouse [35, 36]. Even though the articles by Monkhouse focus on the application of online techniques for the quantification of metals in industrial applications, the principles of these techniques apply as well for other species like tars.

All online measurement devices deal with similar problems. The major difficulty is the harsh environment. Depending on the gasifier type, the product gas has high temperatures (300°C - 800°C or higher), high dust and tar loads (up to 40 g/m^3) and the presence of corrosive gases (HCl and others), which all on their own can cause serious problems for any sensitive equipment. Dust and tars in particular pose a threat for these methods, since they stick at lower temperatures

to surfaces and change the properties of the device (fouling). Sometimes, these problems can be circumvented by keeping the equipment at the same temperatures as the product gas. However, the higher temperature can be challenging for the calibration of the online device.

On the other hand, online devices have a clear advantage: other than offline techniques, online techniques can measure continuous or at least in short time intervals of a couple of seconds (quasi-continuous) and thus eventually allow a real-time analysis. This kind of monitoring has the advantage of being able to understand the effect of changes in the process on the gas composition. This can in the end lead to a better understanding of the process itself and a better control.

In general, it is common to validate a new method by comparing the results achieved with those of offline methods. For tars, this means a comparison with the tar protocol or the SPA method. Depending on the challenges that the tar concentration poses and the questions that should be addressed, a certain method is advantageous.

If the condensation of tars is the target of the investigation, the tar dew point analyser [37] developed by the Energy research Centre of the Netherlands (ECN) might be a solution. A possibility to investigate the amount of total tars and especially the heavier tars is the same ionizing detector (FID) currently used by the University of Stuttgart. It measures the total hydrocarbons and quantifying the amount of non-condensable and condensable hydrocarbons up to 300 °C [38]. The same group is right now developing a new version of this device [39].

If a more detailed tar quantification is necessary, one of the many adaption of the GC method using custom made or ready-made GCs and μGCs might be a solution. These GCs can be equipped with one of several different detectors, e.g., laser absorption mass spectrometry (LAMS) [40], thermal conductimetry detector (TCD) [41] or many others. Defoort et al. have used the so-called ion molecular reaction mass spectrometry (IMR-MS) for online quantification of tars [42]. Another online mass spectrometry device, the molecular beam mass spectrometry (MB-MS) has also been used for more detailed tar quantification [43]. However, most of those techniques are quite costly and require trained personal for the analyses.

In addition to the previously mentioned methods, different optical methods have been proposed and developed for tar analysis. Similar to the FID is the photo ionizing detector (PID) developed by Ahmadi et al.. It can measure the total tar including the BTX. However, the setup is by now prone to fouling even at concentrations below 300 mg/m^3 of total tars [44, 45]. Karellas et al. [13] proposed to use the fluorescence signal of higher hydrocarbons present over a

wide range of the Raman spectrum to calculate the amount of total tars in the gas. The Raman spectrum was initially used for measuring the major gas species. At high tar loads the strong fluorescence signal can strongly influence the measurement of the major gas species. An adaptation using LEDs instead of expensive laser equipment has also been done by the same group [46]. In general, the fluorescence signal has been investigated by other groups, e.g., at the Technical University in Berlin. They analyzed not only the amount of total tar, but also evaluated the concentration of the most important tar species by fitting the individual fluorescence signals to the overall fluorescence signal [47, 48]. A similar approach to identify the single tar species has been done by the group around Roveda and Patuzzi [49, 50]. However, they used the UV absorption principle to evaluate the most important tar species, similar to the one used in this study. To make the sensor cheap, Roveda and Patuzzi used three different UV-LEDs.

All of these online methods extract gas from the product gas stream. A technical more simple and therefore cheaper solution would be to measure the tar components in-situ. This means, to measure directly in the product gas. Optical methods are fitting, however, they need optical access, something that can be diffcult to obtain in industrial applications. This approach can actively avoid the typical condensation problems.

3.3 A Brief Description of the Low Temperature Circulating Fluidized Bed Gasifier

Today, a very large number of different gasification concepts and designs exit and in some cases are commercially used. Each of them has its qualifications with respect to the fuel types and the target application of its product gas. To explain all would be a long study on its own. Therefore, I will only shortly target the idea and the tasks of the low temperature circulating fluidized bed gasifier (LT-CFB).

In Fig. 3.1, the flow diagramm including the major parts of the LT-CFB can be found [51, 52]. The pyrolysis chamber is a circulating fluidized bed that allows strict temperature control. Here, the fuel is added and the temperature is controlled to approx. 650°C. In this stage, only pyrolysis, meaning the release of volatile compounds, takes place. The temperature is chosen to have a complete pyrolysis, but also to still be able to prevent the volatization of inorganic ashes. At the top of the pyrolysis chamber, the flow enters the first cyclone. In this stage, bed material (here silica sand) char and ash are still mixed with the major gas components H_2, CO, CO_2 and CH_4 as well as a high amount of tars. The

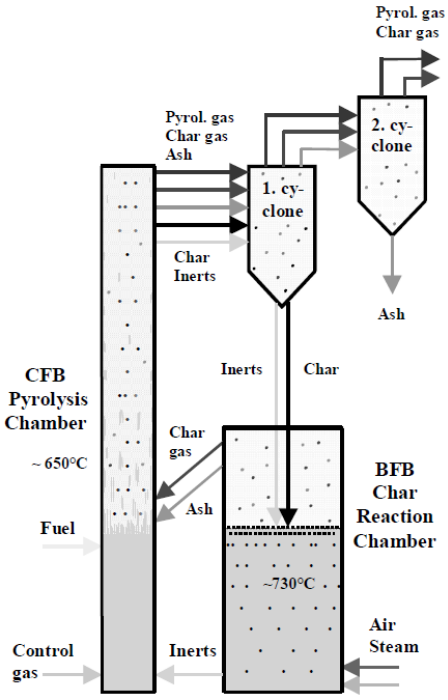

Figure 3.1: Flow diagram of the LT-CFB gasifier according to [3].

first cyclone seperates the solids (char and the bed material) from the gaseous compounds. While the gases enter a second cyclone that filters most of the remaining ashes from the product gas, the bed material and the char enter the char reaction chamber, a bubbling fluidized bed. Here, air is added to initiate partial combustion of the char. The temperature is controlled to about 730°C through the addition of air and the subsequent combustion. The products of the reaction chamber are then added to the pyrolysis chamber.

Because of this design, the LT-CFB generally produces fewer inorganic pollutants. Thus, it can be used for difficult biomasses, which contain rather high amounts of these. Wheat straw, manure, sewage sludge and other low-grade and waste biomasses have been successfully tested [3]. The low temperature, an advantage in preventing volatile ash components ending up in the product gas, results in a higher tar load. Hence, the tars contain a high level of the overall chemical energy in the product gas.

Because the product gas of the LT-CFB is mainly combusted, it is of great interest to analyze the gas composition with respect to especially these gas

species.

Chapter 4

Methods and Equipment

In this work, the ultraviolet (UV) and infrared (IR) absorption spectroscopy were used. For a better understanding of the pro's and con's of the methods, I will shortly describe the principle of the measurements, the Lambert-Beer Law. Afterwards, a detailed explanation of the setups at the gasifier will be given. First, the gas extraction method and the equipment used will be described, before the two different setups for the in-situ measurements will be described.

4.1 Theory of Absorption Spectroscopy in Brief

The principle theory of absorption spectroscopy is relative simple. It is all based on the so called Lambert-Beer Law. Even though the Lambert-Beer-Law describes in principle all absorption phenomena, the focus is on the absorption in gas. The Lambert-Beer-Law relates the measureable dimensions of incoming light of the intensity I_0 and transmitted light of the intensity I_1 to the particle number density N of the investigated species, its absorption cross-section σ and the path length l as follows:

$$I_0 = I_1 \cdot e^{-\sigma \cdot l \cdot N}$$

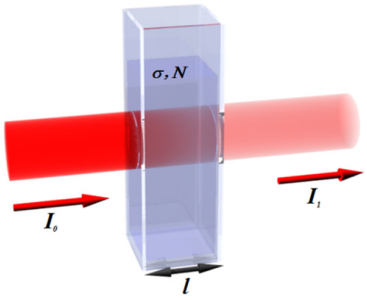

Figure 4.1: Principle of the Labert-Beer law, where the initial light intensity I_0 is absorbed by a material with the absorption cross-section σ and the particle number N in a compartment of the length l to the final intensity I_1

$$A = ln\frac{I_0}{I_1} = \sigma \cdot l \cdot N$$

Here, σ is given in $cm^2/molecule$, l in cm and N in $molecule/cm^3$

That means that the intensity of the incoming light decreases exponationally with the product of the particle number density, the path length and the absorption cross-section (see Fig. 4.1). The logarithm of the ratio of the incoming and transmitted light, also called the absorbance A, is directly proportional to the three mentioned dimensions. As already mentioned, the absorbance A can be calculated from measurable dimensions. If two of the three derived dimensions σ, l and N are known, the third one can be calculated. For quantitative analysis, the particle number density N as a measure of the concentration is the main goal of the measurements. Therefore, the length l and the absorption cross-section σ need to be known. While the length can easily be measured, the cross-section is dependent on the wavelength, the temperature and the pressure and it is specific for each gas. With sufficiant equipment, even structural isomers and the isotopologues can be distinguished. In gas mixtures, the overall absorbance is usually the sum of the absorbances of all components.

As already noted in Chapter 2 and described in the publications (see [28, 29]), measurements in the controlled environment of a laboratory allow the accurate determination of the absorption cross-sections σ. Once known, the absorption spectrum for different concentrations and absorption path length can be calculated from these data. The measurements of absorption cross-sections are however very time consuming and therefore should be used mainly for species not yet measured under the circumstances at hand, e.g., temperature, pressure, resolution, wavelength etc.

A timesaving, yet quite accurate method, is the calculation of the absorption spectrum from databases like HITRAN [53, 54], HITEMP [55] or CDSD [56, 57]. These databases give the so-called line spectrum, which can be mathematically transformed into absorption cross-section or the absorption spectrum under given circumstances with various tools. Even an online version called "HITRAN on the web" [58] is available. However, these databases focus on the IR spectra and only a few UV spectra are available. Often, it is also necessary to have a detailed understanding of the errors and uncertainties and a constant improvement of the databases by comparison of experimental data are essential.

However, the Lambert-Beer-Law is not always valid in the present form, e.g., high concentrations or light emission of the sample in the same wavelength region can be reasons for deviations from the linearity. In addition, the equipment used can also be a source of uncertainties that can play an important role. However, these deviations can be minimized by a careful handling of the setup and proper measurements. An analysis of the deviations in the UV setup can be found in [28]. In the IR, especially the light emission of the hot gas can cause major deviations. By measuring the emission of the light source without gas absorption and the emission of the gas itself, the absorption of the gas can be calculated.

In these properties of optical absorption spectroscopy lay its opportunities and its challenges. While it is possible to identify single compounds with great accuracy, the absorption cross-section σ of each single component needs to be known at a certain temperature, a certain pressure and a certain wavelength. Even though the inaccuracies due to small changes in temperature (a few degrees) and pressure (a few hPa) are for most industrial cases, such as the present one negligible. Nevertheless, accurate data in the investigated wavelength range and the circumstances expected in the process are needed for each component of a multi component environment to be able to identify the gas composition correctly.

Therefore, a product gas, with its strong light attenuation, a high temperature and its many gas components with different cross-sections is a difficult environment for the detemination of gas concentrations by absorption spectroscopy. However, the advantages of the methods, e.g., a simple setup, low operational costs, the possibility of real-time in-situ measurements and the ability to identify single components with high accuracy are striking factors. That and the fact that the obtained data can be used in multiple application justify the time consuming approach.

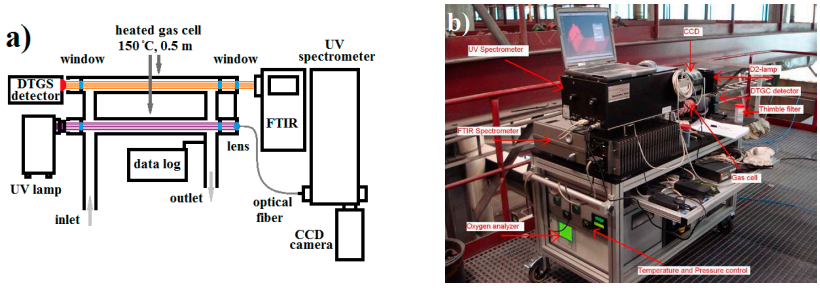

Figure 4.2: Setup of the gas extraction measurement system. Part a) shows the schematic setup and part b) the setup in reality

4.2 Setup for the Extraction Measurements

The system has been designed for measurements identifying and quantifying the major gas species (e.g., CO_2, CO, H_2O and CH_4) and, if possible, minor components of different high temperature applications. In addition, it can be used as a reference to the in-situ meaurements and helps to understand the differences between extraction and in-situ as well as online and offline techniques.

The setup is supposed to be moveable and needs to have the ability to carry both an UV and a FTIR setup as well as a gas cell. To measure at well-controlled conditions and achieve acurate data, temperature, pressure and oxygen levels were recorded as well. A vacuum pump ensured a constant flow through the cell, while a mass flow controller regulated that flow.

Fig. 4.2 shows the setup used for online gas extraction measurements. In part a) of the figure, a principle overview is given, while part b) shows how it looks in reality. The key elements of the setup are two interconnected, heated gas cells, the light sources and the spectrometers, which all were placed on a thin optical table. This setup was previously used successfully in other industrial applications, e.g., flame and hot flue gas analysis.

The gas cells consist of stainless steel which are on the inside covered with a teflon-like material. They have a length of 0.5 m, a diameter of 4.5 cm diameter, and can be heated up to 150°C. On both sides optical windows were installed. The window material was KBr and Suprasil for the IR and UV range, respectively. The equipment (e.g., lenses, detectors or light sources) could be mounted on the gas cells by special optical inserts for easy mounting and demounting.

As FTIR, a Bomem MB-154S system was used. The light source was the internal black body made of silicon carbid typically held at 800°C. The detector, a DTGS

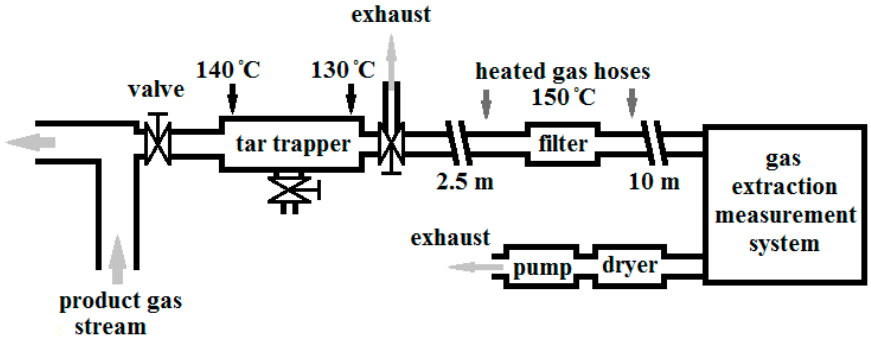

Figure 4.3: Extraction procedure at the LT-CFB gasifier for optical online gas analysis of the product gas

detector, was placed outside the FTIR on the other side of the gas cell. The resolution used in the experiments was 2 cm^{-1}.

In general, the UV setup used the same equipment as for the laboratory experiments [27, 28, 29]. As UV light source, a LOT Oriel deuterium lamp (D_2) was used. On the other side of the gas cell, the light was coupled into an optical fiber and then guided into the Czerny-Turner monochromator. The monochromator, a Princeton Instruments Spectra Pro 2500i of 0.5 m length, was equipped with three different gratings of which the 1800 and 3600 grooves holographic gratings were used. As detector, a CCD camera (PIXIS 100B /Princeton Instruments) was used. Depending on the wavelength, the achieved resolution was 0.045 nm, and 0.019 nm or better for 1800 and 3600 grooves, respectively.

The oxygen levels were measured with an oxygen analyzer (Oxymat 6 from Siemens) and recorded with a data log system from Agilent along with the temperature and the pressure readings.

The recording of the IR and UV measurements were synchronized manually with the datalog system and recorded a single dataset every 10 seconds. Before and after each measurement, the system was purged with nitrogen and background measurements were taken to assure the stability of the baseline.

In Fig. 4.3, a schematic drawing of the extraction procedure at the gasifier is shown. At first, the hot gas (around 300°C or 500°C) entered the tar trapper, where it cooled down. The tar trapper was an isolated and heated tube of 7 cm diameter and a length of 1 m. The temperature was set to 140°C at the entrance and 130°C at the exit of the tube. Its task was to reduce the amount of heavy tars with high dew points, that could block the extraction system and to avoid

water condensations in the system. Of the total amount of gas flowing through the tar trapper only 1-2 l/min were used in the extraction system. This flow was regulated by a combination of a vacuum pump from the company Ilmvac and a highly acurate mass flow controller from Bronkhost were installed at the end of the system. After the tar trapper, a 2.5 m heated gas hose (150°C, inner diameter 4 mm) led the extracted gas to a filter. The filter consisted of a cotton thimble filter that was placed before a second particle filter made of sintered metal. Both filtered the gas from particles larger than 1 μm. The reduction of larger particles reduced the optical density of the gas and allowed to use a 0.5 m path length in the gas cell. Besides, it reduced the fouling of the optical equipment. After the particle filter a 10 m heated gas hose (150°C, inner diameter 4 mm) led the gas stream into the gas extraction measurement system, where the gas was analysed at 150°C. Thereafter, the gas was dried by cooling it down to 5°C to protect the vacuum pump. Under these circumstances, the time until 99% of the product gas concentrations was established in the gas cells was 50 s.

4.3 Setup for the In-situ Measurements

For the in-situ online measurements, two setups have been made. In the first setup, IR and UV measurements at various path length up to 5.7 cm along the cross-section of the product gas flow could be done. A principle scheme of the setup can be found in Fig. 4.4. In this case, the measurements in the UV and the IR region needed to be done seperately.

The principle spectroscopic setup was similar to the one used in the gas extraction setup. In fact the UV setup used the same equipment and the only difference was that the light of the deuterium lamp was coupled in by an optical fiber made of doped quartz. An identical fiber was used for guiding the light back to the spectrometer. In the case of IR, a similar spectrometer, the BOMEM B-155 ES2 with the same resolution was used. The custom-made black body (Risø R800) was the light source. For coupling the light in, no optical fibers were used. However, the transmitted light was guided with an optical IR fiber (CIR fiber) to the spectrometer. This fiber has no transmission in a region of about 100 cm^{-1} to 1500 cm^{-1} and around 2500 cm^{-1}

The optical access to the product gas stream was the most challenging, since the setup needed to meet three specifications. To find a good balance between absorption and detectability in the IR and the UV region, it was necessary to be able to adjust the path length of the light through the product gas, the path length needed to be defined and in addition, the optical windows and lenses

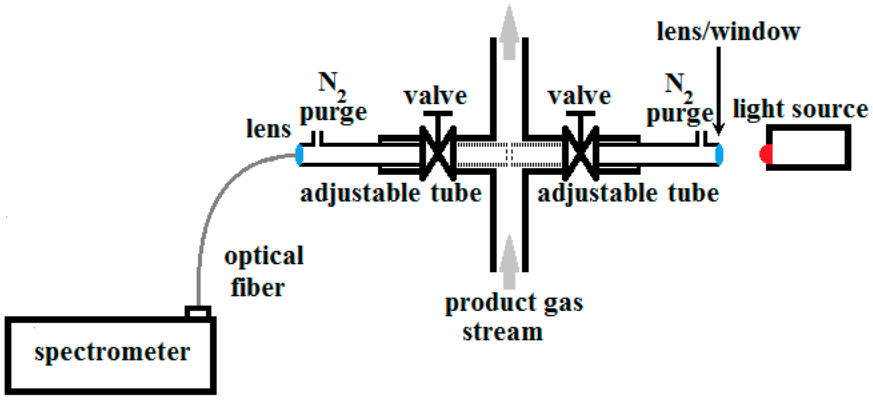

Figure 4.4: Principle setup of the in-situ measurements of the product gas at the LT-CFB. For UV analysis, the light source was coupled in with an optical fiber. For the IR analysis, the direct light of a black body was used.

needed to stay clean. As a result of these specifications, the setup as shown in Fig. 4.4 was chosen. On two opposing sides of the product gas line, a flange allowed an easy access. With two custom-made adapters, two tubes of 15 mm inner 23 mm outer diameter and 36 cm length could be inserted into the product gas line. Valves allowed to mount and demount the devices during operation of the gasifier. The tubes could be adjusted by pushing them further into the gas line or pulling them out. A gasket of two O-rings sealed the adapters to the tubes to prevent leaking of the product gas. The distance was measured by inserting the tubes from both sides until they touched each other. For the UV measurements, a distance of a few millimeters (1-3 mm) was chosen since a larger path length resulted in total absorption of the UV light. In case of the IR, the full diameter (5.7 cm) of the tube was used. To keep the windows and lenses clean, and to have a defined path length, cold nitrogen entered the system close to the lenses. The idea was that the colder nitrogen and the hot product gas flow would then form something similar to the flow windows in the gas cell (see [27]).

The second setup was made to measure in the IR along the gas flow on a length of 5.5 m. The idea of having such a long path length was to be able to detect trace gases that show a weak absorption in the IR region. To be able to detect those, it was necessary to use an FTIR with a high resolution and a high performance black body. The high resolution would make it possible to resolve peaks that are inbetween the peaks of major gas components like H_2O. With lower resolution, the structures of major gases appear to be continuous. Therefore, the Agilent Cary 660 FTIR spectrometer with a linearized broadband MCT detector was

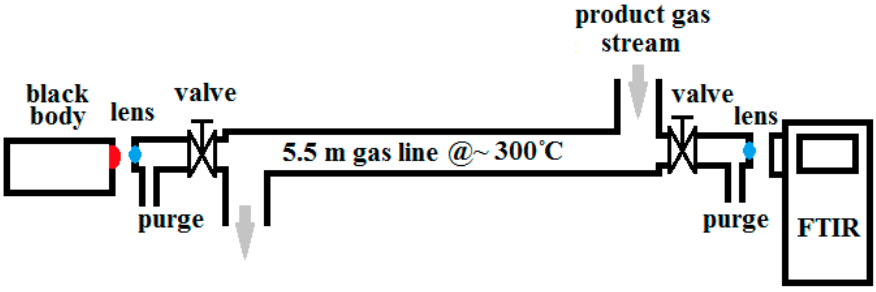

Figure 4.5: The setup of the long path length (5.5 m) in-situ measurements of the product gas.

used. This setup was run at a software controlled resolution of 0.25 cm^{-1}. The black body was custom-made by our group and had a temperature of 1500°C.

In Fig. 4.5, the setup can be seen. It is in principle very similar to the previous setup. From both sides special adapters were mounted to the flanges that held the optical windows and kept them clean. The windows consisted in this case of KBr and were purged from both sides with dry air.

Chapter 5

Results and Discussion

In this chapter, the results of the measurements at the LT-CFB will be discussed. At first, the results of the IR measurements will be given, before the data in the UV region will be examined.

5.1 IR Measurements - The Major Gas Species

In this section, the in-situ and extraction measurements are compared with one another. The emission of some hot gas species (e.g., CO_2 and H_2O) made it necessary to measure four different spectra to be able to get the absorbance A. The four measurements were the emission of the black body without absorbing product gas I_{BB}, the emission of the hot gas without the black body I_G as well as the emission of the black body and the gas I_A and the reference I_R, a measurement without black body or gas. This is a typical way to circumvent the restrictions of the Lambert-Beer-Law that does not include emissions by the gas itself. The absorption is then calculated as:

$$A = \frac{I_{BB} - I_R}{I_A - I_G}$$

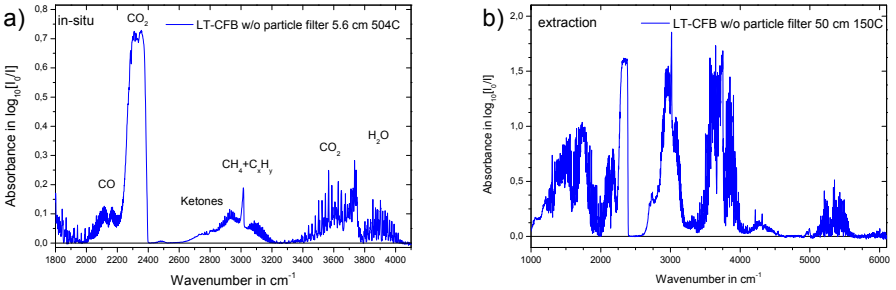

Figure 5.1: Overview over absorbance from a) in-situ measurements at 504°C and 5.6 cm and b) extraction measurements at 150°C and 50 cm at the same gasification conditions

In the first part, a direct comparison between in-situ measurements of the product gas at a temperature of around 500°C and a short path length of 5.6 cm and extraction measurements of 50 cm length at 150°C for CO, CO_2 and H_2O is made. Here, the gasifier was run without an additional particle filter and with straw as a fuel. In the second part, the potential of the FTIR spectroscopy are shown by a single long path length in-situ measurement (550 cm at approx. 300°C) and a detailed analysis of organic compounds by means of extraction measurements (50 cm at 150°C). Since both measurements were taken under the same circumstances (additional particle filter, straw as a fuel) and at the same day, the major gas species are also compared.

5.1.1 IR In-situ Measurements at Short Path Lengths

When the LT-CFB was operated without the particle filter, the temperature of the product gas at the measuring site was 504°C and the pressure around 1200 hPa. The temperature was measured with a thermocouple close to the actual measuring point (about 0.5 m away). The in-situ measurements were performed at an optical path length of 5.6 cm which was the diameter of the product gas line. The use of optical fibers and the InSb detector limited the wavenumber range. Below 1800 cm^{-1} no data could be collected. For the extraction measurements, the gas was cooled down to 150°C and filtered as described in Chapter 4. In the 50 cm gas cell of the extraction measurements, a pressure of 923 hPa was measured. In Fig. 5.1 an overview of the resulting spectra are shown.

Fig. 5.1a shows a typical result of the in-situ measurements and part b, the one of the extraction measurements. The major structures observed in-situ, can also

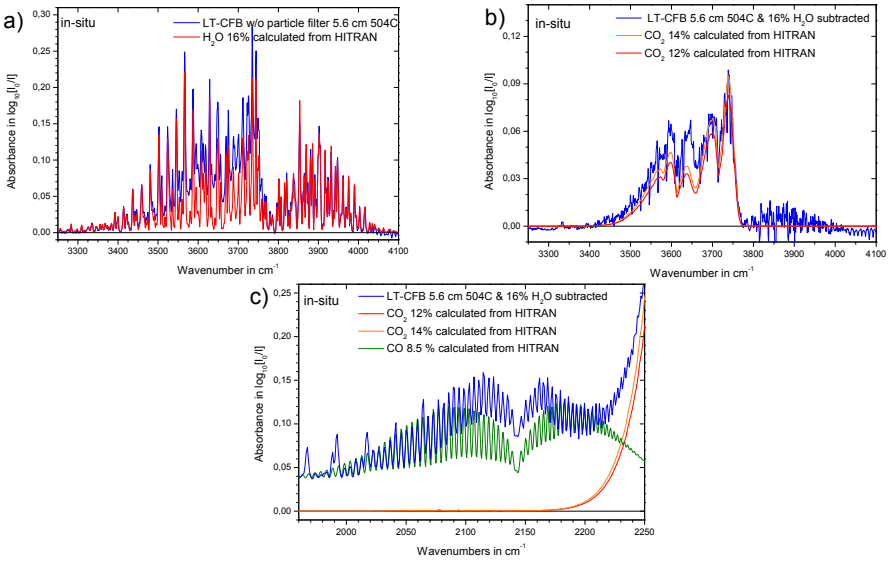

Figure 5.2: Comparison of measured in-situ absorbance (blue) and calculations from the HITEMP database at 5.6 cm, 504°C. a) H_2O (red) at 16% between 3250 cm^{-1} and 4100 cm^{-1}; b) CO_2 at 14% (orange) and 12% (red) in the same region as (a); c) CO (green) at 8.5% and CO_2 at 12% (red) and 14% (orange) between 2010 cm^{-1} and 2250 cm^{-1}. For b) and c), the water bands were subtracted.

be seen in the extraction measurements, where they have a higher absorbance. Since in both experiments, similar equipement was used, the differences are mainly due to the longer path length and the lower temperature in the gas cell compared to the in-situ measurements. The major gas components CO_2, CO and H_2O can be seen clearly. In the region between 2600 cm^{-1} and 3200 cm^{-1}, organic compounds, such as lower hydrocarbons (CH_4, C_xH_y) and aldehydes and ketones (C-H compounds with at least one C=O double bond), can be found.

Fig. 5.2, shows a more detailed view on the major components. In Fig. 5.2a, the bands between 3250 cm^{-1} and 4100 cm^{-1} are magnified. While the blue curve shows the real measurements, the red curve shows the water bands under the same circumstances (5.6 cm, 504°C, 1200 hPa, same resolution) at 16%$_{vol}$ calculated from the HITEMP database. Especially between 3800 cm^{-1} and 4100 cm^{-1} a good agreement can be stated. In regions with lower wavenumbers, the water bands are overlaid with CO_2 bands. After subtracting the calculated water bands at a concentration of 16% from the measured structure, the remaining structure can be compared to calculated CO_2 bands to quantify

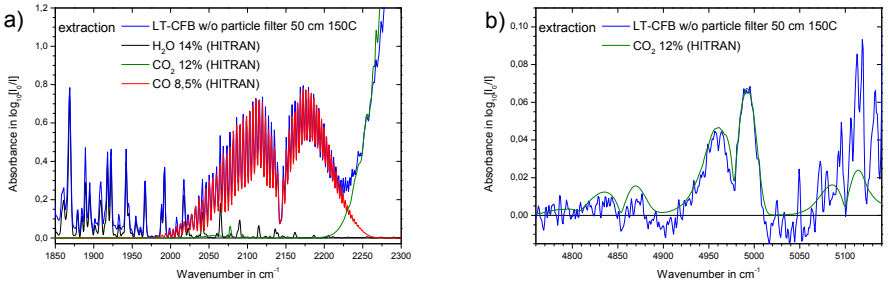

Figure 5.3: Comparison of measured absorbance (extraction - blue) and calculations from the HITEMP database at 50 cm and 150°C. (a) H_2O at 14% (black), CO at 8.5% (red) and CO_2 at 12% (green) between 1850 cm^{-1} and 2300 cm^{-1}; (b) CO_2 at 12% (green) between 4710 cm^{-1} and 5180 cm^{-1}.

the concentration. This is shown in Fig. 5.2b. The CO_2 bands fit at a concentration of 12-14%. In the same way, the structure of CO between 2000 cm^{-1} and 2300 cm^{-1} can be analysed (see Fig. 5.2c). For CO a concentration of 8.5% can be concluded. However, the CO bands are also overlaid by other bands.

Fig. 5.3 shows a more detailed view on the results of the extraction measurements (in blue). In part a, the fit with CO (red) and H_2O between 1850 cm^{-1} and 2300 cm^{-1} are in focus. With the same concentrations for CO (8.5%) and H_2O (14%) as calculated for the in-situ measurements, an excellent agreement can be found. In addition, also the CO_2 (green) shows a good agreement for the slope of the peak around 2250 cm^{-1}, if a concentration of 12% is chosen. In Fig. 5.3b, the CO_2 peak around 5000 cm^{-1} is investigated. Again, an excellent agreement can be found for 12%.

5.1.2 Potential of the FTIR Spectroscopy

In this part, the potential of the FTIR spectroscopy and trial measurements in tracing compounds besides the major gas species CO, CO_2, H_2O and CH_4 will be discussed. Hereby, two methods and their application at the LT-CFB are shown: long path measurements and subtraction of known gas components for the identification of trace gases.

The use of a very long path length is benefitial for the identification of trace gases, because a longer path length results directly in a higher absorbance and therefore lowers the detection limit of each gas. However, this higher absorbance

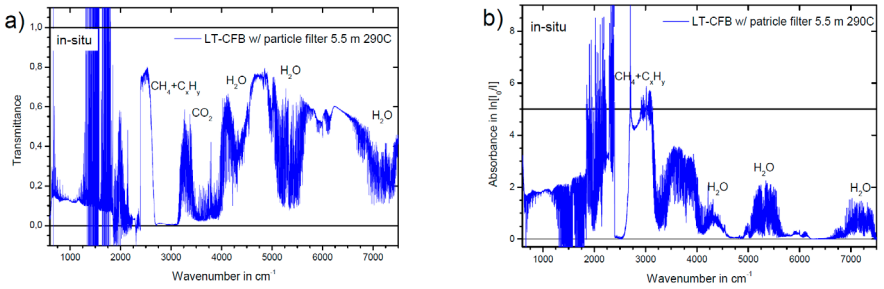

Figure 5.4: Spectra for in-situ measurements at 290°C and 550 cm a) transmittance without baseline correction and b) absorbance.

also applies for the major gases, which in return can cause total absorption in some regions. In the case at hand, a 550 cm path length was used for these trial measurements. For a better differentiation and to be able to trace single indentifying bands, a high resolution spectrometer was used. In addition, a more powerful light source had to be used (see Chapter 4). In this experiment, the gas temperature was 290°C and the pressure 1020 hPa.

The gas in the gas cell of the extraction setup had a temperature of 150°C and a pressure of 963 hPa.

Fig. 5.4 shows the transmittance and the absorbance at 550 cm. For the transmittance, a value of 0 means that the gas is optically dense, while in regions with a transmittance 1, the gas is transparent. Especially at the lower wavenumbers, it can be seen that there is no transmittance. However, even at a transmittance above 0 (e.g., around 1000 cm^{-1} or 3800 cm^{-1}), it seems as if the higher peaks are cut off. In addition, around 1500-2200 cm^{-1} the transmittance shows an unusual behaviour. By looking more carefully at the absorbance (Fig. 5.4b) one can see that between 3100 cm^{-1} and 2600 cm^{-1} and below 2400 cm^{-1}, no individual species can be identified.

Besides the high absorption of water in the spectrum, the unusual signal has mainly two sources: First of all, the use of KBr windows at these circumstances was difficult. The high water concentration and the low temperature of the window resulted in a condensation of water on the KBr window. This effected the transmission of light through the window. After this experiment, the lense was partially opaque. In addition, a partial blocking of the product gas pipe with time due to particle and condensed tar deposition caused a decreasing field of view and difficulties in the general optical alignment.

However, in the spectral range around 5000 cm^{-1}, CO_2 and H_2O can still be

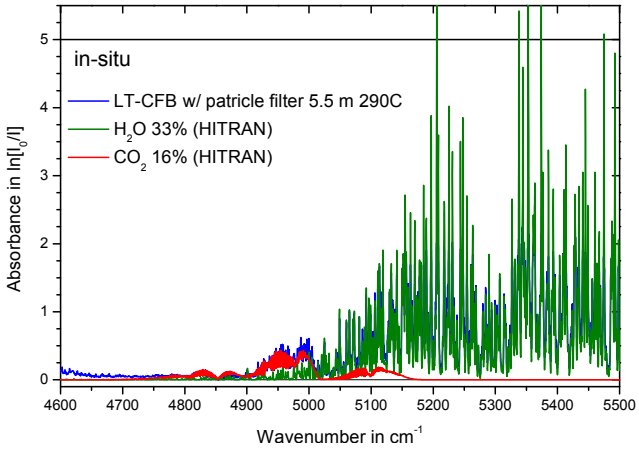

Figure 5.5: Comparison of measured in-situ absorbance (blue) and calculations at 290°C and 550 cm of CO_2 (16% - red) and H_2O (33% - green) between 4600 cm^{-1} and 5500 cm^{-1}.

quantified. This is shown in Fig. 5.5. The figure shows the absorbance of the product gas (blue) and the calculated absorbance of H_2O at 33% (green) and CO_2 at 16% (red) around 4600 cm^{-1} and 5500 cm^{-1}. For both cases a good agreement can be stated.

The same values for water (33%) and carbon dioxide (16.4%) can be found in the extraction measurements conducted at the same day (see Fig. 5.6a). In addition, the concentration of CO can be calculated. At 10% an excellent agreement can be found. These measurements also allow an quantification of CH_4 (methane - Fig. 5.6b) and C_2H_4 (ethylene - see Fig. 5.6c). In Fig. 5.6d), the second approach of subtracting the known gas components from the spectrum was used to identify other organic trace gases. This approach was prefered to simple fitting of all components, because either the presence of some trace gases in the product gas or their absorption cross-sections at higher temperatures were unknown.

While for methane and ethylene calculations from the HITRAN database showed a good agreement with the measurements at 2.5% and approx. 1%, respectively. For the other species mentioned, no HITRAN/HITEMP data or other data at 150°C were available. Thus, the concentrations were estimated by recalculating data at 50°C from the PNNL database [59]. The resulting concentrations are to be handled with care, because the changes in the shape of the spectra (e.g., widening) due to higher temperature are not taken into account. However, some good agreements can be found. Especially acetaldehyde shows a good agreement at a concentration of 0.5%. All other data seem to have part in the structure

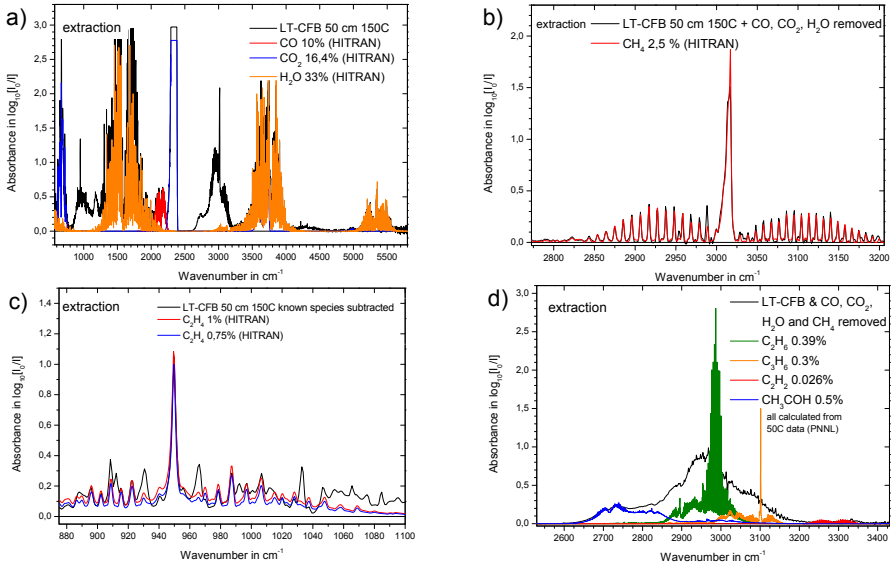

Figure 5.6: Comparison of measured absorbance (extraction - black) and calculations at 150°C and 50 cm of: a) CO (10% - red), CO_2 (16.4% - blue) and H_2O (33% - orange) between 600 cm^{-1} and 5800 cm^{-1}; b) CH_4 (2.5% - red); c) C_2H_4 at 1% (red) and 0.75% (blue); (c) C_2H_6 (0.39% - green), C_3H_6 (0.3% - orange), C_2H_2 (0.026% - red) and CH_3CHO (0.5% - blue) scaled from 50°C data [59].

Table 5.1: Comparison of the concentrations of the IR in-situ short path length and extraction measurements

Technique	CO in vol%	CO_2 in vol%	H_2O in vol%
IR extraction	8.5	12-14	14
IR in-situ (5.6 cm)	8.5	12	14

between 2600 cm^{-1} and 3400 cm^{-1}, however, the temperature dependency of these compounds is not known in the IR. For a better understanding of this structure, the temperature dependency of these species has to be investigated.

5.1.3 Conclusion of the IR Measurements

The comparison of IR extraction and in-situ measurements with a short path length of 5.6 cm at the LT-CFB show that both achieve similar results by using similar equipment. Table 5.1 gives and overview over the most important species. With both methods, the same concentrations are measured. That proves that even under the extreme environment of an heavily tar and particle loaded product gas at pressures around 1200 hPa a good agreement between in-situ and online eaxtraction methods can be found.

The measurements at long path length of 550 cm and a detailed analysis of extraction measurements show the potential of FTIR spectroscopy. If the challenges of the partial blocking, the condensation of water on the KBr windows and the optical alignment can be overcome, the FTIR technique can prove to be a powerful tool in the analysis of trace gases in a product gas. In addition, a larger database for important trace gases at higher temperature could improve the performance of this techique as well and also make an easier quantification possible.

5.2 UV Measurements - Phenol and Naphthalene as Examplary Tars

In this section, the extraction and in-situ UV measurements will be described. To set the stage, extraction measurements will be described first, before the

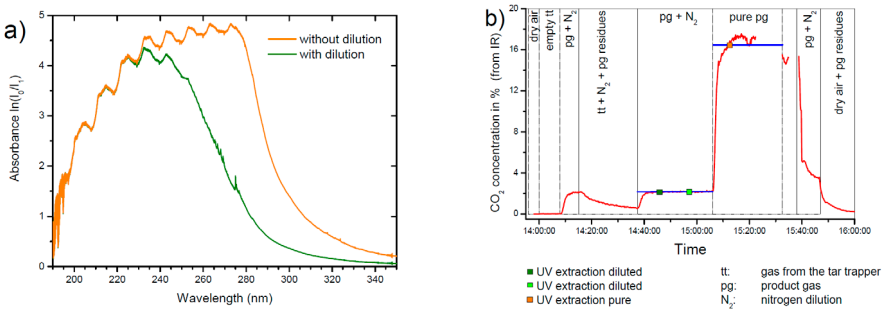

Figure 5.7: a) UV absorbance A the extraction measurements of product gas at 150°C in the wavelength range of 190 nm to 350 nm with dilution (green) and pure (orange). b) concentration of CO_2 over time measured by the IR system. The green squares indicate the time of the UV measurements in part a) of the figure (green - diluted product gas; orange - pure product gas).

findings in the in-situ measurements will be discussed. Both parts focus on the absorption of the two major aromatic compounds phenol and naphthalene and therefore directly show the application of the measured absorption cross-sections published in the third paper (see Chapter 2).

5.2.1 UV Extraction Measurements

The first UV measurements with the extraction system showed that the product gas in the 0.5 m gas cell at 150°C is optically dense for the UV radiation emitted by the deuterium lamp in the wavelength range between 190 nm and 280 nm. This means that the transmittance in this wavelength range was close to zero. Consequently, a total absorption can be observed. In Fig. 5.7, the orange curve is an example for that.

To avoid the total absorption, either the absorption path length, or the gas concentration had to be reduced. In the measurements at hand, the only variable was the concentration, which could be changed by introducing a constant flow of nitrogen to the system. Thereby, the product gas was diluted. The green curve in Fig. 5.7a resembles an exemplary result of this effort and the appearance of a distinct structure around 270 nm can be seen. However, dilution ratio of product gas to nitrogen was unknown. In Fig. 5.7b the CO_2 concentrations over the time including the time of the measurements measured by the IR spectroscopy system in the adjacent (connected) gas cell are shown. The green and orange squares in the plot mark the time of the UV measurements presented here. From these

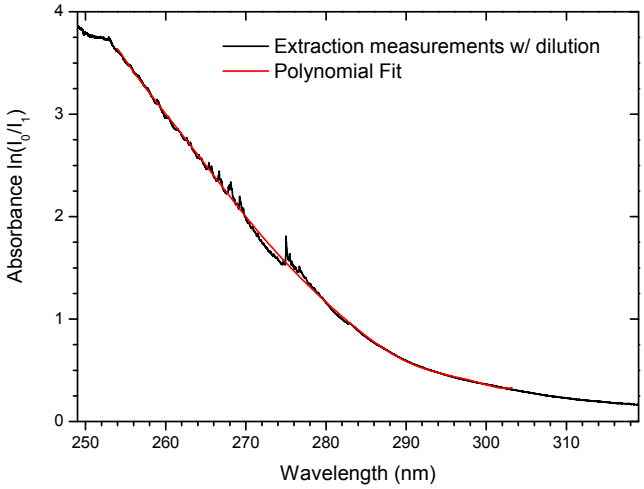

Figure 5.8: Polynomial fit (red) to the absorbance A of the extraction measurements with dilution at the 150°C.

concentrations, the dilution factor can be determined to 7.6 in the measurements presented in this section. In the following, for all concentrations mentioned the dilution is already accounted for.

The structure on the black curve around 270 nm in Fig. 5.7 can be identified as phenol that is heavily overlaid by other absorbing gas species. It is also difficult to evaluate their composition, because most aromatic species absorb in this region [60]. To circumvent this problem the differential optical absorption spectroscopy (DOAS) aproach can be done [61]. Here, only the fine structure is investigated. To obtain the fine structure, a polynomial fit in the spectral range of interest is subtracted from the original signal (see Fig. 5.8). Then, the same polynomial fit (order and range) is done for the absorption cross-sections to which the signal will be compared. In the case at hand, the polynomial fit was of the order 9 between 254 nm and 304 nm.

The advantage of this method is that all constant shifts in signal intensity in the area of investigation (e.g., base-line shifts) are canceld out. The result of this procedure is shown in Fig. 5.9. Here, two different extraction measurements taken about 10 minutes apart at the LT-CFB are shown. It can be seen, that over the time between the measurements, the signal was stable. Subsequently, only one of those curves will be used to quantify the phenol and naphthalene.

In Fig. 5.10, a fitting of the differential optical absorption spectra from the laboratory data of phenol and naphthalene at 150°C to the extraction measure-

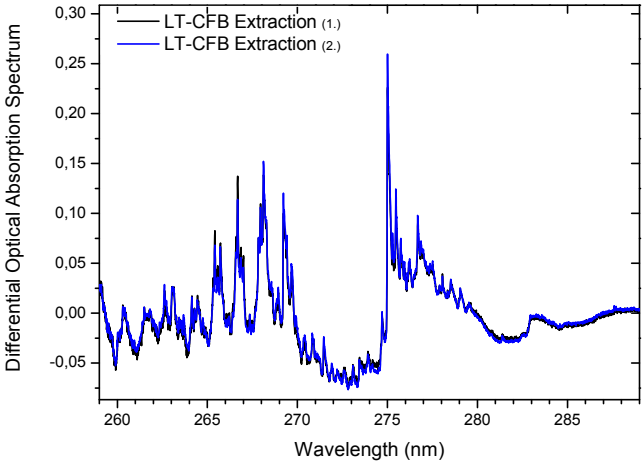

Figure 5.9: Two differential optical absorption spectra of the extraction measurements at 150°C with dilution.

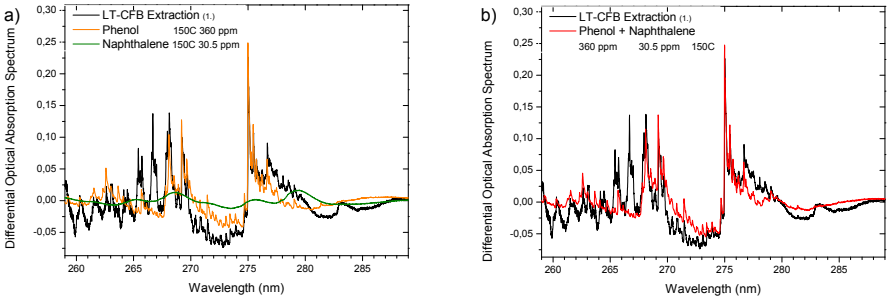

Figure 5.10: UV extraction measurements of the product gas at 150°C with phenol and naphthalene fits. a) shows the individual structure at 360 ppm of phenol (orange) and 30.5 ppm of naphthalene (green). b) shows their summation

ments at the LT-CFB can be seen in the wavelength range between 259 nm and 289 nm. The laboratory spectra for phenol and naphthalene were calculated from the differential absorption cross-sections using the conditions in the gasifier experiment: a temperature of 150°C, a pressure of 972 hPa, a path length of 50 cm. Only the concentrations were fitted to the spectra obtained at the gasifier. In Fig. 5.10a, the orange curve accounts to a concentration of 360 ppm phenol and the green curve to 30.5 ppm of naphthalene in the product gas. The figure also shows that the contribution of phenol to the fine structure at 150°C is very large, whereas naphthalene only contributes an uneven offset.

Fig. 5.10b compares the summation of both signals (red) to the extraction measurements at the gasifier (black). In general, a good agreement of the data can be found. In addition to the good fit in some regions, e.g., between 273 nm and 277 nm, there is a good agreement of the fine structure with offset in other regions, e.g., betwenn 267 nm and 273 nm. However, additional peaks can also be found, e.g., around 266 nm. Both deviations are most likely due to the absorption of unknown species. It is very difficult to evaluate these species, mainly because the chemical structure of a compound determines their ability to absorb UV light, which means that the strongest absorption does not equal to the highest concentration. Another reason is that the absorption of many higher aromatics are less distinct and contribute an offset, such as naphthalene.

5.2.2 UV In-situ Measurements

To be able to quantify phenol and naphthalene in-situ, it was necessary to find a right path length in the gas on site. Similar to extraction, the gas was optically dense in the UV range for the setup used, when the path length equalled the full inner diameter of the gas pipe (5.7 cm). Therefore, it was necessary to adjust the path length. Due to strong absorbance, the characteristic peaks of phenol could be observed only at very small path length of a couple of millimeter. Measurements have been performed at a distance of 1 mm, 2 mm, and 3 mm between the tubes (see Fig. 4.4 in Chapter 4). Fig. 5.11a shows the simplified flow diagram that was assumed. In this case, the distance between the tubes equals to the path length (see Fig. 5.11b). This assumption proved to be correct for larger distances as it has been seen in the IR measurements. Even shifts of a couple of millimeter would still give the right order of magnitude in concentrations. The measurements at 3 mm proved to have the acceptable signal-to-noise ratio and will be discussed here.

In Fig. 5.12, the differential absorption spectrum of the in-situ measurements at the LT-CFB is shown at a wavelength range between 264 nm and 286 nm. The temperature of the product gas was 306°C and was measured with a thermocou-

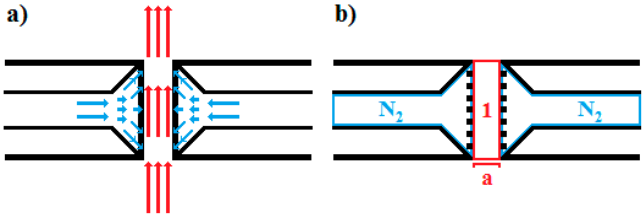

Figure 5.11: Simplified flow diagram of the conditions at the end of the optical tubes. a) The red arrows depict the product gas stream at 306°C and the blue the nitrogen flow at lower temperature. b) The red region 1 of the length a describes where UV light is absorbed by the product gas.

ple less than 0.5 m away from the measuring point. The pressure was assumed to be 1030 hPa. In general, the shape of the curve seems to be similar to the one at 150°C (see Fig. 5.9). Around 275 nm the peak of phenol can be seen and also the peaks below 270 nm are visible. As expected from the measurements at the laboratory, the peaks are less distinctive than at lower temperature.

Again, the differential absorption spectrum of phenol and naphthalene were calculated on basis of the differential absorption cross-sections of both species at 300°C under the conditions mentioned above. The results can be seen in Fig. 5.13a with phenol at 7700 ppm in orange and naphthalene at 1000 ppm in green. 5.13b shows the summation of both (red). It is visible that naphthalene has a higher influence on the overall structure than at lower temperature, which is due to the decreasing of the fine structure of phenol at higher temperatures (see Appendix C / [29]). Especially in the summation, a remarking agreement between 275 nm and 286 nm and below 267 nm can be stated. However, between 267 nm and 275 nm there is a strong deviation in the overall structure while the individual peaks still seem to match. In addition to the strong deviations in the structure between 267 nm and 275 nm, there is a huge difference in concentrations compared to the results of the extraction measurements.

Many different explanations for this difference can be made up. It may be due to chemical convertion and condensation due to the cooling and the processing of the product gas during the extraction process, wrong calibration of the distance between the tubes or hot product gas penetration into the tubes and therefore wrong assumption of the path length or a combination of these.

The later posibility, the combination of penetration of hot product gas into the tube and its cooling due to the mixing with colder nitrogen, shall be discussed further: Fig. 5.14a illustrates this in a simple flow chart. From the outside,

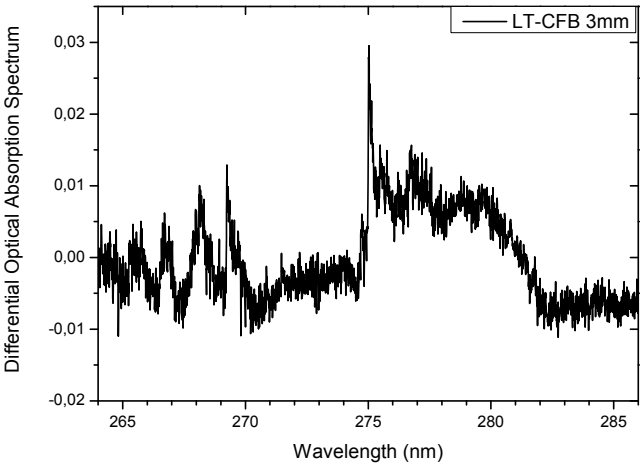

Figure 5.12: Differential optical absortpion spectrum of the in-situ UV measurements at the LT-CFB

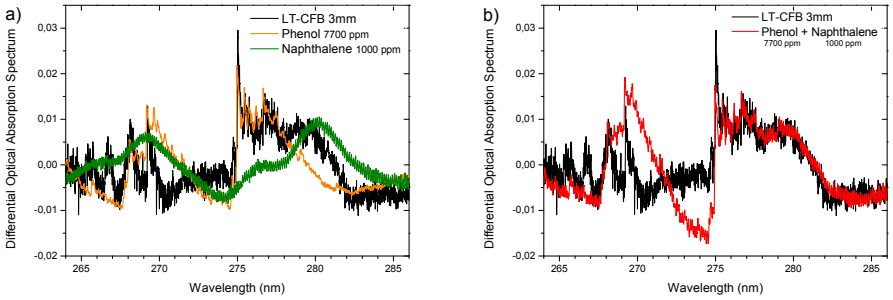

Figure 5.13: UV in-situ measurements at 306°C and fits of phenol and naphthalene. a) shows the individual structure at 7700 ppm of phenol (orange) and 1000 ppm of naphthalene (green). b) shows their summation

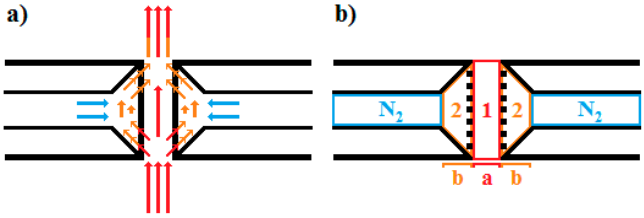

Figure 5.14: Simplified flow diagram of possible conditions at the end of the optical tubes. a) the red arrows depict the product gas stream at 306°C, the blue ones the nitrogen flow at lower temperature and the orange ones, the mixture of cooler nitrogen and hotter product gas. b) The region 1 of length a describes the region where the UV light is absorbed by the product gas at full concentration and 306°C and region 2 of length b, where the UV light is absorbed by the cooler nitrogen/product gas mixture.

nitrogen at room temperature is introduced into the optical tubes to keep the optical windows clean of dust, tar and other condensations. In the tube, the nitrogen is heated. Due to a short residence time of the nitrogen in the tube, it can be assumed that the nitrogen is not heated to the full 300°C. In fact, it probably has a significantly lower temperature than 300°C when it reaches the product gas. When the product gas flow itself enters the relative small gap of 3 mm at a significant velocity, it spreads. This creates vortexes of hot and cold gas directed into the tubes, which are probably further enhenced by the V-shaped geometry of the tubes. The mixed gas, has a temperature that is above the one of colder nitrogen but below the 300°C of the product gas. To be able to evaluate the influence of such effects, a simplified three section model is applied (see Fig. 5.14b). The product gas in the middle (section 1 - red) has the temperature T_1 of 300°C and an width a of 3 mm. To both sides of the product gas, a section of lower temperature T_2 and width b are adjacent (section 2 - orange). For the following calculations, T_2 was set to 150°C, because the absorption cross-sections of both, phenol and naphthalene at temperatures between 150°C and 300°C are unknown. The width b of the outer sections was set to 6 mm each, to a total path length of 12 mm at 150°C and half the concentration in the product gas to resemble a dilution. The pressure was assumed to be the same as in the product gas pipe. It is important to mention that the temperatures and penetration lengths were set to achieve concentrations in similar to the ones observed in the extraction measurements.

Fig. 5.15a shows the result for phenol in each section with orange being the absorption signal at 300°C and red the one at 150°C. Fig. 5.15b shows the same for naphthalene with light green being 150°C and dark green being 300°C.

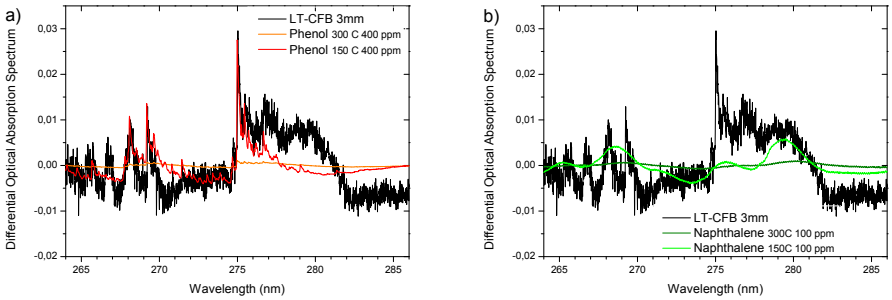

Figure 5.15: UV in-situ measurements at 306°C and fits of phenol and naphthalene according to the three section model. a) shows the individual structure at 400 ppm of phenol (orange) and 100 ppm of naphthalene (green). b) shows their summation

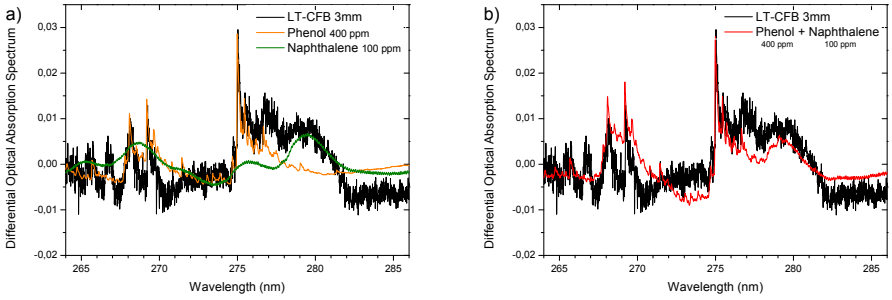

Figure 5.16: UV in-situ measurements at 306°C and fits of phenol and naphthalene according to the three section model. a) shows the individual structure at 400 ppm of phenol (orange) and 100 ppm of naphthalene (green). b) shows their summation

At concentrations of 400 ppm for phenol and 100 ppm for naphthalene in the product gas, a good agreement can be found. The influence of the absorption at lower temperatures are higher in both cases. Especially for phenol, the influence of the higher temperature is almost negligible.

In Fig. 5.16a the summation for each species can be seen and part b shows the summation of both, sections and species. Again, a good agreement can be stated. Especially the structure between 275 nm and 277 nm (mainly phenol) and below 266 nm fit nicely. In addition, the heights of the fine structure fits perfectly with the exception of the structure around 267 nm. Again, an offset in some regions can be found. This may be due to other unidentified gas species and because of the assumed temperatures, path lengths in the outer sections.

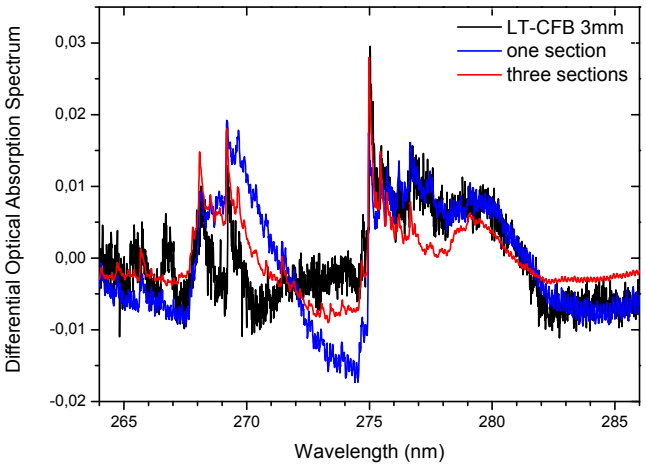

Figure 5.17: Comparison of the one and three section models in blue and red, respectively, with different concentrations of phenol and naphthalene.

All mentioned concentrations in the three section model have the only purpose to show that a different view on the quantification process is possible. For both species, these concentration depend on the penetration length b, the concentration, temperature and presence of other species. While the major factor that changes the calculations of the phenol concentrations is the temperature (due to its strong temperature dependency), the most influencial factor for naphthalene is the presence of other species (because of its lack of fine structure).

5.2.3 Comparison of the UV Results

Fig. 5.17 shows the comparison of the two models. While the black line depicts the original product gas measurements, the blue line depict the one section model with no product gas penetration into the optical tubes and the red line the three sections model with simplified penetration, respectively. In general, both give a good agreement with the real measurements. In case of the one section model, a mismatch between 268 nm and 275 nm can be seen, but a good to excellent agreement in the other regions can be stated. For the three section model, the mismatch is smaller, but more constant. From these data alone, it can not be concluded which model is to favor.

Therefore, a comparison with the sampling and subsequent GC-MS analysis at the same circumstances and during the same measurement campaign might pro-

Table 5.2: Comparison of different phenol and naphthalene values obtained from different measurements including the temperature of the measurement.

Technique	temperature in °C	phenol in ppm	naphthalene in ppm	Sum of both in g/m^3
UV extraction	150	360	30.5	1.77
UV in-situ (1 section)	300	7700	1000	35.4
UV in-situ (3 sections)	300	400	100	2.10
GC-MS 1 [62]	25	203	16.9	0.885
GC-MS 2 [62]	25	226	15.8	0.963

Table 5.3: Results of gravimetric tar measurements at the LT-CFB measurement campaign from [62].

	amount of total tars in g/m^3
Sample 1	32.68
Sample 2	28.51

vide more evidence. In Table 5.2, the concentrations of phenol and naphthalene in ppm as well as their summation in g/m^3 are presented for the three different analysis, extraction, in-situ (one section) and in-situ (three sections) and also the concentrations obtained by sampling with a Petersen column and GC-MS analysis [62].

In general, the GC-MS analyses show the lowest results for phenol and napthalene. The analysis of the UV extraction measurements and the UV in-situ three sections analysis are of a factor of 1.7 higher but still in the same order of magnitude. In this comparison, only naphthalene in the three section model shows a significant higher value. However, the different temperatures of the gas during the sampling/analysis might be a reason for the different concentrations.

As already mentioned before, the gravimetric measurements measure the amount of total tar in the product gas. These measurements show an average mass concentration of 30 g/m^3. Given the uncertainties in both methods, the value is in the same range as the 35.4 g/m^3 calculated for the one section model of the UV in-situ measurements. This means, if the one section model is correct, almost all tars of the product gas at 300°C are in form of phenol and naphthalene. This,

however, is contradictory to the GC-MS analysis, which states that phenol and naphthalene are only minor species. In addition, it would mean that the majority of tars in the product gas are either lost in the processing and cooling (e.g., in filters or due to condensations) or converted to heavy tars, which can not be identified by GC-MS.

That leaves two options:

1. processing changes gas composition (e.g., by conversion, filtering, condensation)
2. flawed measurements (either UV or sampling)

The first option seems to be a fitting choice from the data presented here. However, chemical conversion seems unlikely considering the fact that a lower temperature also means a lower reactivity. The filters should also have a negligible impact since phenol and naphthalene in their gaseous form have a smaller size than the 1μm. According to calculations made with the complete tar dew point model of the Energy research Centre of the Netherlands (see ECN-website Thersites [63]), who specialized on dew point calculations and measurements, the dew point of a mixture of around 36 g/m^3 tars mainly consisting of phenol (30 g/m^3) and naphthalene (5 g/m^3) but also traces of higher aromatics (scaled according to the GC-MS analysis) is at 112°C and thereby below the temperature in the gas extraction system. A lower temperature could only happen, if despite careful insulation and heating of the extraction system, cold spots appeared. From this point of view none of the above mentioned changes in the gas composition seem to be very likely.

The first part of the second option are flawed UV measurements. The IR measurements show that the in-situ and extraction measurements are in agreement. Therefore, the only source of such high deviations in the setup might be the small gap between the tubes as discussed in the two different models above. However, both models can explain the findings, and none can be favored from this point of view.

In the second option, the sampling measurements have to be addressed as well. Even though traditional sampling methods, are often unprecise and deviations of a factor of 2 are not unusual, a difference of almost 30 times is unusually high. In addition, other reported comparison of online and sampling methods at other gasifiers at similar temperatures but different tar loads have not shown these huge differences in phenol and naphthalene concentrations [41, 43, 45, 46, 50]. In the mentioned publications, also the more precises SPA method has been used. Therefore also this option seems to be unlikely.

5.2.4 Conclusion of the UV Measurements

In this section, the UV measurements have been presented. On a first look, a huge difference in phenol and naphthalene concentrations between the extraction measurements and the in-situ measurements have been found. This is in contradiction to the IR measurements, were a good agreement was reported. On a closer investigation of the geometry and the situation inside the product gas pipe, a second explanation to the measured spectra could be found. Through consideration of sampling and subsequent GC-MS and gravimetric measurements, the problem could be reduced to two possible explanations: flawed measurements (either UV or sampling) or change of gas composition due to processing. A discussion of the different possibilities has shown that all options seem to be equally likely or unlikely and none of them can be definitely excluded.

A simple, yet effective way to evaluate which of the two mentioned models is to be favored, might be to repeat the UV in-situ measurements in a similar setup but with windows closing the optical tubes. It is possible, that during such kind of measurements, the windows may get dirty (depositions) or might even be damaged. Maybe flushing the tubes with hot, clean gas could keep the windows unharmed.

Chapter 6

Conclusion and Outlook

6.1 Conclusion

The thesis has two major parts. The first part, the laboratory experiments, has a strong optical focus by building up a hot gas cell and executing experiments on the optical properties of specific gases under the influence of temperature. These experiments provide a solid background knowledge for any applications using the investigated gases in the the temperature range between room temperature and 500°C. In the second part, the applied part with technical focus, one application of the absorption cross-sections at different temperatures is given. This part provides a close investigation and discussion of in-situ measurements of the product gas of the LT-CFB in the IR and the UV range as well as the attached challenges.

At first, a novel gas cell, the HGC, was build and validated, in which the optical properties of reactive gases could be measured at temperatures up to 500°C. The HGC used a special design of so called flow windows to protect the optical windows, which can change their optical properties under the influence of reactive and sticky gases and higher temperatures over time. The cell enables the measurements of a wide variety of reactive and sticky gases in the UV and the IR range under defined circumstances (e.g., concentration, temperature, pressure), from which the absorption cross-sections of the investigated gas species can be

calculated. Afterward the build-up of the HGC, measurements of different gas species relevent in the field of biomass gasification at relevent temperatures were conducted. In these experiments, the UV absorption cross-sctions of the sulfur compounds H_2S, COS and CS_2 and the aromatic compounds phenol and naphthalene were determined at room temperature, 150°C, 300°C and 500°C. These species were chosen, because they were the most important species for the low-temperature circulating fluidized bed gasifier at Risø Campus. The results of these works are published in three individual articles in the *"Journal of Quantitative Spectroscopy and Radiative Transfer"*. Copies of the works can be found in the appendix.

In the second part, the UV and FTIR spectroscopy were applied at the product gas of the LT-CFB. The measurements consisted of direct online measurements inside the product gas stream (in-situ) and online measurements by extraction and cooling of the gas. In the IR, the spectra were compared to calculations from the HITRAN/HITEMP databases. Here, a good agreement between in-situ and extraction measurements could be stated for the major gas components. In addition to the sole measurement of the major gas components CO, CO_2 and H_2O, it was shown that measurements at long path length and measurements of organic compounds of minor concentration are possible. This shows that it is possible, to identify minor gas species with the chosen setup. In the UV, the spectra were heavily overlaid by coarse structures. Therefore, the differential optical absorption spectroscopy approach was chosen to compare the calculated concentrations of phenol and naphthalene from the in-situ and extraction measurements with one another and with the results from GC-MS analysis. Between the results of the extraction measurements and the GC-MS analysis, a fair agreement could be found. At the same conditions, the concentrations of phenol and naphthalene were of a factor of more than 20 higher than in extraction and GC-MS measurements. A closer investigation of the conditions during the in-situ measurements (geometry and possible flows) gave a second plausible explanation that is in better agreement with the other measurements. However, a detailed analysis of the various possible explanations could not find a concluding answer to the question, which of the two models describes the situation best. Further investigations on this specific question needs to be done to allow a definite answer.

All in all, the thesis provides the tools for measuring important major and minor gas species in a real gasification application. In addition, these tools have been tested under the harsh environment (high temperature, high tar load, high dust load) of the product gas of the LT-CFB.

6.2 Outlook

The following outlook provides two different future paths: the extension of the absorption cross-sections database and a possible design and setup of a sensor.

Through build-up and validation of the novel design of the HGC, the possibilites for measuring different reactive compounds in the UV and IR region are very broad. Especially compounds of unknown temperature dependency are a possible target for future analysis. However, it is also important to keep possible applications and the value in relation to the effort in mind. Including the measurements, analysis and possible remeasurements for understanding the behaviour of a specific compound best, the investiagtions of a single compound may easily take a couple of weeks. Therefore, it is important to select the compounds carefully. Considering this, it might be of interest to investigate different inorganic, organic and aromatic compounds in the UV and/or IR region. An incomplete list of compounds specifically interesting for biomass gasification are HCl, HCN, NH_3 lower hydrocarbons like C_2H_4, CH_3COH or also formaldehyde (CH_2OH), typical aromatic compounds are, e.g., benzene, fluorene, phenantrene, anthracene, pyrene, acenaphtylene, acenaphtene. In all cases, detailed literature research on the optical properties of the mentioned compounds needs to be done to be able to understand the necessity of the particular investigations. In addition to the gas species interesting for biomass gasification, other gases of interest for high temperature processes can be investigated.

The second approach, the sensor design and setup, is of interest for both UV and IR or even a combination. In the following, a UV sensor for phenol and naphthalene will be discussed. However, most of the statements can be easily adapted to the IR range.

For an (semi-)industrial in-situ UV sensor, there are technical needs and economical and operational limitations.

From the technical point of view, our experiments have shown that a variable path length, a powerful light source and a suitable spectrometer are necessary. The variable path length is needed, since biomass gasifiers often run on different fuel that result in significant differences in the gas, tar and particle concentration. A variable path length can react to these differences and still achieve resonable results. The powerful light source is necessary to achieve a good signal to noise ratio. At the same time it is necessary to be able to resolve the structure of the different gas species. In case of phenol, a resolution of 0.05 nm should be sufficiant to investigate the major peaks at least up to 300°C. At higher temperatres, the structure of phenol changes to a quasicontinious one.

For naphthalene a lower resolution of about 0.1 nm would still be sufficiant, because its structure has less peaks and is more continuous.

On the other hand, the setup should be reasonably priced, robust, long lasting and easy to use. In order reduce the cost, a modular spectrometer with a fixed wavelength range and resolution (e.g., Maya 2000Pro from Ocean Optics) could be used. These spectrometers are also robust enough to be used in industrial environments. The major challenges are the possible contamination of the optics that are in contact with the product gas and the lifetime of the lamp. The first part can partially circumvented by using a probe and place it directly and uncooled in the product gas, maybe supplemented by a low hot gas purge. First experiments in this direction have been done with an IR sensor. An unserviced operational time of the sensor of a couple of weeks could be achieved. As a light source, a modulated pulsed xenon lamp might be a solution. Most measurements are not needed continuously, but in intervals of ten seconds to one minute. Thus, a pulsed lamp seems to be a good choice to increase the lifetime to a couple of years. It is of course also a long-term ideal to have an easy to use. However, it is the last step after the mentioned changes have been tested and approved.

Appendix A

Article 1

Article 1: "The Hot Gas Flow Cell for Optical Measurements on Reactive Gases"

Helge Grosch, Alexander Fateev, Karsten L. Nielsen, Sønnik Clausen

Reprinted from *Journal of Quantitative Spectroscopy and Radiative Transfer* 130 (2013) 392-399

Journal of Quantitative Spectroscopy & Radiative Transfer 130 (2013) 392–399

Contents lists available at ScienceDirect

Journal of Quantitative Spectroscopy & Radiative Transfer

journal homepage: www.elsevier.com/locate/jqsrt

Hot gas flow cell for optical measurements on reactive gases

Helge Grosch, Alexander Fateev*, Karsten L. Nielsen, Sønnik Clausen

Danish Technical University, Insitute for Chemical and Biochemical Engineering, Frederiksborgvej 399, 4000 Roskilde, Denmark

ARTICLE INFO

Article history:
Received 6 March 2013
Received in revised form
26 June 2013
Accepted 28 June 2013
Available online 6 July 2013

Keywords:
Gas cell
Absorption coefficients
Spectroscopy
FTIR
UV
High resolution
SO_2
High temperature

ABSTRACT

A new design is presented for a gas flow cell for reactive gases at high temperatures. The design features three heated sections that are separated by flow windows. This design avoids the contact of reactive gases with the material of the exchangeable optical windows. A gas cell with this design was validated for high resolution measurements at temperatures of up to 800 K (527 °C) in the ultraviolet (UV) and infrared (IR) regions (190–20 000 nm). Verification of the gas temperature in the cell is provided by a thermocouple and emission/transmission measurements in the IR and UV regions. High-resolution measurements are presented for the absorption cross-section of sulfur dioxide (SO_2) in the UV range up to 773 K (500 °C).

1. Introduction

Spectroscopic methods are used in a wide variety of applications for the identification and the quantification of gas components. Accurate molecular spectroscopic data (e.g., effective absorption cross-sections, or cross-sections measured by an instrument with finite spectral resolution) play an essential role in many applications, such as astrophysics (determination of the gas composition of the atmosphere of exoplanets [1,2]) and environmental control (flue gas composition in combustion and gasification processes [3,4]).

Although there are already databases of measured and/or calculated spectra for many compounds at room temperature, there is a lack of reliable data at higher temperatures. This gap in the data applies in particular to experimental data. Although the effective absorption cross-sections for many gases of interest can be calculated from or found in, e.g., the HITRAN/HITEMP/ CDSD databases [5–8], the values must be carefully validated and sometimes improved using experimental data [9]. This requirement is especially true at high temperatures. Accurate measurements of the effective absorption cross-sections in a gas cell at high temperatures require high uniformity of temperature, concentration and pressure of the gas sample in the cell. Various gas cells that suit this purpose have been described by Modest and Bharadwaj [10]. More recent approaches have been described, e.g., by Hofmann et al. [11] and Hargreaves et al. [12].

Gas cells suitable for use with reactive gases for measurements in the spectral range from 190 nm (UV) up to 20 000 nm (mid IR) at temperatures up to 800 K are rare because reactive gases interact with the surfaces and either harm the windows or react with the gas cell walls to form unwanted products (especially at high temperatures). In both cases, the spectroscopic properties of either the windows or the gas can change dramatically, and the gas cell becomes unsuitable for the accurate measurement of effective absorption cross-sections.

A new gas cell suitable for work with reactive gases is presented in the article. The gas cell has been designed and manufactured to minimize the impact of surface

* Corresponding author. Tel.: +45 4677 4564; fax: +45 4677 4565.
E-mail address: alfa@kt.dtu.dk (A. Fateev).

0022-4073/$ - see front matter © 2013 Elsevier Ltd. All rights reserved.
http://dx.doi.org/10.1016/j.jqsrt.2013.06.029

reactions and to perform high-resolution UV/IR optical emission/transmission measurements on gases at temperatures of up to 800 K.

The article has the following outline. In the second section, the design of the high temperature gas flow cell (HGC) is described in detail, and the experimental setup is presented. In the third section, the validation of the gas cell (performance of the flow windows and temperature/path length) by IR and thermocouple measurements is presented. Afterwards, a comparison of available effective UV absorption cross-sections for SO_2 at room temperature from literature and experimental measurements with the validated HGC is given. New effective UV absorption cross-sections of SO_2 at temperatures of up to 773 K are presented, and at the end, a conclusion is given.

2. Design and experimental setup

2.1. Design of the high temperature gas flow cell

The basic principle of the HGC is the same as described in [13]. The cell is designed to operate at pressure of approximately 1 bar. There are three heated sections in the HGC separated about 1 mm from each other. The inner section is fully heated, and the outer sections of the gas cell are only partially heated (see Fig. 1). With this three-zone design, a uniform temperature profile can be achieved (see also Section 3). While the two outer sections are purged with a buffer gas (e.g., nitrogen split into two equal flows, half from each side), the potentially reactive gas is introduced into the central section.The buffer gas flow and the reactive gas flow meet between the outer and inner sections. In this area the net velocity in the horizontal direction is zero. Due to this and the different viscosities of the gases, a laminar flow sheet is established. The gas flows can exit through the gap between the sections. Thus, the reactive sample gas is not in contact with a optical windows and can therefore not react with them or form deposits on it, but still can react with the internal surface of the gas cell. To avoid or at least minimize hetero-phase reactions of the reactive gases, inner section of the HGC is made from quartz. The inner section consists of several quartz parts specially made and assembled during the glassblowing process. The inner part includes three quartz tubes with a diameter of 35 mm; two flow windows with an internal diameter of 9.4 mm; a gas inlet for the reactive gas that consists of 8 small holes uniformly distributed around the central quartz tube. The quartz component is mounted into a sandwich construction between two aluminum blocks that support the cell. With 16 heating elements mounted into the body of the aluminum blocks, the cell can be uniformly heated to 800 K to maintain the heat, the aluminum blocks are first covered with 25 mm insulation boards and later with a 20 mm thick Kerline outer insulation. The heating of the gas cell is performed with 16 $\times$ 230 V/15 W heating elements controlled by an ELK 3/3/5 temperature controller together with a type K thermocouple mounted on one of the aluminum blocks near the quartz component. A transformer is integrated into the heating circuit to reach the maximum temperature. Stainless steel inserts are mounted from both ends of the cell and act as inlets for the buffer gas and outlets for both the reactive and buffer gases. Additionally, the inserts seal the cell and hold the cold, exchangeable optical windows. Depending on the application, either UV or IR outer windows can be used. Further details about the HGC can be found in Section 3.

2.2. The high temperature gas flow cell

The setup can be divided into three major parts: the gas mixing unit with a quartz reactor, the HGC and a spectrometer with an external light source. The gas mixing unit consists of the pre-mixed (with N_2) reactive gases in gas bottles, three high precision mass flow controllers (Bronkhost), a quartz reactor that can be heated to 473 K and a heated Teflon line that connects the quartz reactor and the heated gas inlet to the HGC. The heated line and the gas inlet are maintained at 293–473 K to prevent a significant temperature drop when the gas enters the cell. The quartz reactor is a simple quartz tube, variable in length (30–60 cm, diameter $\varnothing = 5$ cm), with one inlet/outlet where several gases can be mixed and reactions among them can be performed, if desired. Therefore, a complete mixture leading to a stable reactive gas concentration in the HGC is guaranteed. By using two different mass flow controllers variable concentrations of the reactive gas in nitrogen at a constant flow could be achieved. A third mass flow controller regulated the nitrogen flow that was used as a buffer gas in the HGC.

For the IR emission/transmission measurements, an FTIR spectrometer (Bomem 155) with an InSb detector and an external IR light source (a black body at 1073 K) was used. The measurements have been performed at 2 cm^{-1} spectral resolution. For the UV absorption measurements, a highly stable deuterium lamp (30 W, LOT Oriel) as the UV light

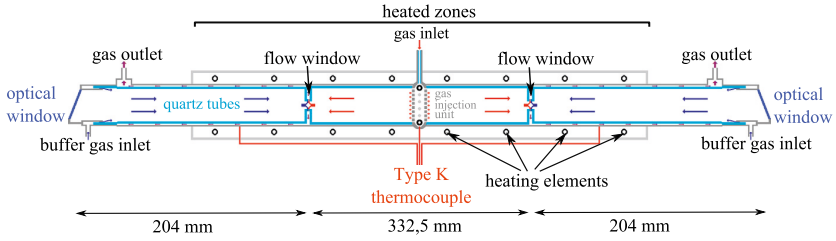

Fig. 1. Setup of the gas cell. The red arrows indicate the hot reactive gas, while the blue arrows show the colder buffer gas. (For interpretation of the references to color in this figure caption, the reader is referred to the web version of this article.)

source and a 0.5 m monochromator (Spectra Pro 2500i/ Princeton Instruments) with a 3600 grooves/mm holographic grating equipped with a CCD camera (Princeton Instruments PIXIS 100B) were used. With this setup, a spectral resolution of 0.019 nm is achieved.

3. Validation of the HGC

The validation of the gas cell has been performed in several steps. First, the function of the flow windows at various temperatures and gas flow rates has been proven. Additionally, the temperature inside the cell has been measured, first by the infrared emission/transmission method and later by the measurement of the temperature profiles with a calibrated thermocouple.

The verification of the function of the flow windows was performed using N_2 as the buffer gas and CO_2 (100%) as the reactive gas. The CO_2 flow was kept constant at 0.795 ln/min during measurements, but the N_2 flow has been varied from 0.2 to 3 ln/min. In Fig. 2, part of an IR emission spectrum from the HGC is shown with the temperature controller of the cell set to $T_{set}=573$ K. The temperature on the heated line (T_{line}) was set to 473 K, and the temperature on heated inlet (T_{inlet}) was set to 423 K. The shown spectra are single beam spectra obtained by measurements without external source. To minimize the impact of the gray body radiation from the walls a J-stop was set up before the external port of the spectrometer. When the N_2 and CO_2 flows are balanced (red lines), the emission spectrum shows a continuum-like gray body emission from the cell and a strong CO_2 emission band (2150–2400 cm^{-1}), which is affected by CO_2 self-absorption (from cold CO_2 as a trace gas in the setup). A decrease in the buffer gas flow from 0.795 to 0.2 ln/min leads to a collapse of the laminar sheet of the flow windows, a penetration of the hot reactive gas into the buffer sections of the cell (i.e., inserts) and a cooling of the buffer gas (see Fig. 1). The cooling of the gas can be perceived as an increase of CO_2 self-absorption in Fig. 2 (a). Conversely, an increase of the buffer gas flow from 0.795 to 3.0 ln/min causes penetration of the cold buffer gas into the central (hot) section of the cell and gradual cooling of this section. The cooling of the section is observed as a decrease in the emission signal from the cell (see Fig. 2(b)).

The same measurements have been performed at $T_{set}=423$ K and 761 K. The limits of existence of the flow windows are shown in Table 1 (columns 2–4). Here, Δ stands for the difference in the flow of the buffer gas nitrogen and the reactive gas carbon dioxide.

The table shows that the flow windows have a higher tolerance to deviations in the flow at higher temperatures. Thus the flow windows will cease to exist and a mixing of the gases in the quartz cell will occur more easily at lower temperatures. At higher temperatures, the viscosity of gases is higher, which means that a laminar flow is more easily established. To maintain a stable flow window, the use of accurate mass-flow controllers is an essential component of the setup especially at low temperatures. In the following discussions, a flow rate of 0.795 ln/min has been set for both the buffer and reactive gases.

The effective gas temperature profiles in the HGC have been validated by infrared emission and transmission FTIR spectroscopy, and detailed temperature mapping inside the central zone of the cell has been made by thermocouple (TC) measurements.

The infrared emission/transmission method for measuring the gas temperature has been described in detail in [14]. The measurements have been performed at $T_{set}=423$, 573 and 761 K. The temperature in the heated line and gas cell inlet was set to 423 K for $T_{set}=423$ K and 473 K for $T_{set}=573$ and 761 K, respectively. The emission and transmittance spectra calculated from the experimental data for CO_2 at 573 K are shown in Fig. 3 in the upper and lower panels, respectively. To calculate the transmittance spectrum correctly, and minimize the effect of the CO_2 self-absorption in the spectrum, the interferrograms both with and without black body radiation were taken for both cases, with and without CO_2. After subtracting the interferrograms without black body radiation from the

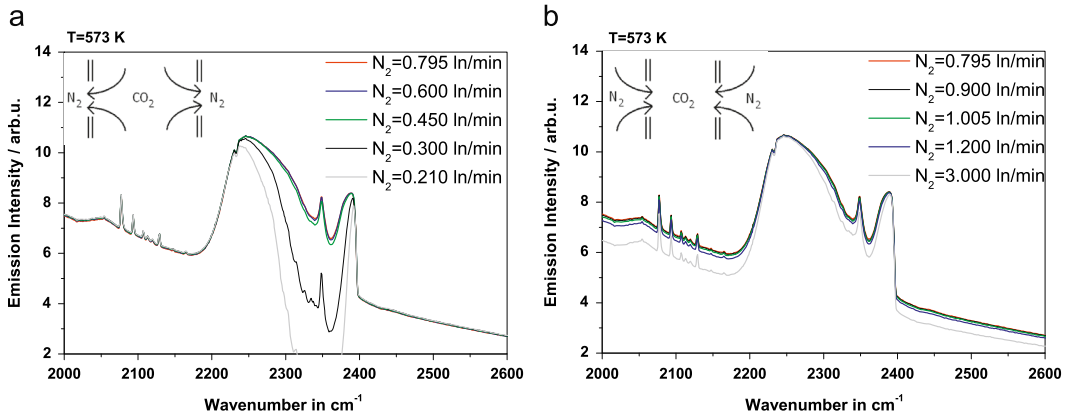

Fig. 2. Part of the emission spectrum from HGC at $T_{set}=573$ K. The lines (from red to gray) show the CO_2 self-absorption at 2350 cm^{-1} when the buffer gas flow (N_2) (a) decreases and (b) increases. The reactive gas flow (CO_2) is kept constant at 0.795 ln/min. The flow diagram in top left corner depicts schematically what happens in the cell. (For interpretation of the references to color in this figure caption, the reader is referred to the web version of this article.)

Table 1
Limits of existence of gas flow windows produced by cold and hot gas flows.

$\langle T_{eff}\rangle/T_{set}$ in K	CO_2 flow ln/min	$\Delta = N_2 - CO_2$ ln/min (% of CO_2 flow)	
(421.57 ± 0.22)/423.15	0.795	−0.045 (6%)	+ 0.105 (13%)
(571.58 ± 1.14)/573.15	0.795	−0.180 (23%)	+ 0.168 (21%)
(750.13 ± 1.84)/753.15	0.795	−0.342 (43%)	+ 0.3 (38%)

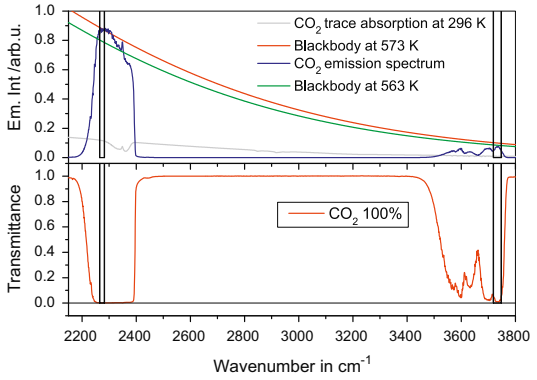

Fig. 3. Top: FTIR emission spectrum calculated from the experimental CO_2 (100%) data at 573 K (blue) and black body spectra calculated at T_{set}=573 K (red) and 563 K (olive). Typical CO_2 absorption at ambient temperature on the black body background is shown by a gray line for a reference. Bottom: Transmittance spectrum (red) calculated from the experimental CO_2 (100%) data. The black boxes show the spectral ranges used for the calculation of the gas temperature. (For interpretation of the references to color in this figure caption, the reader is referred to the web version of this article.)

ones with blackbody radiation for each of the two resulting data sets, the single beam spectrum is calculated. The quotient of the single beam spectrum with CO_2 and the one only with nitrogen is equal to the transmittance. The emission spectrum is then given as 1 minus the transmittance spectrum. A more detailed description of the procedure can be found in Evseev et al. [15].

Because the CO_2 band at 2200–2400 cm^{-1} approaches black body continuum at the relevant temperature (i.e., transmittance is zero, see Fig. 3, lower part), it can be used for gas temperature (or more precisely, brightness temperature) calculations. Due to traces of CO_2 in the setup, it is impossible to use the entire band. However, in the region marked by the first black box (approximately 2270 cm^{-1}), the contribution of the absorption from cold CO_2 (tail of the structure) to the shape of the strong CO_2 emission band is negligible. Therefore, calculations of the gas temperature can be performed in this spectral range. This region corresponds to the transitions from high vibrational CO_2 levels; therefore, this emission intensity is highly temperature-dependent. The best fit of the CO_2 emission spectrum by a black body curve gives a gas temperature of 573 K, which can be considered the highest gas temperature in the cell. In addition, the transmittance of CO_2 near 3734 cm^{-1} is approximately zero. Therefore, the part of the CO_2 band at 3500–3800 cm^{-1} marked by the second black box in Fig. 3 can also be used for gas temperature calculations. The major contribution in the peak maximum at 3734 cm^{-1} (see Fig. 3, top) is due to transitions from low vibrational levels that are mostly populated and are less sensitive to small temperature variations (or temperature non-uniformity) in the cell.

The black body fit to the CO_2 emission spectrum in this region gives the lowest gas temperature in the cell (in this case 563 K). In conclusion, the infrared emission/transmission

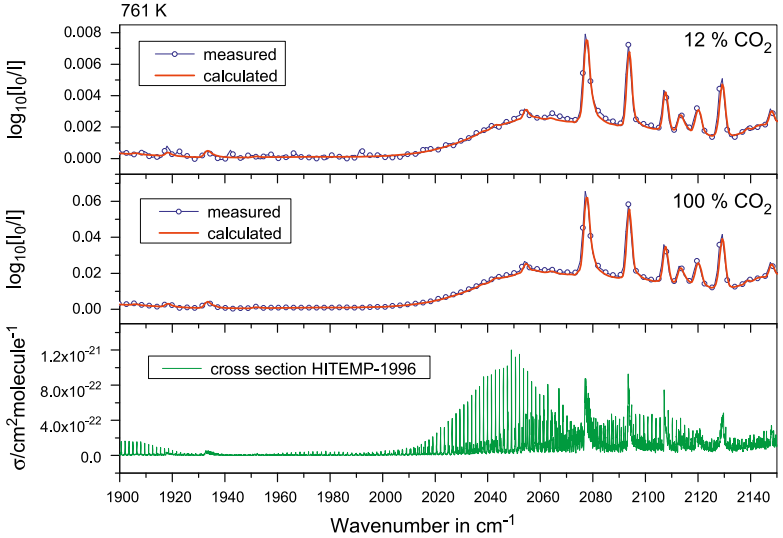

Fig. 4. Parts of the measured (blue) and calculated (red) CO_2 absorption spectra in the HGC at 761 K. The top panel shows 12% and the middle panel 100% CO_2. In the lower panel, the CO_2 true absorption cross-sections are calculated using the HITEMP-1996 database at the corresponding temperature. The pressure was 1.0156 bar, and the spectral resolution was 2 cm^{-1} at an absorption path length of L=33.25 cm. (For interpretation of the references to color in this figure caption, the reader is referred to the web version of this article.)

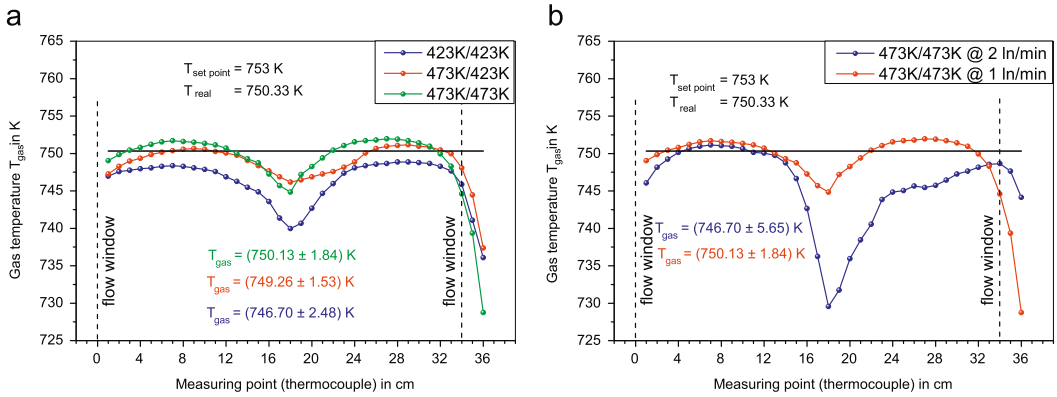

Fig. 5. Gas temperature profile in the HGC at a set point on the temperature controller of 753 K. (a) shows the profile for different T_{line} and T_{inlet}, whereas in (b), the effect of different flow rates can be observed. The locations of the flow windows are indicated.

method evaluates the effective gas temperature in the cell to be $T_{eff}=568\pm5$ K. The same measurements were performed at 423 K and 761 K and gave similar results ($T_{eff}=423\pm5$ K and $T_{eff}=757\pm5$ K, respectively).

The validation of the effective gas temperature has been conducted by comparison of the measured and calculated CO_2 absorption spectra at various temperatures (T_{set}) and CO_2 concentrations in nitrogen. Calculations can be made on the basis of known high-temperature databases, e.g., HITEMP or CDSD. In this work, the HITEMP-1996 database has been used. The database is an extension of HITRAN database, which is extensively used in atmospheric research, into the high-temperature range. All calculations were done below a temperature of 800 K. In this way, the known errors of the HITEMP-1996 database at temperatures higher than 1000 K were circumvented.

In Fig. 4 (upper and middle panels), parts of the measured CO_2 absorption spectra in the HGC at $T_{set}=761$ K at two CO_2 concentrations are shown by blue lines. T_{line} was set to 473 K and T_{inlet} to 423 K. In the same figure, the calculated CO_2 absorption spectra are shown by red lines. The optical absorption path length (L) has been assumed to be equal to the geometrical absorption path length (33.25 cm) measured on the assembled HGC. There is an excellent agreement between the calculations and measurements at both CO_2 concentrations, which confirms that the optical absorption path length is, in fact, defined by the flow windows and has the value of 33.25 cm.

There is only a small difference between the measured and calculated spectra in the range of 2060–2100 cm^{-1}. The small difference can be explained by uncertainties in the intensities of the weak lines in the HITEMP-1996 database and also by a line mixing effect. These lines start to provide a definite contribution to the band structure at higher CO_2 concentrations and temperatures. The lower panels in Fig. 4 show the calculated true (i.e., unaffected by an instrument) absorption cross-sections of CO_2. In the range 2060–2100 cm^{-1}, many extra lines appear at 761 K, which influence the band structure. The calculated spectra are insensitive to small variations in the gas temperature (approximately $\pm$5–10 K).

In conclusion, the CO_2 absorption measurements and calculations validate the effective temperature profile in the HGC and the optical absorption path length, as defined by the flow windows. For a deeper insight, the temperature profiles along the axis of the cell have been measured by a calibrated thermocouple (TC). The TC was calibrated by the Temperature Laboratory of DTU. The set temperatures (T_{set}) at the temperature control were 423 K, 573 K and 753 K. For the measurements, a type K thermocouple and an Ametek (at $T_{set}=423$ K) and a Fluke (at $T_{set}=573$ K and 753 K) thermometers were used. The TC was first placed 1 cm after the first flow window in the central HGC section and was moved in 1 cm increments along the axis of the HGC toward the second flow window. The last measured point was 2 cm behind the second flow window. In the following, only the results of $T_{set}=753$ K will be shown.

In Fig. 5(a), the gas temperature (T_{gas}) profile at $T_{set}=753$ K is shown for various T_{line}/T_{inlet} settings with the location of the flow windows indicated. In general, the temperature distribution varies with a value of up to $\pm$2.48 K with a small but broader temperature drop centered at the reactive gas inlet (at 18 cm). This temperature drop is due to a slight cooling of the gas as it expands from the narrow gas inlet (4 mm) into the wider central zone of the cell (30.95 mm). Nevertheless, the distribution can be perceived as uniform. Comparing the different T_{line}/T_{inlet} settings (blue – $T_{line}=423$ K/$T_{inlet}=423$ K, red – $T_{line}=473$ K/$T_{inlet}=423$ K and olive – $T_{line}=473$ K/$T_{inlet}=473$ K) shows that preheating the reactive gas is essential to maintain the highest possible uniformity of the gas temperature profile in the cell. At $T_{line}=473$ K/$T_{inlet}=473$ K, temperature uniformity along the axis of the hot part of the cell is $\pm$1.84 K.

At $T_{line}=473$ K/$T_{inlet}=473$ K, the temperature drop at the reactive gas inlet point (18 cm) was higher than at $T_{line}=473$ K/$T_{inlet}=423$ K. This difference has not been observed at 573 K. A possible explanation might be that the TC has been bending toward the gas inlet during the measurements, which caused lower TC readings. Nevertheless, from comparison of the two mentioned measurements,

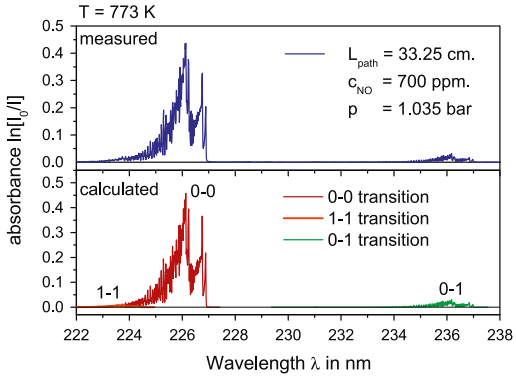

Fig. 6. Measurements (blue) and calculation (brown: 0–0 transition, green: 0–1 transition, red: 1–1 transition) of the absorbance of nitric oxide at 773 K between 222 nm and 238 nm at 1.035 bar, a path length of 33.25 cm and an NO concentration of 700 ppm. (For interpretation of the references to color in this figure caption, the reader is referred to the web version of this article.)

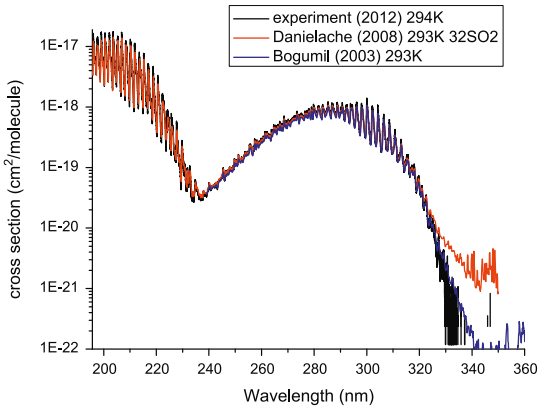

Fig. 7. Comparison of the derived absorption cross-sections from the absorption spectra of SO_2 at 294 K on a logarithmic scale from 197 nm to 360 nm with previously published data of lower resolution. Both Danielache et al. [17] (red) and Bogumil et al. [18] (blue) were obtained at 293 K. The data of Danielache, in particular, were obtained with the ^{32}S isotope. (For interpretation of the references to color in this figure caption, the reader is referred to the web version of this article.)

one can conclude that gas temperature uniformity is in between ± 1.53 and ± 1.84 K.

In Fig. 5(b), the temperature profile of the two primarily used flows of 1 ln/min (red) and 2 ln/min (blue) is compared. At lower flows, the temperature drop is less than at higher flows, and a higher uniformity is achieved (± 1.84 K at 1 ln/min compared to ± 5.65 K at 2 ln/min). However, the higher flow was also used in the gas mixing to achieve lower ratios of reactive gas to nitrogen.

In general, a gas temperature uniformity better than ± 2 K at 1 ln/min and ± 6 K at 2 ln/min for all temperatures in such a gas cell can be considered to be a satisfactory result. Moreover, such a small value has no influence on the quality of the high resolution IR (0.1 cm^{-1})/UV (0.019 nm) absorption measurements for the gases of interest (e.g., IR: SO_3, SO_2, H_2O and UV: SO_2, H_2S, phenol) because of the value's minor impact on the line shape profiles. Effective gas temperatures (T_{eff}), which are averaged values of T_{gas} calculated from TC measurements, are used for the temperature calibration of the HGC. The results are summarized in Table 1 (first column). From this finding, a linear relation between the set temperature (T_{set}) and the desired gas temperature (T_{eff}) can be obtained.

In addition to these measurements, a comparison between a measured and calculated UV spectrum of nitric oxide (NO) at T_{eff}=773 K was performed. This comparison is feasible because the vibrational and rotational transitions are well-known, and the structure of the resulting spectra can be used as a measure of the rotational and vibrational temperatures [13]. Fig. 6 shows the results of this comparison. For a gas temperature of 773 K, a cell length of 33.25 cm, a matching pressure of 1.035 bar and a concentration of 700 ppm, excellent agreement between the calculations and the experiment is shown. Both the rotational and the vibrational temperatures matched the effective gas temperature.

4. High resolution UV measurements of sulfur dioxide

As mentioned above, the HGC is designed for UV and IR absorption measurements. In this section, the performance of the HGC is shown in high resolution SO_2 UV absorption measurements ($\Delta\lambda = 0.019$ nm). The SO_2 was chosen because it has a broad UV absorption spectrum (190–360 nm), and there is an extensive information regarding the UV absorption cross-sections of SO_2 at low temperatures (160–300 K) [16]. Therefore, measurements at room temperature (294 K) were performed first.

Afterward, measurements at 423 K, 573 K and 773 K were conducted. Measurements were performed at three different SO_2 concentrations (215 ppm, 350 ppm and 1000 ppm in nitrogen) to cover the spectral ranges of high/low SO_2 absorption without non-linear effects. The absorption spectra were converted to the effective absorption cross-section spectra through use the of Lambert–Beer Law. In Figs. 7 and 8, a comparison between the measured effective absorption cross-sections and previously published SO_2 UV absorption cross-sections is shown. In Fig. 7, the lower resolution data of Danielache et al. [17] (0.026 nm) and Bogumil et al. [18] (0.21–0.22 nm) over a spectral range from 197 nm to 360 nm are shown. Strong agreement between the different data can be observed. The small difference in the heights of the single peaks is a result of the different spectral resolutions used. Because the spectral resolution in the current measurements is $\Delta\lambda = 0.019$ nm, the black lines show the higher peaks. Comparing the presented data with the high resolution data of Rufus et al. [19] and Woods et al. [20] (see Fig. 8), a strong agreement can be stated. Thus, our spectrum can be considered as a result of smoothing of the high resolution spectrum obtained from Rufus et al. [19]. Only a slight shift of 0.1 nm in the wavelength compared to Rufus et al. and to Danielache et al. and a slight difference in the fine structure compared to Woods et al. (298 nm)

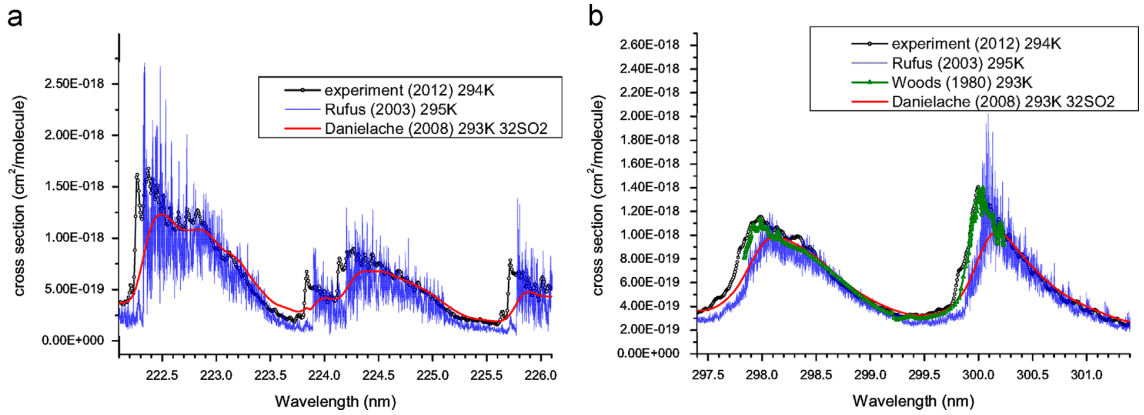

Fig. 8. A closer look at the absorption cross-section of SO_2 at 294 K in comparison with the high resolution measurements of Rufus et al. [19] (light blue, 293 K) and Woods et al. [20] (green, 295 K) and Danielache et al. [17] (red, 293 K) at two different spectral locations. Absorptions cross-sections from (a) 222.1 nm to 226.1 nm and (b) 297.4 nm to 301.4 nm. (For interpretation of the references to color in this figure caption, the reader is referred to the web version of this article.)

can be observed. The shift is most likely due to a wavelength calibration error of the UV grating spectrometer, although there is strong agreement in line positions between our measurement and Woods et al. measurement at 298 nm. The calibration of the UV spectrometer was conducted in the 185–350 nm range with a calibration Hg/Ar pen lamp and standard spectrometer software calibration tools. In the works of Rufus et al. and Danielache et al., a UV-FT spectrometer, which has significantly higher precision in wavelength calibration, was used. Strong agreement of the measured SO_2 cross-sections at 294 K with recently published data shows that all components of the experimental set up (gas mixing system, HGC and the spectrometer and the light source) are properly working and can be used for further measurements. In Fig. 9, the effective absorption cross-sections of SO_2 at 294 K, 423 K, 573 K and 773 K on logarithmic scale are shown. The overall structure of the spectrum remains the same. However, at higher temperatures, there are certain changes in the band shapes and fine band structures. The bands become broader, and the fine band structure begins to disappear with the increasing temperature.

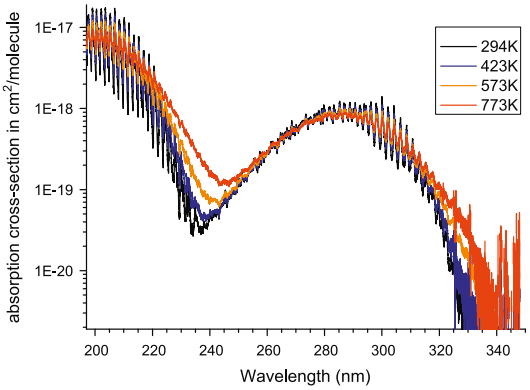

Fig. 9. Comparison of the spectra obtained at 294 K (black), 423 K (blue), 573 K (orange) and 773 K (red) on a logarithmic scale between 197 nm and 350 nm. (For interpretation of the references to color in this figure caption, the reader is referred to the web version of this article.)

5. Conclusions and outlook

In this work, a new gas flow cell suitable for work with corrosive gases at temperatures up to 800 K was designed, built and validated. The three-section design with a quartz body and two flow windows allows the performance of high-quality high-temperature UV/IR absorption measurements with various reactive gases while preventing their reactions with the optical windows of the HGC. The validation of the HGC was performed by IR emission/transmission measurements and TC measurements. The effective gas temperature and optical absorption path length were verified by measurements and modeling of the CO_2 absorption spectra at various temperatures in the HGC. Effective SO_2 UV absorption cross-sections measured at 294 K were compared with previously published data, and strong agreement was found. The new SO_2 UV effective absorption cross-sections up to 773 K are presented.

Future works will focus on the cross-sections of other reactive compounds, such as sulfur- and nitrogen-containing compounds, as well as aromatic hydrocarbons, in the ultraviolet and infrared ranges, and their behavior at temperatures up to 800 K will be determined.

Acknowledgments

We would like to thank Energinet.dk for providing financial support (Project no. 2011-1-10622).

References

[1] Tennyson J, Yurchenko SN. ExoMol: molecular line lists for exoplanet and other atmospheres. Mon Not R Astron Soc 2012;425:21–33.
[2] Hill C, Tennyson J, Yurchenko SN. Temperature-dependent molecular absorption cross-sections for exoplanets and other atmospheres. Icarus, http://dx.doi.org/10.1016/j.icarus.2012.07.028, in press.

[3] Becher V, Clausen S, Fateev A, Spliethoff H. Validation of spectral gas radiation models under oxyfuel conditions. Part A: gas cell experiments. Int J Greenhouse Gas Control 2011;5S:S76–99.
[4] Fateev A, Clausen S. On-line non-contact gas analysis. Report Ris-R-1636(EN) (2008).
[5] Rothman LS, Jacquemart D, Barbe A, Chris Benner D, Birk M, Brown LR, et al. The HITRAN 2004 molecular spectroscopic database. J Quant Spectrosc Radiat Transfer 2005;96:139–204.
[6] Rothman LS, Gordon IE, Barbe A, Chris Benner D, Bernath PF, Birk M, et al. The HITRAN 2008 molecular spectroscopic database. J Quant Spectrosc Radiat Transfer 2009;110:533–72.
[7] Rothman LS, Gordon IE, Barber RJ, Dothe H, Gamache RR, Goldman A, et al. HITEMP, the high-temperature molecular spectroscopic database. J Quant Spectrosc Radiat Transfer 2010;111:2139–50.
[8] Tashkun SA, Perevalov VI. CDSD-4000: high-resolution, high-temperature carbon dioxide spectroscopic databank. J Quant Spectrosc Radiat Transfer 2011;112:1403–10.
[9] Fleckl T, Jäger H, Obernberger I. Experimental verification of gas spectra calculated for high temperatures using the HITRAN/HITEMP database. J Phys D: Appl Phys 2002;35:3138–44.
[10] Modest MF, Bharadwaj SP. Medium resolution transmission measurements of CO_2 at high temperature. J Quant Spectrosc Radiat Transfer 2002;73:329–38.
[11] Hofmann JP, Eifert B, Mellau GC. Near infrared emission spectrum of $H^{13}CN$. J Mol Spectrosc 2010;262:75–81.
[12] Hargreaves RJ, Li G, Bernath PF. Hot NH_3 spectra for astrophysical applications. Astrophys J 2011;735(111):11.
[13] Fateev A, Clausen S. In situ gas temperature measurements by UV-absorption spectroscopy. Int J Thermophys 2009;30:265–75.
[14] Bak J, Clausen S. FTIR emission spectroscopy methods and procedures for real time quantitative gas analysis in industrial environments. Meas Sci Technol 2002;13:150–6.
[15] Evseev V, Fateev A, Clausen S. High-resolution transmission measurements of CO_2 at high temperatures for industrial applications;. J Quant Spectrosc Radiat Transfer 2012;113:2222–33.
[16] Keller-Rudek H, Moortgat G. Database of the Max-Planck-Institut für Chemie - Atmospheric Chemistry Division, Mainz ⟨http://www.atmosphere.mpg.de/enid/2295⟩, Website.
[17] Danielache SO, Eskebjerg C, Johnson MS, Ueno Y, Yoshida N. High-precision spectroscopy of ^{32}S, ^{33}S, and ^{34}S sulfur dioxide: ultraviolet absorption cross-sections and isotope effects. J Geophys Res D 2008;113:D17314.
[18] Bogumil K, Orphal J, Homann T, Voigt S, Spietz P, Fleischmann OC, et al. Measurements of molecular absorption spectra with the SCIAMACHY pre-flight model: instrument characterization and reference data for atmospheric remote sensing in the 230–2380 nm region. J Photochem Photobiol A: Photochem 2003;157:167–84.
[19] Rufus J, Stark G, Smith PL, Pickering JC, Thorne AP. High-resolution photoabsorption cross-section measurements of SO_2, 2: 220 to 325 nm at 295 K. J Geophys Res Planets 2003;108:5011.
[20] Woods PT, Jollife BW, Marx BR. High resolution spectroscopy of SO_2 using a frequency-doubled pulsed dye laser, with application to the remote sensing of atmospheric pollutants. Opt Commun 1980;33:281–5.

Appendix B

Article 2

Article 2: "UV absorption cross-sections of selected sulfur-containing compounds at temperatures up to 500°C"

Helge Grosch, Alexander Fateev, Sønnik Clausen

Reprinted from *Journal of Quantitative Spectroscopy and Radiative Transfer* 154 (2015) 28-34

Journal of Quantitative Spectroscopy & Radiative Transfer 154 (2015) 28–34

Contents lists available at ScienceDirect

Journal of Quantitative Spectroscopy & Radiative Transfer

journal homepage: www.elsevier.com/locate/jqsrt

UV absorption cross-sections of selected sulfur-containing compounds at temperatures up to 500 °C

H. Grosch, A. Fateev*, S. Clausen

Technical University of Denmark, Department of Chemical and Biochemical Engineering, Frederiksborgvej 399, 4000 Roskilde, Denmark

ARTICLE INFO

Article history:
Received 29 August 2014
Received in revised form
25 November 2014
Accepted 28 November 2014
Available online 5 December 2014

Keywords:
Absorption coefficients
UV Spectroscopy
Sulfur containing compounds
High temperature
H_2S, CS_2, OCS/COS

ABSTRACT

The temperature dependence of the ultraviolet absorption cross-sections of three different sulfur containing compounds, hydrogen sulfide (H_2S), carbon disulfide (CS_2) and carbonyl sulfide (OCS), are presented between 200 nm and 360 nm at a resolution of 0.018 nm. The absorption cross-sections for each compound are initially compared with those available in the literature, followed by the discussion of the measurements and their spectral features at three temperatures up to 500 °C/773 K. Uncertainties in the measured absorption cross-sections are also addressed.

1. Introduction

Absorption cross-sections of molecules are important spectroscopic data and are used in a variety of applications for identification and quantification of the compounds in various multi-component environments such as environmental monitoring and control and sensor developments [1]. Although absorption cross-sections for many compounds have been investigated thoroughly at room temperature (approximately 21 °C/294 K) both theoretically and experimentally, their temperature dependence, especially at higher temperatures, has not been investigated extensively. In the ultraviolet (UV) range most of the available absorption cross-section data are reported at low temperatures, which are of interest for laboratory and atmospheric research [2]. For many high-temperature applications (e.g., flue gas monitoring, combustion and gasification) data are limited and normally cover major gas compounds such as e.g., CO_2, CO, CH_4 and H_2O [3–6].

Due to their environmental impact, sulfur containing compounds are of growing interest, especially in the field of energy production. Although the absorption cross-sections of sulfur dioxide (SO_2) have been investigated heavily in the UV range for various applications, wavelengths [1,7], temperatures [8] and isotopic variances [9], the same has not been done for other small sulfur containing molecules. Particularly, the absorption cross-sections of hydrogen sulfide (H_2S), carbon disulfide (CS_2) and carbonyl sulfide (OCS or COS) have not been adequately determined above room temperature. However, these compounds are released at high temperatures in combustion and gasification processes [10,11] as well as volcanic activities on earth [12,13] and other planets [14–17]. The knowledge of the UV absorption cross-sections of these three compounds at high temperature is beneficial for multiple applications such as flue gas/product gas analysis but also in atmospheric research.

Experimental data have been determined mainly by two methods. For the shorter wavelengths in the vacuum ultraviolet (VUV) range ($\leq$ 190 nm) the dipole strength has been measured by (e,e)- or (e,2e)-spectroscopy [18–22]. For longer wavelengths (190–400 nm), traditional transmission measurements in a gas cell containing a continuous

* Corresponding author. Tel.: +45 46774564; fax: +45 46774565.
E-mail address: alfa@kt.dtu.dk (A. Fateev).

http://dx.doi.org/10.1016/j.jqsrt.2014.11.020
0022-4073/

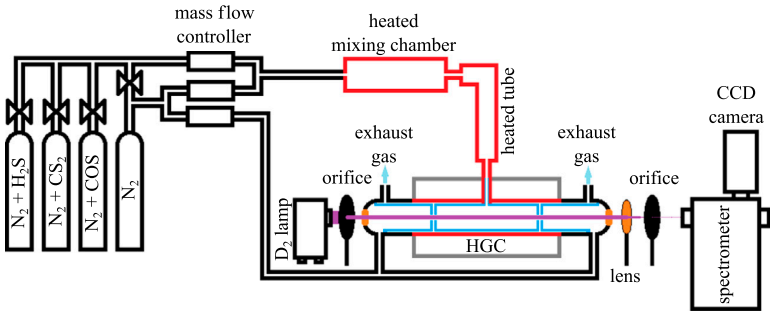

Fig. 1. Principle scheme of the experimental setup. It consisted of a mixing unit, the high temperature gas flow cell (HGC) and a grating spectrometer unit.

broad-band light source have been employed. Most measurements are recorded with purified gases at low pressures. It is also common to measure the absorption cross-section with very high resolution at one specific wavelength [23,24]. In this study, the focus will be on investigating the temperature-dependent UV absorption cross-sections of S-compounds in the 200–360 nm range.

While the major absorption of H_2S lies in the VUV light between 40 nm and 160 nm, it does contain a less prominent characteristic band between 160 nm and 250 nm. The overall UV absorption band at longer wavelengths has been measured by Watanabe [25], Thompson [26] and Wu and Chen [27]. In addition, single wavelength measurements have been performed by Wine at 185 nm [28] and by Wight and Leone at 248 nm [29]. The first temperature-dependent absorption cross-sections have been published by Thompson et al., who have presented data for temperatures below room temperature (down to 190 K). These data have been extended by Wu et al., who also presented data between 170 K and 370 K with a resolution of 0.06 nm. This work has also been the basis for the JPL recommendation in 2011 [30], in which the data are given in 2 nm-increments.

CS_2 has its major UV absorption band between 160 nm and 240 nm with an additional characteristic band between 280 nm and 360 nm, with an intensity four orders of magnitude lower than its major band. These two bands make it possible to identify and quantify carbon disulfide over a wide range of concentrations, allowing for a wide range of concentrations to be measured using its absorbance in different spectral regions. Different groups have reported data for both bands at room temperature [32,31,33–35]. The work of Hearn and Joens [36], as basis for the JPL recommendation [30], as well as Vandaele [37] and Schneider and Moortgat [38], as the most recent studies have to be considered. As is also the case for the other molecules, few publications can be found that address high temperature spectra of CS_2. To the best of our knowledge, only Dove et al. [39] and Chen and Wu [40] have investigated this matter. In the first work, CS_2 has been investigated with a low spectral resolution over a long range of wavelengths and coarse temperature steps, and in the second one, CS_2 absorption measurements in the range 180 nm and 230 nm have been performed up to 383 K.

The absorption cross-sections of OCS have two major bands in the VUV region, one between 20 nm and 120 nm [41] and a second between 130 nm and 190 nm. A minor band (approximately two to three orders of magnitude lower) can be found between 190 nm and 260 nm. In contrast to H_2S and CS_2, a number of publications on the band between 190 nm and 260 nm [42,43], its temperature dependency below [44,45] and above room temperature [46–48] exist and even the isotopology has been investigated [49]. Nevertheless, these spectra have either a low resolution [46,47] or do not exceed 370 K [48].

The aim of this paper is to present absorption cross-sections of the three sulfur compounds H_2S, CS_2 and OCS in the temperature range from 293 K to 773 K between 195 nm and 370 nm measured with a high spectral resolution (0.018 nm). The experimental setup is described, and then the obtained absorption cross-sections for each of the compounds are presented. For each compound, a comparison between the previously published data and the present ones at approximately 293 K will be given before the results at higher temperatures are presented. The uncertainties in the measurements will also be discussed and conclusions presented.

2. Experimental setup

A principle scheme of the experimental setup is shown in Fig. 1. The setup consisted of the gas mixing unit, a heated connection line, the high temperature gas flow cell (HGC) [8] and the UV spectrometry unit.

The gas mixing unit consisted of a set of gas cylinders, highly stable mass flow controllers (MFC, Bronkhost) and heated mixing chamber. The four gas cylinders, with H_2S, CS_2, OCS, each premixed at 1000 ppm nominal in nitrogen (N_2) and N_2 (purity 99.8%) were provided by Air Liquide. Two MFCs were used to achieve further dilution of the sample gases with N_2 and thereby yield different concentrations. One additional MFC was used to control the buffer gas flow in the HGC. The gases are pre-heated in the mixing chamber, where additional mixing of the gases took place. The chamber was connected with the HGC through a heated Teflon line. The temperature in the chamber could be set to 423 K, whereas the temperature on the heated Teflon line could be set up to 473 K to minimize the gas temperature drop at the inlet of HGC for temperatures higher than 473 K inside the HGC. The buffer

gas flow was introduced into the HGC without pre-heating.

The HGC, consisting of quartz, was designed for the use of reactive gases at temperatures up to 800 K in the UV and FTIR range and was based on the use of flow windows. A detailed description of the HGC and its validation is given in [8]. The idea of the HGC is to prevent the reactive gas to reach the optical windows and to keep the windows cooled. To achieve the later, the HGC consists of three section: two partially heated outer sections for the buffer gas and one fully heated inner section for the reactive gas. To prevent the contact between the optical windows and the reactive gases, the HGC used a principle of the so-called flow windows. In the region of flow windows, the cooler buffer gas and the heated reactive gas meet with similar velocity and establish a laminar flow sheet. The net velocity in axial direction is zero and both gases exit the gas cell through a small gap in this region. The pressure in the cell was measured with a pressure sensor (PTX series from Druck Ltd.) and was slightly above ambient pressure.

The UV spectrometry unit consisted of a UV lamp, focusing optics and a UV spectrometer with a CCD camera. A highly stable deuterium lamp (LOT Oriel) was used as a UV light source. After passing the HGC, the light was focused by a quartz lens onto the entrance slit of a 0.5 m grating spectrometer (Spectra Pro 2500i/Princeton Instruments) equipped with a CCD camera (Princeton Instruments PIXIS 100B). With a holographic UV grating (3600 gr/mm) the spectral resolution of 0.018 nm could be achieved between 190 and 400 nm. To match the gas cell and the spectrometer and to reduce the impact of stray light, two orifices were added, one between the HGC and the D_2-lamp (larger diameter compared to the size of internal apertures in the HGC) and one of smaller diameter between the UV spectrometer and the focusing lens.

The absorption measurements were performed for each compound at various temperatures and concentrations, and the absorption cross-sections were calculated. The different concentrations allowed for the creation of composite absorption cross-section spectra where non-linear absorption effects due to high absorbance can been eliminated. In addition, the reproducibility of the absorption cross-sections under different circumstances could be checked and the signal to noise ratio for the different structures could be enhanced.

3. Results and discussion

In this section, obtained absorption cross-sections for each compound are compared with those available from the literature. Then, temperature-dependent absorption cross-sections are presented. Finally, uncertainties in the measurements are discussed.

3.1. Hydrogen sulfide

As previously mentioned, several publications about the absorption cross-sections of H_2S at room temperature already exist. H_2S absorption starts approximately 160 nm and extends towards longer wavelengths with its maximum approximately 195 nm. Due to the experimental setup used in this work, comparisons can be performed only in the region from 195 nm and upwards.

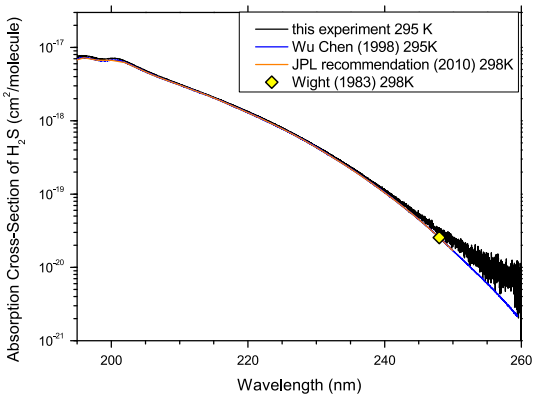

Fig. 2. Comparison of the absorption cross-sections of hydrogen sulfide at hand (black) with Wu and Chen ([27] – blue), Wight ([29] – yellow) and the JPL-2010 recommendation ([30] – orange) on a logarithmic scale. (For interpretation of the references to color in this figure caption, the reader is referred to the web version of this article.)

In Fig. 2, a comparison of the original data from Wight et al., Wu et al. and the derived JPL-2010 recommendation with the data obtained here is shown. Although the overall structure is the same, the maximum of the absorption cross-section spectrum in the present work is higher than that in the JPL-2010 recommendation by approx. 10%. However, this has a minor influence on the value of the integrated absorption cross-section between 195 and 280 nm. The difference in the absorption cross-sections between the present work and JPL-2010 recommendation is within uncertainties reported in [30].

To the best of our knowledge, only Wu and Chen [27] published data at higher temperatures (up to 370 K). However, these data were obtained at a different temperature than in the present work. In Fig. 3 absorption cross-sections spectra of H_2S at various temperatures are shown. In contrast to most other gases, the H_2S absorption cross-sections have a weak temperature dependence. Only minor changes in the shape of the spectrum are observed up to 673 K without a significant decrease of the absorption cross-section at 673 K.

At temperatures higher than 573 K, a second structure appears in the area between 250 nm and 320 nm. This structure can be identified as S_2 [50,51] (see Fig. 3 bottom left). S_2 appears due to thermal decomposition of H_2S on the surfaces of the gas cell and in the gas phase [52]. While the decomposition of H_2S is very low at temperatures up to 673 K, it increases at higher temperatures (see Section 3.4).

3.2. Carbon disulfide

Similar to H_2S, the structure of CS_2 exceeds the minimum wavelength of 195 nm. However, in the case of CS_2 the structure only ranges down to 180 nm, and a second, less intensive structure between 290 nm and 360 nm can be investigated.

In Fig. 4, comparisons with the available literature at room temperature for the peaks between (a) 205 nm and 230 nm [40] (orange) and (b) 280 nm and 360 nm [30] (yellow), [38] (blue), [37] (red) are shown. The overall structure is in good agreement with the literature. In part (a) of the figure, the peaks of the fine structure are cut off below approx. 205 nm. This occurred as the result of absorption of the CS_2 being in saturation at room temperature. Nevertheless, down to the wavelength of 205 nm, the measurements at hand are in good agreement.

For a better comparison between the single data, a detailed view of the region between 318 nm and 323 nm is shown in Fig. 5, where a very good agreement with Schneider et al. and the JPL recommendation can be seen. The largest deviations originate from the higher resolution of the data at hand. Compared to Vandaele et al., a slight shift in wavelength and a slightly lower intensity can be seen. Otherwise, no significant deviations are observed.

In Fig. 6, the variation of the spectrum with temperature from 195 nm to 360 nm is shown. For 773 K, the fine structure at approximately 200 nm can be fully resolved without running into full absorption.

As expected, the heights of individual peaks are lowered with an increase in temperature, making the fine structure disappear. Meanwhile, the width of the overall structure increases with the temperature by raising the coarse structure at higher wavelengths and shifting the overall maximum towards higher wavelength. Up to 573 K, the absorption reaches the maximum at approximately 205 nm. This behavior has already been reported by Dove et al. [39] for the coarse structure up to 4000 K and by Chen and Wu [40] for the structure between 280 nm and 360 nm at 383 K and is similar as the behavior of SO_2 at higher temperatures [36,8].

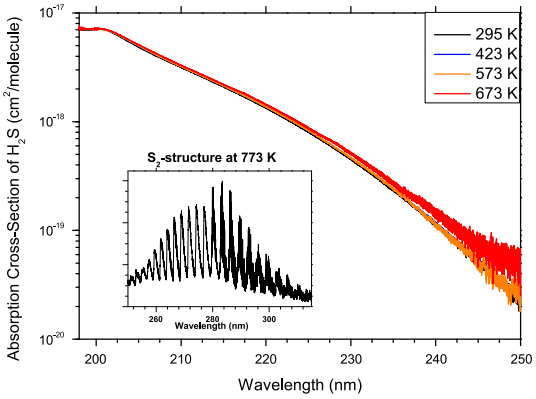

Fig. 3. Absorption cross-sections of hydrogen sulfide at room temperature (black), 423 K (blue) and 573 K (orange) and 673 K (red) on a logarithmic scale. (For interpretation of the references to color in this figure caption, the reader is referred to the web version of this article.)

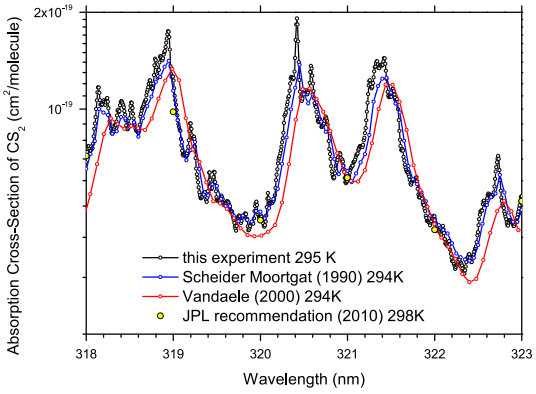

Fig. 5. Detailed comparison of the absorption cross-sections of carbon disulfide at hand (black) with Schneider and Moortgat ([38] – blue), Vandaele ([37] – red) and the JPL recommendation ([30] – yellow dots) between 318 nm and 323 nm on a logarithmic scale. (For interpretation of the references to color in this figure caption, the reader is referred to the web version of this article.)

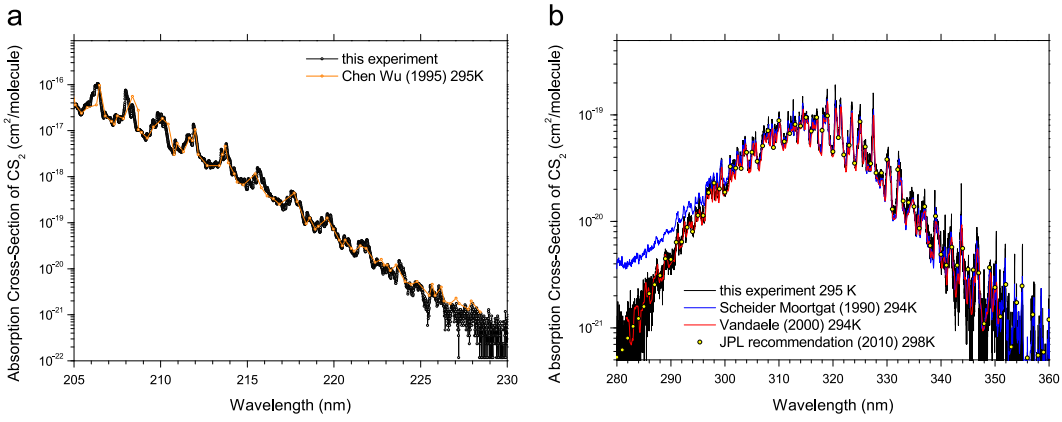

Fig. 4. Comparison of the absorption cross-sections of carbon disulfide at hand (black) in two different ranges: (a) between 195 nm and 230 nm with Chen and Wu ([40] – orange) and (b) between 280 nm and 360 nm with Schneider and Moortgat ([38] – blue), Vandaele ([37] – red) and the JPL recommendation ([30] – yellow dots) on a logarithmic scale. (For interpretation of the references to color in this figure caption, the reader is referred to the web version of this article.)

3.3. Carbonyl sulfide

As reported by Molina et al. [44] and Locker [47], some additional absorption caused by an impurity of CS_2 can be found in the OCS absorption spectra. To obtain the pure OCS absorption structure, the CS_2 structure obtained in the same experiments at the same temperature was subtracted. It was found that CS_2 is present in the ppb-range (approximately 65 ppb at 100 ppm OCS in nitrogen), which is likely the result of impurities in the gas bottle.

A comparison of the obtained OCS absorption cross-section spectrum with the available data from the literature has been done in Fig. 7. In part (a) of the figure, a good agreement with the overall structure between 205 nm and 275 nm can be observed. Although the older data ([44] – blue) and the derived JPL data ([30] – yellow dots) range above the measured curve, newer data ([48] – green and [49] – orange) are slightly below the measured curve, and yet the derivation of the data at hand is less than 5%. Only at approximately 206 nm does a different peak appear. This peak belongs to CS_2 and was present even after its subtraction due to the problems with total absorption discussed above. Upon closer examination, (Fig. 7b) between 215 nm and 230 nm, a very good agreement of the fine structure with the measurements of Hattori et al. can be found, with only a slight shift in wavelength of approximately 0.1 nm.

In Fig. 8, the temperature dependency of the absorption cross-section of OCS is shown over the wavelength between 205 nm and 315 nm. The maximum of the overall Gaussian-like shape stays the same, with only the height and the position of the maximum changing. Both the height and the wavelength of the maximum increase with temperature. Moreover, the peaks of the superimposed fine structure stay at the same wavelength, but their amplitude decreases. This is in good agreement with the temperature dependent behavior reported by Locker et al. [47].

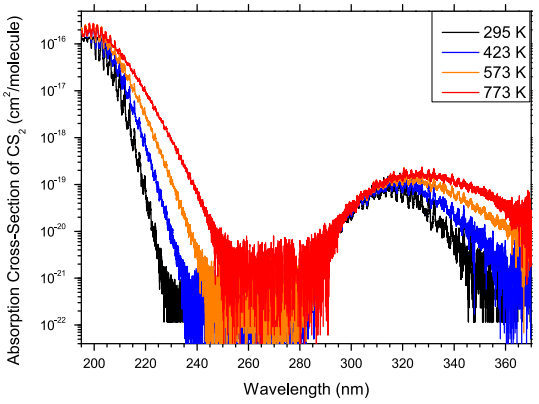

Fig. 6. Absorption cross-sections of carbon disulfide at room temperature (black), 423 K (blue), 573 K (orange) and 773 K (red) on a logarithmic scale. (For interpretation of the references to color in this figure caption, the reader is referred to the web version of this article.)

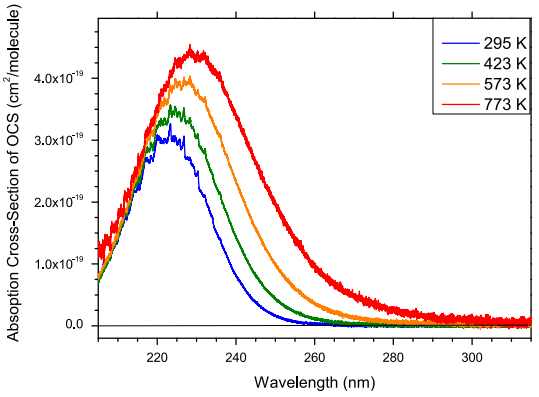

Fig. 8. Absorption cross-sections of carbonyl sulfide at room temperature (blue), 423 K (green), 573 K (orange) and 773 K (red). (For interpretation of the references to color in this figure caption, the reader is referred to the web version of this article.)

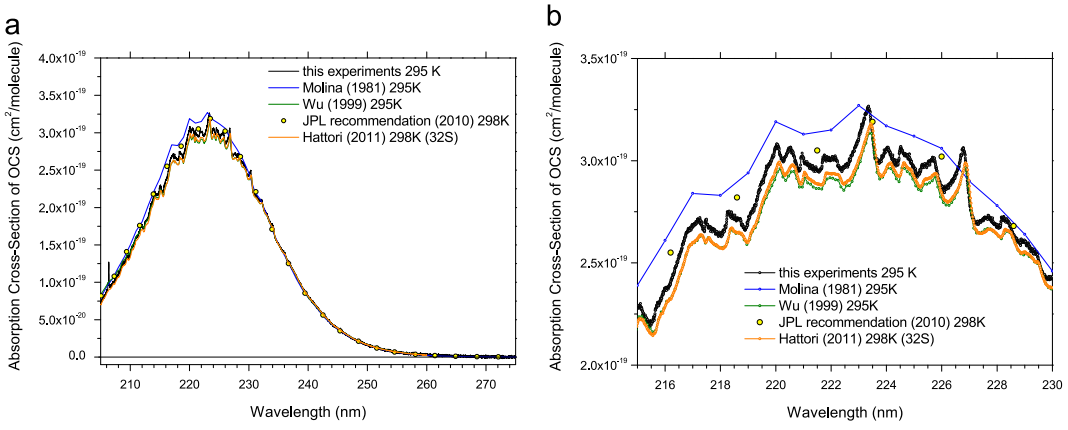

Fig. 7. Comparison of the absorption cross-sections of carbon disulfide at hand (black) with Molina et al. ([44] – blue), Wu et al. ([48] – green), Hattori et al. ([49] – orange) and the JPL recommendation ([30] – yellow dots). (a) Overview from 205 nm to 275 nm and (b) detailed view between 215 nm and 230 nm. (For interpretation of the references to color in this figure caption, the reader is referred to the web version of this article.)

3.4. Uncertainties

To evaluate the measured cross-sections, the sources of uncertainties in the measurements and their impact on the data have to be evaluated. The methodological uncertainties, the quality of the gas composition, the wavelength shift due to the grating and the stray light and shifts in the stability of the deuterium lamp, residues in the gas cell and the conversion into other compounds can be seen.

As stated on the certificates of the gas bottles, the uncertainty on the concentration of CS_2 and H_2S was below 3%, whereas it was 5% for OCS. Because this experimental setup was calibrated by a UV pen lamp (Hg/Ar) and the standard spectrometer software, a shift of the wavelength might have occurred. In [8], a comparison of SO_2 data obtained with this setup and data obtained by FT-UV measurements with higher spectral precision from Rufus [7] were done. The wavelength difference was found to be $\Delta\lambda \approx 0.1$ nm.

A potential third source of uncertainty, the stray light, was also considered. This can play a significant role when the absorption peaks are close to total absorption. For H_2S and OCS, the uncertainties due to stray light at the maximum peak heights were always below 1%. For CS_2 the peaks below 207 nm the uncertainties due to the stray light exceeded 5%, whereas it was below 0.5% between 280 nm and 360 nm.

As a highly stable deuterium lamp was used as light source, the uncertainties due to changes in the light intensity were below 1% in the region investigated.

To reduce the influence of residues on the spectra, the setup was purged with N_2 for a sufficient amount of time after each measurement. To verify this, the absorption background spectrum before and after the measurement and after the N_2 purging was taken in all cases.

As a potential source of impurities, a chemical conversion of the gases was also taken into account. With the gas–wall interaction and the thermal decomposition, the impurities can have two sources and might affect the spectrum by reducing the effective heights of it and interfering by 'adding' new peaks. Although the cell was built to minimize the surface effects, in the case of OCS, an interference with the strong CS_2 below 220 nm could be observed. Here, the impact of the conversion was negligible (0.065%), and a simple subtraction of the unwanted spectra was sufficient.

In case of H_2S, trace S_2 gas was observed. Here, the impact of the conversion was determined by measuring the difference of the concentration of H_2S before and after the heating of the HGC by a second cell. Up to 673 K, no difference in the height or shape of H_2S other than the additional S_2-structure could be found. Due to surface effects, such as adsorption of H_2S at the stainless steel walls in the outlet of the HGC, the exact decomposition rates at temperatures higher than 673 K could not be evaluated, and the obtained data cannot be published. For that reason, only H_2S absorption cross-sections at 673 K rather than 773 K are reported here.

In addition to the already mentioned uncertainties, the deviations from the Lambert–Beer law due to instrumental effects have been investigated. According to Mellqvist and Rosén [53], the apparent spectrum can be considered as true spectrum, if the width of instrumental line shape is one-fifth of the linewidth of the absorption line. This is true for OCS, H_2S and in most parts also for CS_2. Only in very few cases, the CS_2 structure between least 3.5 and 5 times is wider than the instrumental line shape. In these few cases, the optical depth is small (below 0.1). This means that the presented spectra are within 1% of the true spectra.

4. Conclusion

In this paper, absorption cross-section for CS_2, H_2S and OCS in the UV range between 200 nm and 360 nm has been presented. The results were obtained by using premixed gases at atmospheric pressure, a high temperature gas flow cell and a UV grating spectrometer setup. Comparison of available literature data at room temperature was made to evaluate the quality of the absorption cross-sections at hand and all three cases a very good agreement was found. Afterwards, absorption cross-sections for the three compounds at 423 K, 573 K and 773 K were presented, for the first time. Finally, an overview of possible uncertainties was given.

Acknowledgments

We would like to thank Energinet.dk for providing financial support (Project no. 2011-1-10622).

Appendix A. Supplementary data

Supplementary data associated with this paper can be found in the online version at http://dx.doi.org/10.1016/j.jqsrt.2014.11.020.

References

[1] Woods PT, Jollife BW, Marx BR. High resolution spectroscopy of SO_2 using a frequency-doubled pulsed dye laser with application to the remote sensing of atmospheric pollutants. J Opt Commun 1980;33:281–5.
[2] Keller-Rudek H, Moortgat G, Sander R, Sörensen R. The MPI-Mainz UV/VIS spectral atlas of gaseous molecules of atmospheric interest. http://satellite.mpic.de/spectral_atlas.
[3] Fateev A, Clausen S. On-line non-contact gas analysis. Report Risø-R-1636(EN); 2008.
[4] Teichert H, Fernholz T, Ebert V. Simultaneous in situ measurement of CO, H_2O, and gas temperatures in a full-sized coal-fired power plant by near-infrared diode lasers. Appl Opt 2003;42:2043–51.
[5] Webber ME, Wang J, Sanders ST, Baer DS, Hanson RK. in situ combustion measurements of CO, CO_2, H_2O and temperature using diode laser absorption sensors. Proc Combust Inst 2000;28:407–13.
[6] Sur R, Sun K, Jeffries JB, Hanson RK. Multi-species laser absorption sensors for in situ monitoring of syngas composition. Appl Phys B 2014;115:9–24.
[7] Rufus J, Stark G, Smith PL, Pickering JC, Thorne AP. High-resolution photoabsorption cross section measurements of SO_2, 2: 220–325 nm at 295 K. J Geophys Res E: Planets 2003;108:5011.
[8] Grosch H, Fateev A, Nielsen KL, Clausen S. Hot gas flow cell for optical measurements on reactive gases. J Quant Spectrosc Radiat Transf 2013;130:392–9.
[9] Danielache SO, Eskebjerg C, Johnson MS, Ueno Y, Yoshida N. High-precision spectroscopy of ^{32}S, ^{33}S, and ^{34}S sulfur dioxide: ultraviolet absorption cross sections and isotope effects. J Geophys Res D: Atmos 2008;113:D17314.

[10] Ståhlberg P, Lappi M, Kurkela E, Simell P, Oesch P, Nieminen M. Sampling of contaminants from product gases in biomass gasifiers. Research Note 1903, VTT Technical Research Centre of Finland; 1998.
[11] Ma RP, Felder RM, Ferrell JK. Evolution of hydrogen sulfide in a fluidized bed coal gasification reactor. Ind Eng Chem Res 1989;28:27–33.
[12] Halmer MM, Schmincke HU, Graf HF. The annual volcanic gas input into the atmosphere, in particular into the stratosphere: a global data set for the past 100 years. J Volcanol Geotherm Res 2002;115:511–28.
[13] Crutzen PJ. The possible importance of CSO for the sulfate layer of the stratosphere. Geophys Res Lett 1976;3:73–6.
[14] Kaltenegger L, Henning WG, Sasselov DD. Detecting volcanism on extrasolar planets. Astron J 2010;140:1370–80.
[15] Tinetti G, Encrenaz T, Coustenis A. Spectroscopy of planetary atmospheres in our Galaxy. Astron Astrophys Rev 2013;21:63.
[16] Seager S, Bains W, Hu RA. Biomass-based model to estimate the plausibility of exoplanet biosignature gases. Astrophys J 2013;775:104.
[17] Kasting JF, Kopparapu R, Ramirez RM, Harman CE. Remote life-detection criteria, habitable zone boundaries, and the frequency of Earth-like planets around M and late K stars. Proc Natl Acad Sci USA 2014;111:12641–6.
[18] Brion CE, Iida Y, Thompson JP. Absolute oscillator strengths for the photoabsorption, ionic photofragmentation and photoionization of H_2S (10–40 eV). Chem Phys 1986;101:449–60.
[19] Feng R, Cooper G, Brion CE. Absolute oscillator strengths for hydrogen sulphide. I. Photoabsorption in the valence-shell and the S 2p and 2s inner-shell regions (4–260 eV). Chem Phys 1999;244:127–42.
[20] Carnovale F, White MG, Brion CE. Absolute dipole oscillator strengths for photoabsorption and photoionization of carbon disulphide. J Electron Spectrosc 1981;24:63–76.
[21] Feng R, Cooper G, Brion CE. Quantitative studies of the photoabsorption of carbonyl sulphide in the valence-shell, S 2p, 2s and C 1s inner-shell regions (4–360 eV) by dipole electron impact spectroscopies. Chem Phys 2000;252:359–78.
[22] White MG, Leung KT, Brion CE. Absolute dipole oszillator strength for the photoionization and photoabsorption of COS (5–50 ev). J Electron Spectrosc 1981;23:127–45.
[23] Starr WL, Loewenstein M. Total absorption cross sections of several gases of aeronomic interest at 584 Å. J Geophys Res 1972;77:4790–6.
[24] Vatsa RK, Volpp H-R. Absorption cross-sections for some atmospherically important molecules at the H atom Lyman-alpha wavelength (121.567 nm). Chem Phys Lett 2001;340:289–95.
[25] Watanabe K, Jursa AS. Absorption and photoionization cross sections of H_2O and H_2S. J Chem Phys 1964;41:1650–3.
[26] Thompson ST, Carrol DG, Watson F, O'Donnell M, McGlynn SP. Electronic spectra and structure of sulfur compounds. J Chem Phys 1966;45:1376–9.
[27] Wu CYR, Chen FZ. Temperature-dependent photoabsorption cross sections of H_2S in the 1600–2600 Å region. J Quant Spectrosc Radiat Transf 1998;60:17–23.
[28] Wine PH, Kreutter NM, Gump CA, Ravishankara AR. Kinetics of OH reactions with the atmospheric sulfur compounds H_2S, CH_3SH, CH_3SCH_3, and CH_3SSCH_3. J Phys Chem 1981;85:2660–5.
[29] Wight CA, Leone SR. Vibrational state distributions and absolute excitation efficiencies for T–V transfer collisions of NO and CO with H atoms produced by excimer laser photolysis. J Chem Phys 1983;79:4823–9.
[30] Sander SP, Friedl RR, Abbatt JPD, Barker JR, Burkholder JB, Golden DM, et al. Chemical kinetics and photochemical data for use in atmospheric studies. JPL Publication 10-6; 2011. Evaluation Number 17.
[31] Wine PH, Chameides WL, Ravishankara AR. Potential role of CS_2 photooxidation in tropospheric sulfur chemistry. Geophys Res Letters 1981;8:543–6.
[32] Ahmed SM, Kumar V. Measurement of photoabsorption and fluorescence cross section for CS_2 at 188.2–213 and 287.5–339.5 nm. Pramana J Phys 1992;39:367–80.
[33] Wu CYR, Judge DL. SO_2 and CS_2 cross section data in the ultraviolet region. Geophys Res Lett 1981;8:769–71.
[34] Xu H, Joens JA. CS_2 absorption cross section measurements. Geophys Res Lett 1993;20:1035–7.
[35] Cook GR, Ogawa M. Photoionization, absorption, and fluorescence of CS_2. J Chem Phys 1969;51:2419–24.
[36] Hearn CH, Joens JA. Absorption spectrum of CS_2 and SO_2 at 300 K. J Quant Spectrosc Radiat Transf 1991;45:69–75.
[37] Vandaele AC. Thesis. Développement d'instruments pour la détection de constituants troposphériques minoritaires par DOAS UV-visible. Université Libre de Bruxelles, Brussels, Belgium; 1997. http://satellite.mpic.de/spectral_atlas.
[38] Schneider W, Moortgat GK, Berichte des Forschungszentrums Jülich; 1997. http://satellite.mpic.de/spectral_atlas.
[39] Dove JE, Hippler H, Plach HJ, Troe J. Ultraviolet spectra of vibrationally highly excited CS_2 molecules. J Chem Phys 1984;81:1209–14.
[40] Chen FZ, Wu CYR. High, room and low temperature photoabsorption cross sections of CS_2 in the 1800–2300 Å region. Geophys Res Lett 1995;22:2131–4.
[41] Cook GR, Ogawa M. Photoionization and absorption coefficients of OCS. J Chem Phys 1969;51:647–52.
[42] Sidhu KS, Csizmadia IG, Strausz OP, Gunning HE. The reactions of sulfur atoms. VII. The ultraviolet spectrum, the photolysis, and the mercury sensitization of carbonyl sulfide. J Am Chem Soc 1966;88:2412–7.
[43] Breckenridge WH, Taube H. Ultraviolet absorption spectrum of carbonyl sulfide. J Chem Phys 1970;52:1713–5.
[44] Molina LT, Lamb JJ, Molina MJ. Temperature dependent UV absorption cross sections for carbonyl sulfide. Geophys Res Lett 1981;8:1008–11.
[45] Rudolph RN, Inn ECY. OCS photolysis and absorption in the 200–300 nm region. J Geophys Res 1981;86:9891–4.
[46] Ferro BM, Reuben BG. Temperature dependence of absorption spectrum of carbonyl sulphide in quartz ultra-violet. Trans Faraday Soc 1971;67:2847–51.
[47] Locker JR, Burkholder JB, Balr EJ, Webster III HA. Thermally excited vibrational components of the $A \leftarrow X^1\Sigma^+$ system of OCS. J Phys Chem 1983;87:1864–8.
[48] Wu CYR, Chen FZ, Judge DL. Temperature-dependent photoabsorption cross sections of OCS in the 2000–2600 Å region. J Quant Spectrosc Radiat Transf 1999;61:265–71.
[49] Hattori S, Danielache SO, Johnson MS, Schmidt JA, Kjæregaard HG, Toyoda S, et al. Ultraviolet absorption cross section of carbonyl sulfide isotopologues $OC^{32}S$, $C^{33}S$, $OC^{34}S$ and $O^{32}CS$: isotopic fractionation in photolysis and atmospheric implications. Atmos Chem Phys 2011;11:10293–303.
[50] Rosen B, Barrow RF. Constantes Sélectionnées: Données spectroscopiques concernant les molécules diatomiques. Paris, France: Pergamon; 1951.
[51] Brewer L, Brabson GD, Meyer BUV. Absorption spectrum of trapped S_2. J Chem Phys 1965;42:1385–9.
[52] Olschewski HA, Troe J, Wagner HGUV. Absorption study of the thermal decomposition reaction $H_2S \leftrightarrow H_2+S(^3P)$. J Phys Chem 1994;98:12964–7.
[53] Mellqvist J, Rosén A. DOAS for flue gas monitoring. II. Deviations from the Beer-law for the UV/visible absorption spectra of NO, NO_2, SO_2 and NH_3. J Quant Spectrosc Radiat Transf 1996;56:209–24.

Appendix C

Article 3

Article 3: "UV absorption cross-sections of phenol and naphthalene at temperatures up to 500°C"

Helge Grosch; Zsuzsa Sárossy; Helge Egsgaard; Alexander Fateev

Reprinted from *Journal of Quantitative Spectroscopy and Radiative Transfer* 156 (2015) 17-23

Journal of Quantitative Spectroscopy & Radiative Transfer 156 (2015) 17–23

Contents lists available at ScienceDirect

Journal of Quantitative Spectroscopy & Radiative Transfer

journal homepage: www.elsevier.com/locate/jqsrt

UV absorption cross-sections of phenol and naphthalene at temperatures up to 500 °C

H. Grosch, Z. Sárossy, H. Egsgaard, A. Fateev *

Technical University of Denmark, Department of Chemical and Biochemical Engineering, Frederiksborgvej 399, 4000 Roskilde, Denmark

ARTICLE INFO

Article history:
Received 24 October 2014
Received in revised form
16 January 2015
Accepted 24 January 2015
Available online 7 February 2015

Keywords:
Absorption coefficients
Spectroscopy
UV
Phenol
High temperature
Naphthalene

ABSTRACT

Absorption cross-sections and their temperature dependency, especially in the UV spectral range, of organic compounds such as phenol and naphthalene are of great interest in atmospheric research and high temperature processes. Due to the challenges of producing premixed gases of known concentration, it is difficult to determine absorption cross-sections in experiments, especially at higher temperatures. In this paper, a gas flow of nitrogen with a stable but unknown concentration of phenol or naphthalene is produced, and their UV absorption spectra between 195 and 350 nm have been measured at higher resolution than before (0.019 nm) in a hot gas flow cell at temperatures of up to 500 °C/773 K. A Petersen column is used to sample the organic compounds in the gas mixture to determine their concentration by GC–MS. The absorption cross-sections are calculated with the use of the Lambert–Beer law. Consequently, the absorption cross-sections for phenol and naphthalene at room temperature, 423 K, 573 K and 773 K in the range of 195–360 nm are presented in this study.

1. Introduction

Simple aromatic compounds, such as benzene, toluene, xylene (BTX), and phenolic and polyaromatic hydrocarbons, are known to be hazardous for health and the environment. Nevertheless, in their gaseous form, they play an important role in interstellar [1] and atmospheric chemistry [2] as well as in the chemical industry. They are also known as an intermediate product in different high temperature processes, such as combustion [3] and biomass gasification [4,5]. With new regulations that lower pollution threshold values, the energy sector has a particular interest in monitoring and controlling these compounds to minimize their release into the environment.

There are several techniques, including ultraviolet (UV) spectroscopy, gas chromatography–mass spectrometry (GC–MS) and laser-induced fluorescence (LIF), for the quantification of organic compounds in gaseous mixtures, particularly phenolic and polyaromatic compounds. Among the methods used, optical techniques such as UV spectroscopy and LIF play only a minor role in high temperature processes, particularly the analysis of the producer gas from gasification processes. This is due to a lack of spectroscopic reference data for these organic compounds, especially at higher temperatures. It would still be beneficial, however, to use optical techniques because they can avoid the typical problems associated with sampling methods (e.g., gas cooling, sample handling) and make continuous, online and in situ measurements possible. Continuous and in situ measurements are of special interest for long term monitoring of gas flows. Moreover, atmospheric research also has a strong interest in obtaining reliable data of organic compounds at different temperatures and at a reasonable resolution to quantify these compounds.

Analyses of phenolic and polycyclic aromatic hydrocarbon compounds in the product gases of biomass gasification

* Corresponding author. Tel.: +45 46774564; fax: +45 46774565.
E-mail address: alfa@kt.dtu.dk (A. Fateev).

http://dx.doi.org/10.1016/j.jqsrt.2015.01.021
0022-4073/

have been well established using chromatographic techniques that may be coupled with mass spectrometry [5–7]. These compounds are most commonly part of the tar fraction in gasification. Analysis and detection of tar compounds from the sampled gas is often performed using GC–MS techniques. Such techniques may be used with isotope-labeled compounds as internal standards and quantification aids [5,8,9].

The absorption cross-sections in the UV range for aromatic compounds, in general, are scarce and need to be extended [10]. In the case of phenol and naphthalene, the subject of this investigation, the number of reports in the literature is more limited. However, especially in high temperature applications where strong changes in the structure of the cross-sections can occur, reliable absorption cross-sections are necessary to obtain consistent gas concentrations. To our knowledge, no data have been published to date for these compounds at higher temperatures.

There are only a few publications for phenol covering the spectral range between 200 nm and 360 nm. The studies of Breho and Lesclaux [11] from 1997 covers almost the full range but only shows the absorption cross-sections in very coarse steps of 2–20 nm, while Trost et al. [12] and Etzkorn et al. [13] investigated only the characteristic bands between 240 and 290 nm. These papers used a setup of a UV lamp (either a deuterium lamp [11,12] or a xenon high pressure lamp [13]) with a bandpass for the lower UV ranges, a monochromator (e.g., Czerny–Turner spectrograph) and a detector (either a photomultiplier [11] or a photodiode array detector [12,13]). While Trost et al. could achieve a spectral resolution of 0.11 nm and Etzkorn et al. obtained a resolution of 0.146 nm, Breho et al. did not report the resolution in his report.

Three datasets of absorption cross-sections at room temperature are available for naphthalene in the spectral range investigated in this study. All experiments were obtained by absorption measurements with a grating spectrometer in a gas cell of different length and light sources. In all cases, the vapor of purified naphthalene was investigated at low pressures. The report published by Ferguson et al. [14] in 1957 at 313 K covered the characteristic bands between 245 nm and 285 nm and introduced small amounts of argon to the naphthalene vapor to achieve thermal equilibrium more rapidly. George et al. [15] in 1968 covered the full spectrum between 187 nm and 327 nm in three steps. The results were presented in one graph with the factor of magnification. The most recent study by Suto et al. [16] investigated the spectrum of naphthalene between 190 nm and 290 nm with a spectral resolution of 0.1 nm. The study itself focused on the fluorescence spectrum but also presented quantitative absorption cross-sections. Moreover, a study by Orain et al. [17] measuring the laser induced fluorescence of naphthalene at higher temperatures included the measurement of the absorption cross-section of naphthalene at 266 nm at 350 K.

Due to the nature of the studied compounds, no commercial gas mixture is available, and it is difficult to produce gas of known and stable concentration. However, three methods can be used to achieve this. As reported in a previously published procedure, a small stable amount of vapor can be produced in a gas cell [12]. This, however, can cause deposits of organic compounds on the windows of the gas cell and therefore change the optical properties. In a second method, a known volume of the compound in question is continuously evaporated directly in a gas stream of known velocity. In this case, problems through concentration changes due to droplet formation during evaporation of the compound can occur. In the third method, a gas mixture is prepared by passing nitrogen gas over the solid crystallized compound. Here, the vapor pressure of the compound and a constant flow ensure stable concentration over the course of the measurements. The concentration is then determined using an appropriate analytical method e.g., GC–MS. In all cases, either heating of the whole system or dilution of the gas is necessary to stabilize its concentration and prevent condensation.

In the approach described in this paper, the UV absorption spectra of phenol and naphthalene from room temperature up to 773 K at unknown but stable concentrations were measured. The concentrations were obtained from a GC-MS analysis of samples taken with a Petersen column during UV absorption measurements. From the data obtained, an averaged value for the absorption cross-sections at each temperature could be calculated. In the first section, the paper presents the experimental set-up with a brief description of the different devices applied. Afterwards, the results for the UV absorption cross-sections for phenol and naphthalene are presented and a comparison with existing data is given. In the end, a short conclusion is given.

2. Experimental setup

The experiment was conducted in two steps. In the first step, a flow of the aromatic compound in nitrogen with a stable concentration was generated, which was then analyzed by UV absorption spectroscopy and sampled using a Petersen column. In the second step, the samples taken by the Petersen column were analyzed using GC–MS.

The objective of the two-step experiment was to obtain absorption cross-sections for phenol and naphthalene at different temperatures. Therefore, measurements were conducted in four temperature steps (296 K, 423 K, 573 K and 773 K). The measurements at room temperature (296 K) were used to compare the results with previously published absorption cross-sections. At each temperature step, four samples for GC analysis were taken, two at a lower concentration and two at a higher concentration. This was performed to show data reproducibility and to minimize errors in the UV spectra due to total absorption (at high concentrations) and signal noise (at low concentrations). During each sampling, three UV spectra were taken (at the beginning, the middle and the end) to document the stability of the concentrations.

In Fig. 1, a scheme of the experimental set-up is shown. The set-up consists of three parts: the gas mixing part (1), the optical analysis part including the hot gas flow cell (HGC) and the UV spectrometer (2), and a sampling part (3),

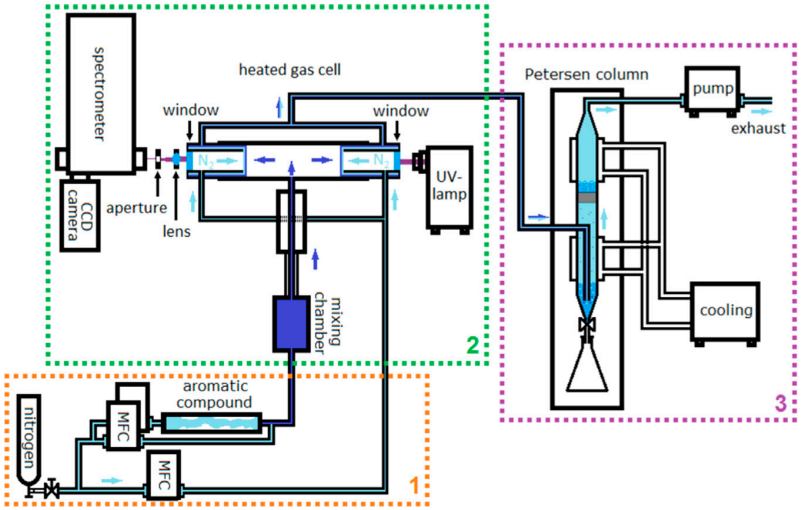

Fig. 1. Setup of the experiments including a gas mixing unit (1), an optical unit (2) for UV measurements with a HGC and a sampling unit (3) with a Petersen column.

where the sampling with the Petersen column for the GC–MS takes place.

To enrich the UV inactive nitrogen (N_2) with the aromatic compound, a steady flow of 0.5 l_N/min controlled by a high precision mass flow controller (MFC, Bronkhost) was passed through a tube coated with melted crystals of the compound. Because of the relatively high vapor pressure of the volatile aromatic compound, a significant amount of the compound could be added to the flow. The steady flow and a long waiting time of 30 min before each measurement assured that the concentration of the aromatic remained stable in the whole system. The higher concentrations were achieved by diluting the enriched nitrogen flow by a flow of 0.5 l_N/min of pure nitrogen. For the lower concentrations, the flow was diluted with 1.5 l_N/min of pure nitrogen controlled by a second MFC. The resulting higher flow rate did not change the quality of the optical measurements and was taken into account in the GC–MS sampling. Afterwards, the gas mixture entered the HGC. A third MFC provided an equal flow of buffer gas (N_2), which was needed to run the HGC.

The optical setup for the measurements of the UV absorption spectra consisted of two major parts, the optical spectroscopy and the heated gas flow cell system, which has already been described in [18] and will be addressed only briefly here.

A highly stable deuterium lamp (30 W, LOT Oriel) was used as the light source for the spectroscopy and placed directly in front of the gas cell. On the other side of the gas cell, a lens focused the light through an orifice on the entrance slit of a 0.5 m monochromator (Spectra Pro 2500i/Princeton Instruments). The monochromator used a holographic grating of 3600 grooves/mm and was equipped with a CCD camera (Princeton Instruments PIXIS 100B). The spectral resolution of this setup was determined to be 0.019 nm. The setup was calibrated with an UV pen lamp (Hg/Ar) and the standard spectrometer software. This led to a wavelength shift of $\Delta\lambda \approx 0.1$ nm (see [19]). The uncertainties of the absorption cross-sections depend on stray light, the stability of the deuterium lamp and deviations of the Lambert–Beer law as well as chemical conversion or residues in the gas cell and the precision of the determination of the concentration. The uncertainties due to stray light, and the deuterium lamp as well as the deviations of the Lambert–Beer law have been discussed in [19] and are in each case below 1%. Chemical conversion and residues have not been found for the two compounds under investigation. The precision of the determination of the concentration is stated later in the paper.

At first, the gas mixture entered a mixing/reaction chamber, where it could be heated up to 423 K. Then, the gas was led through a heated Teflon line (up to 473 K) into the HGC (up to 800 K). The HGC was made of quartz glass and consisted of three sections, one active gas section (inner section) and two buffer gas sections (outer section). Thus, the gas mixture enters the HGC at the center section, where it splits into two equal flows to the left and to the right. The pure nitrogen flow, as mentioned above, enters the outer sections as a buffer gas with the same overall flow rate (half on each side). The flows from the inner section and the outer section meet between the two sections. Here, the net flow velocity in the axial direction is zero and a laminar flow sheet is established due to different viscosities of the gases. This area is called the flow window. The gas could exit in a radial direction through a gap between the sections. Thus, the reactive gas is never in contact with the optical windows. This has the advantage that the optical window is not subject to corrosion or deposition, thereby providing a well-defined gas cell length. Validation of the HGC (defined path length, stable temperature profile etc.) can be found in the report published by Grosch et al. [18]. The combined, and therefore diluted (by the factor 0.5), flows were then directed through a Teflon tube. Here, a rotameter and pressure sensor were used to measure the flow rate and the pressure in the system, respectively.

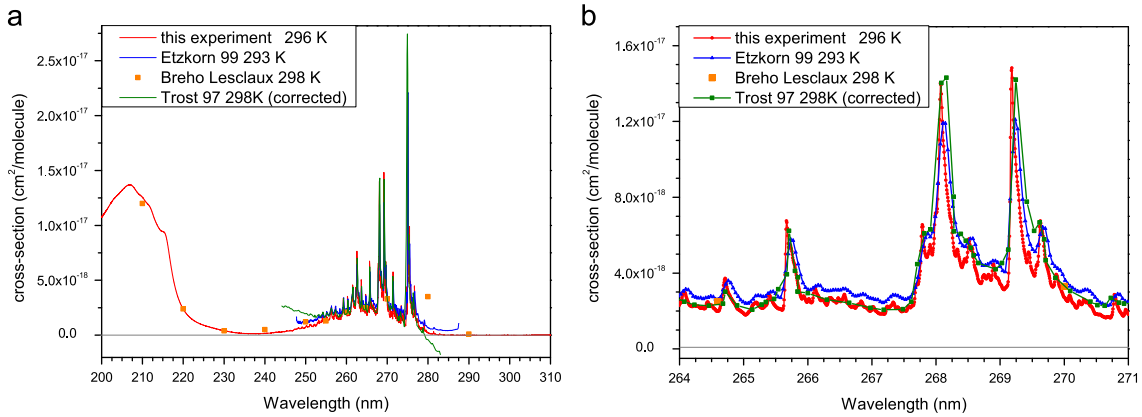

Fig. 2. UV absorption cross-sections of phenol at room temperature. Comparison of available literature data (green – [12]; blue – [13]; orange squares – [11]) and data obtained in this paper (red) between 200 nm and 310 nm (a) and a close-up between 264 nm and 271 nm (b). (For interpretation of the references to color in this figure caption, the reader is referred to the web version of this article.)

Afterwards, the gas mixture entered the Petersen column, a cooled two-stage sampling device for organic and inorganic aerosols, where acetone was used as the solvent. In the first stage, the gas was directly led into acetone, and as a result, the gas flow was cleaned to a large extent from the aromatic compounds. The second stage consisted of a porous membrane followed by a larger amount of acetone. The porous membrane produced a diffuse gas flow resulting in much smaller bubbles in the acetone than the first stage. The higher diffusivity resulted in higher absorption of the remaining aromatic compounds. As a result of this, the slip of sampling compound was negligible. Due to the high backpressure caused by this device, it was necessary to install a pump after the Petersen column. The installation of a pump made active pressure control necessary. The cooling of the system made sure that the sample was always taken at the same temperature of 289 K. The sampling time was 30 min in every case. After each sampling period, absorbed aromatic compound in acetone was filled into a volumetric flask and then prepared for analysis by GC–MS in the second step.

The collected samples were filled to a known volume, kept in the dark and refrigerated. An aliquot was taken from each sample, and known amounts of deuterated standards, phenol D_6 and naphthalene D_8 solutions (29.7 mg and 26.5 mg in 100 ml methanol, respectively), were added. After mixing, phenol and naphthalene were identified and quantified using a GC–MS system. Samples were analyzed using a Hewlett Packard HP 6890 gas chromatograph interfaced to a HP5973 Mass Selective Detector (Agilent, Denmark). Samples (1 µl) were injected in the split mode (1:20) using an HP 7683 autosampler (Agilent, Denmark). The source and rod temperatures were 230 °C and 150 °C, respectively. The products were separated using a 0.32 mm i.d. × 30 m WCOT-fused silica column coated with VF 23 ms at a thickness of 0.25 µm (Analytical, Denmark). The carrier gas was He at a flow rate of 1.2 ml/min. Separation of products was achieved using a temperature program from 70 to 250 °C at 10 °C/min. The applied ionization energy was 70 eV. Full mass spectra were recorded every 0.3 s (mass range m/z 40-450). Products were identified using the NIST search engine version 2.0 f. (Agilent, Denmark).

Four samples for GC analysis were taken for each temperature, and three absorption spectra were recorded for each sample. Taking multiple spectra per sample assured that the errors of the UV spectrometry were in the same range as previous experiments performed with the same setup [19]. To minimize the deviations in concentration due to sampling and sample preparation in the GC–MS analysis, the analysis was run six times for each sample. The resulting six concentrations per sample were averaged. The high concentrations of phenol and naphthalene were approximately 450 ppm and 15 ppm, respectively, whereas the low concentrations measured at 220 ppm and 7.4 ppm, respectively. The standard deviation for each sample was below 3% for naphthalene up to 573 K and for naphthalene at 773 K, and all phenol measurements were approximately 5%. From the three absorption spectra and the average of the concentrations, the absorption cross-section for each sample was calculated using the Lambert–Beer law. The absorption cross-sections presented in this paper are the average value of the four absorption cross-sections at each temperature.

3. Results and discussion

3.1. Phenol

Fig. 2 presents the absorption cross-section of phenol at room temperature from the experiments conducted in this study and data available from literature. Fig. 2a covers the whole spectrum between 195 nm and 310 nm, and Fig. 2b provides a closer look and therefore a better comparability of the fine structure in the 264–271 nm range.

The data from Trost et al. presented in this paper are used for differential optical absorption spectroscopy (DOAS). As a result, they were more interested in the difference in the fine structure rather than the absolute values. Therefore, their data show a considerably high

offset of approximately 10^{-17} cm^2/molecule. While it is valid for their application, this offset needs to be corrected for comparison with other absolute measurements.

In comparison to the overall structure, a good agreement between all absorption cross-sections can be stated. Moreover, the measurements of Etzkorn et al. (blue) and the ones from Trost et al. show a very good agreement in the fine structure (see Fig. 2b). The only differences observed are at the edges of the measurement range and appear only in a shift of the absolute heights of the given publication. The relative differences between the peaks as well as the peak positions stay the same. Therefore, the method for the determination of the cross-sections of phenol in this paper can be considered as valid, and the results at higher temperatures can be presented.

In Fig. 3, the absorption cross-sections for the four temperature steps 296 K, 423 K, 573 K and 773 K are presented in the 200–310 nm range. As observed for other compounds [19], the fine structure of the spectrum disappears with rising temperature. At the same time, the overall structure gets broader and slightly shifts to higher wavelengths. This results in an elevated intensity between 280 nm and 290 nm. At higher temperatures, the minimum between the two major structures is shifted to a higher wavelength. At room temperature, it is at approximately 235 nm and shifts to approximately 245 nm at 773 K. It is interesting to see that at lower wavelengths, the coarse structure of phenol rises (between 200 and 230 nm) with temperature.

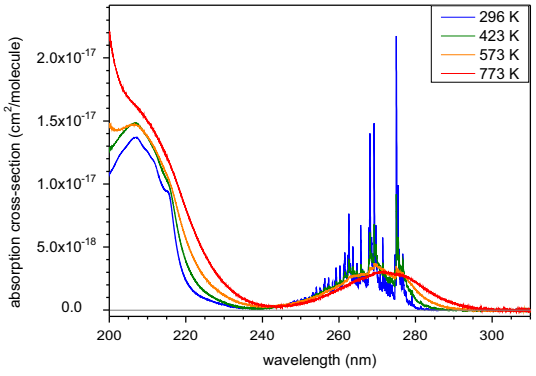

Fig. 3. UV absorption cross-sections of phenol between 200 nm and 310 nm at 296 K (blue), 423 K (green), 573 K (orange) and 773 K (red). (For interpretation of the references to color in this figure caption, the reader is referred to the web version of this article.)

3.2. Naphthalene

In Fig. 4, the absorption cross-sections obtained from these experiments are compared with data published by Ferguson et al., George et al., Suto et al. and Orain et al. The paper of Orain et al. mentioned the height of the absorption cross-section at the measured wavelength of 266 nm to be between 1.25×10^{-17} cm^2/molecule and 1.35×10^{-17} cm^2/molecule.

In Fig. 4a, the absorption cross-sections of naphthalene between 200 nm and 235 nm are presented. In general, the absorption cross-sections are in good agreement with the literature, especially with Suto et al. (green curve). The differences are mainly in the absolute heights at the maximum near 211 nm and at wavelengths below 210 nm. These deviations at lower wavelengths have been addressed in their publication [16]. Deviations at wavelength above 210 nm mainly originate from low spectral resolution, but can also be a product of the digitization process.

In Fig. 4b, the characteristic bands of the absorption cross-sections of naphthalene between 235 nm and 290 nm as well as the structures between 290 nm and 320 nm are presented and compared with previously published results. A good agreement between the relative heights of the peaks can be found, especially between 240 nm and 290 nm. The more recent publications by Suto (green) and Orain (black) also show agreement in terms of absolute heights of the absorption cross-sections within the limits of error of the corresponding experiments and the digitization process. In case of the structures at

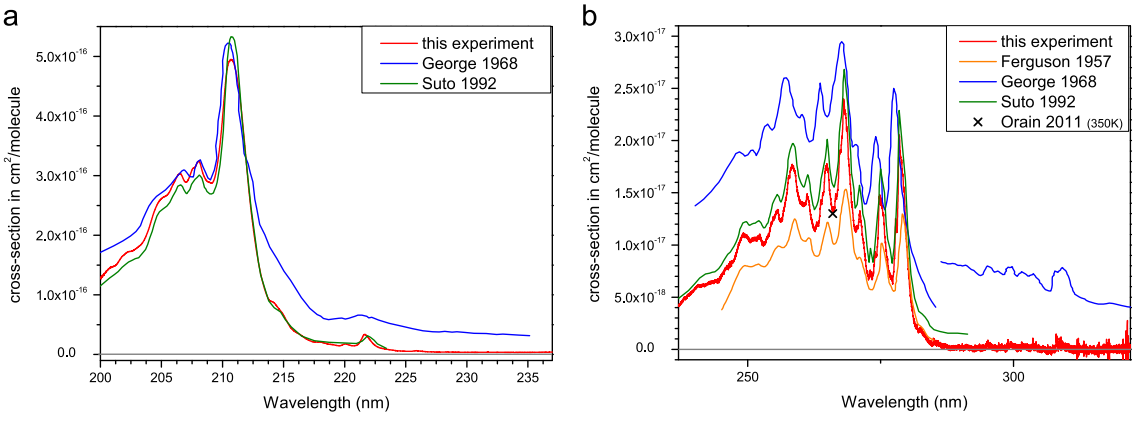

Fig. 4. UV absorption cross-sections of naphthalene at room temperature. Comparison of available literature data (green – [16]; blue – [15]; orange – [14]; black cross - [17]) and data obtained in this paper between 200 nm and 237 nm (a) and a between 237 nm and 320 nm (b). (For interpretation of the references to color in this figure caption, the reader is referred to the web version of this article.)

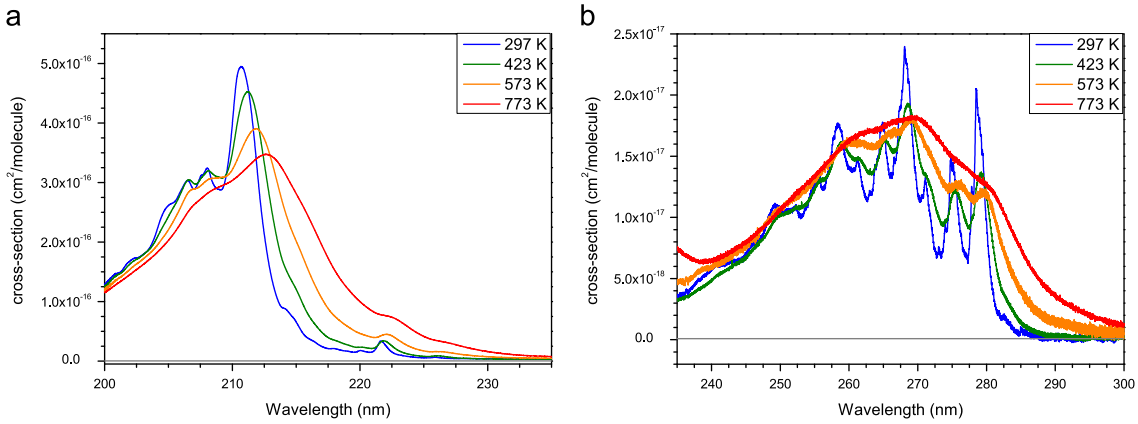

Fig. 5. UV absorption cross-sections of naphthalene between 200 nm and 235 nm (a) and a between 235 nm and 300 nm (b) at 296 K (blue), 423 K (green), 573 K (orange) and 773 K (red). (For interpretation of the references to color in this figure caption, the reader is referred to the web version of this article.)

wavelengths higher than 290 nm, a good agreement of the position of the peaks between George et al. (blue) and the cross-sections obtained here can be observed. Similar to phenol, the method used achieved comparable results and the presentation of results for higher temperatures can be justified.

In Fig. 5, the absorption cross-sections of naphthalene at room temperature (blue), 423 K (green), 573 K (orange) and 773 K (red) are presented. Fig. 5a shows the spectral features of naphthalene between 200 nm and 235 nm. Similar to phenol, the fine structure disappears and the structure becomes wider with increasing temperature. Moreover, the maximum shifts from 210.7 nm at 297 K to 212.6 nm at 773 K and its absolute intensity decreases significantly from 4.95×10^{-16} cm^2/molecule to 3.47×10^{-16} cm^2/molecule. In Fig. 5b, the effect of temperature on the naphthalene spectrum between 235 nm and 300 nm is presented. Analogous to phenol in that region, increasing temperature makes the fine structure disappear and the overall structure wider, until almost no fine structure can be observed at 773 K. Again, the widening of the structure results in higher cross-sections between 280 nm and 300 nm.

4. Conclusion

Absorption cross-sections of two important aromatic compounds, namely phenol and naphthalene, at four different temperatures between room temperature and 773 K were presented in the UV region between 200 nm and 360 nm at higher resolution than before. The cross-sections were obtained by a combined measurement of UV absorption spectroscopy and GC–MS, where the absorption measurements delivered the spectral features of the compounds and GC–MS measurements provided the concentration values necessary for the calculations using the Lambert–Beer law. The absorption cross-sections obtained at room temperature were compared with data available in literature. These data were in good agreement. Consequently, the absorption cross-sections of phenol and naphthalene at 423 K, 573 K and 773 K were presented for the first time in this paper.

Acknowledgments

We would like to thank Energienet.dk for providing financial support (Project no. 2011-1-10622).

Appendix A. Supplementary data

Supplementary data associated with this paper can be found in the online version at http://dx.doi.org/10.1016/j.jqsrt.2015.01.021.

References

[1] Salama F, Allamandola LJ. The Ultraviolet and visible spectrum of the polycyclic aromatic hydrocarbon $C_{10}H_8$: possible contributions to the diffuse interstellar bands and to the ultraviolet–visible extinction. Astrophys J 1992;395:301–6.

[2] Schauer JJ, Kleemann MJ, Cass GR, Simoneit BRT. Measurement of emissions from air pollution sources. 3. C_1–C_{29} Organic compounds from fireplace combustion of wood. Environ Sci Technol 2001;35:1716–28.

[3] Kjällstrand J, Ramnäs O, Petersson G. Gas chromatographic and mass spectrometric analysis of 36 lignin-related methoxyphenols from uncontrolled combustion of wood. J Chromatogr A 1998;824:205–10.

[4] Brage C, Yu Q, Chen G, Sjöström K. Tar evolution proles obtained from gasification of biomass and coal. Biomass Bioenerg 2000;18:87–91.

[5] Dufour A, Girods P, Masson E, Normand S, Rogaume Y, Zoulalian A. Comparison of two methods of measuring wood pyrolysis tar. J Chromatogr A 2007;1164(1–2):240–7. http://dx.doi.org/10.1016/j.chroma.2007.06.049.

[6] Li C, Suzuki K. Tar property, analysis, reforming mechanism and model for biomass gasification—an overview. Renew Sust Energ Rev 2009;13(3):594–604. http://dx.doi.org/10.1016/j.rser.2008.01.009.

[7] Michel R, Rapagnà S, Burg P, Mazziotti di Celso G, Courson C, Zimny T, et al. Steam gasification of Miscanthus X Giganteus with olivine as catalyst production of syngas and analysis of tars (IR, NMR and GC/MS). Biomass Bioenerg 2011;35(7):2650–8. http://dx.doi.org/10.1016/j.biombioe.2011.02.054.

[8] Dufour A, Masson E, Girods P, Rogaume Y, Zoulalian A. Evolution of aromatic tar composition in relation to methane and ethylene from

biomass pyrolysis-gasification. Energy Fuel 2011;25(9):4182–9. http://dx.doi.org/10.1021/ef200846g.
[9] Ortiz González I, Pérez Pastor RM, Sánchez Hervás JM. Assessment uncertainty associated to the analysis of tar from gasification of sewage sludge. Talanta 2011;87:60–6. http://dx.doi.org/10.1016/j.talanta.2011.09.041.
[10] Orphal J, Chance K. Ultraviolet and visible absorption cross-sections for HITRAN. Quant Spectrosc Rad Trans 2003;82:491–504.
[11] Breho F, Lesclaux R. The phenoxy radical: UV spectrum and kinetics of gas-phase reactions with itself and with oxygen. Chem Phys Lett 1997;279:289–96.
[12] Trost B, Stutz J, Platt U. UV-absorption cross sections of a series of monocyclic aromatic compounds. Atmos Environ 1997;31:3999–4008.
[13] Etzkorn T, Klotz B, Sørensen S, Patroescu IV, Barnes I, Becker KH, et al. Gas-phase absorption cross sections of 24 monocyclic aromatic hydrocarbons in the UV and IR spectral ranges. Atmos Environ 1999;33:525–40.
[14] Ferguson J, Reeves LW, Schneider WG. Vapor absorption spectra and oscillator strengths of naphthalene, anthracene, and pyrene. Can J Chem 1957;35:1117–36.
[15] George GA, Morris GC. The intensity of absorption of naphthalene from 30 000 cm^{-1} to 53 000 cm^{-1}. J Mol Spectrosc 1968;26:67–71.
[16] Suto M, Wang X, Shan J, Lee LC. Quantitative photoabsorption and fluorescence spectroscopy of benzene, naphthalene, and some derivatives at 106–295 nm. J Quant Spectrosc Rad Trans 1992;48:79–89.
[17] Orain M, Baranger P, Rossow B, Grisch F. Fluorescence spectroscopy of naphthalene at high temperatures and pressures: implications for fuel-concentration measurements. Appl Phys B 2011;102:163–72.
[18] Grosch H, Fateev A, Nielsen KL, Clausen S. Hot gas flow cell for optical measurements on reactive gases. J Quant Spectrosc Rad Trans 2013;130:392–9.
[19] Grosch H, Fateev A, Clausen S. UV absorption cross-sections of selected sulfur-containing compounds at temperatures up to 500 °C. J Quant Spectrosc Rad Trans 2015;154:28–34.

Bibliography

[1] Y. Neubauer. Nutzung von Biomasse zur Energiegewinnung. *Chemie Ingenieur Technik*, 83(11):1880–1889, 2011.

[2] S.P. Babu. Perspective on Biomass Gasification. Technical report, IEA Bionenergy Agreement, 2006.

[3] J. Ahrenfeldt; T.P. Thomsen; U. Henriksen; L.R. Clausen. Biomass gasification cogeneration - A review of state of the art technology and near future perspectives. *Applied Thermal Engineering*, 50:1407–1414, 2013.

[4] U. Henriksen; J. Ahrenfeldt; T.K. Jensen; B. Gøbel; J.D. Bentzen; C. Hindsgaul; L.H. Sørensen. The design, construction and operation of a 75 kW two-stage gasifier. *Energy*, 31:1542–1553, 2006.

[5] S. Nilsson; A. Gómez-Barea; D. Fuentes-Cano; P. Ollero. Gasification of biomass and waste in a staged fluidized bed gasifier: Modeling and comparison with one-stage units. *Fuel*, 2012:730–740, 2012.

[6] J.I. Hayashi; S. Hosokai; N. Sonoyama. Gasification of Low-Rank Solid Fuels with Thermochemical Energy Recuperation for Hydrogen Production and Power Generation. *Process Safety and Environmental Protection*, 84:409–419, 2006.

[7] A. Demirbas. Gaseous products from biomass by pyrolysis and gasification: effects of catalyst on hydrogen yield. *Energy Conversion and Management*, 43:897–909, 2002.

[8] P. Basu; B. Achary; A. Dutta. Gasification in Fluidized Beds - Present Status and Design. In *Proceedings of the 20th International Conference on Fluidized Bed Combustion*, pages 97–103, 2010.

[9] H.A.M. Knoef, editor. *Handbook Biomass Gasification Chapter 6*. 2. edition.

[10] P. Basu. *Biomass gasification and pyrolysis: practical design and theory*. 1. edition.

[11] C. Li; K Suzuki. Tar property, analysis, reforming mechanism and model for biomass gasification - An overview. *Renewable and Sustainable Energy Reviews*, 13:594–604, 2009.

[12] J. Han; H. Kim. The reduction and control technology of tar during biomass gasification/pyrolysis: An overview. *Renewable and Sustainable Energy Reviews*, 12:397–416, 2008.

[13] S. Karellas; J. Karl. Analysis of the product gas from biomass gasification by means of laser spectroscopy. *Optics and Lasers in Engineering*, 45:935–946, 2007.

[14] R. Sur; K. Sun; J.B. Jeffries; R.K. Hanson; R.J. Pummill; T. Waind; D.R. Wagner; K.J. Whitty. TDLAS-based sensors for in situ measurement of syngas composition in a pressurized, oxygen-blown, entrained flow coal gasifier. *Applied Physics B: Lasers and Optics*, 116:33–42, 2013.

[15] R. Sur; K. Sun; J.B. Jeffries; R.K. Hanson. Multi-species laser absorption sensors for in situ monitoring of syngas composition. *Applied Physics B: Lasers and Optics*, 115:9–24, 2014.

[16] H. Teichert; T. Fernholz; V. Ebert. Simultaneous in situ measurement of CO, H_2O, and gas temperatures in a full-sized coal-fired power plant by near-infrared diode lasers. *Applied Optics*, 42:2043–2051, 2003.

[17] M.E. Webber; J. Wang; S.T. Sanders; D.S. Baer; R.K. Hanson. In Situ Combustion Measurements of CO, CO_2, H_2O and Temperature Using Doode Laser Absorption Sensors. In *Proceedings of the Combustion Institute*, volume 28, pages 407–413, 2000.

[18] P. Ståhlberg; M. Lappi; E. Kurkela; P. Simell; P. Oesch; M. Nieminen. Sampling of contaminants from product gases of biomass gasifiers. Technical report, VTT Technical Research Centre of Finland, 1998.

[19] R.P. Ma; R.M. Felder; J.K. Ferrell. Evolution of Hydrogen Sulfide in a Fluidized Bed Coal Gasification Reactor. *Industrial and Engineering Chemistry Research*, 28:27–33, 1989.

[20] H. Cui; S.Q. Turn; V. Keffer; D. Evans; T. Tran; M. Foley. Contaminant Estimates and Removal in Product Gas from Biomass Steam Gasification. *Energy and Fuels*, 24:1222–1233, 2010.

[21] M.D. Kaufman Rechulski; T.J. Schildhauer; S.M.A. Biollaz; C. Ludwig. Sulfur containing organic compounds in the raw producer gas of wood and grass gasification. *Fuel*, 128:330–339, 2014.

[22] A. Attar. Chemistry, thermodynamics and kinetics of reactions of sulphur in coal-gas reactions: A Review. *Fuel*, 57:201–212, 1977.

[23] X. Meng; W. de Jong; R. Pal; A.H.M. Verkooijen. In bed and downstream hot gas desulphurization during solid fuel gasification: A review. *Fuel Processing Technology*, 2010:964–981, 2010.

[24] H.A.M. Knoef. *Handbook Biomass Gasification Chapter 10.* 2. edition.

[25] R.P.W.J. Struis; T.J. Schildhauer; I. Czekaj; M. Janousch; S.M.A. Biollaz; C. Ludwig. Sulphur poisoning of Ni catalysts in the SNG production from biomass: A TPO/XPS/XAS study. *Applied Catalysis A: General*, 362:121–128, 2009.

[26] J.H. Seinfeld; S.N. Pandis. *Atmospheric Chemistry and Physics: From Air Pollution to Climate Change.* John Wiley, New York, 2006.

[27] H. Grosch; A. Fateev; K.L. Nielsen; S. Clausen. Hot gas flow cell for optical measurements on reactive gases. *Journal of Quantitative Spectroscopy and Radiative Transfer*, 130:392–399, 2013.

[28] H. Grosch; A. Fateev; S. Clausen. UV absorption cross-sections of selected sulfur-containing compounds at temperatures up to 500°C. *Journal of Quantitative Spectroscopy and Radiative Transfer*, 154:28–34, 2015.

[29] H. Grosch; Z. Sárossy; H. Egsgaard; A. Fateev. UV absorption cross-sections of phenol and naphthalene at temperatures up to 500°C. *Journal of Quantitative Spectroscopy and Radiative Transfer*, 156:17–23, 2015.

[30] DIN Deutsches Institut für Normung e. V. *Biomassevergasung - Teer und Staub in Produktgasen - Probenahme und analytische Bestimmung*, 2006.

[31] A. Dufour; P. Girods; E. Masson; S. Normand; Y. Rogaume; A. Zoulalian. Comparison of two methods of measuring wood pyrolysis tar. *Journal of Chromatography A*, 1194:240–7, 2007.

[32] A. Dufour; E. Masson; P. Girods; Y. Rogaume; A. Zoulalian. Evolution of aromatic tar composition in relation to methane and ethylene from biomass pyrolysis-gasification. *Energy and Fuels*, 25:4182–4189, 2011.

[33] R. Michel; S. Rapagná; P. Burg; G. Mazziotti di Celso; C. Courson; T.Zimny; R. Gruber. Steam gasification of miscanthus x giganteus with olivine as catalyst production of syngas and analysis of tars (IR, NMR and GC/MS). *Biomass and Bioenergy*, 35:2650–2658, 2011.

[34] C. Brage; Q. Yu; G. Chen; K. Sjöström. Use of amino phase adsorbent for biomass tar sampling and separation. *Fuel*, 76:137–142, 1997.

[35] P. Monkhouse. On-line diagnostic methods for metal species in industrial process gas. *Progress in Energy and Combustion Science*, 28:331–381, 2002.

[36] P. Monkhouse. On-line spectroscopic and spectrometric methods for the determination of metal species in industrial processes. *Progress in Energy and Combustion Science*, 37:125–171, 2011.

[37] B. van der Drift. Tar Dew Point; past, present and future. In *19th European Biomass Conference and Exhibition, Berlin Germany*, 2011.

[38] O. Moersch; H. Spliethoff; K.R.G. Hein. Tar quantification with a new online analyzing method. *Biomass and Bioenergy*, 18:79–86, 2000.

[39] A. Gredinger. Continuous tar monitoring via FID - Actual status of the further development of an online tar measurement device. In *Chemical Analysis in Bioenergy Conversion Processes*, pages available online at http://www.gas–analysis–webinars.org, 2014.

[40] Y. Neubauer. *Online-Analyse von Teer aus der Biomassevergasung mit Lasermassenspektrometrie*. PhD thesis, Technical University Berlin, January 2008.

[41] Thiery S. Dufour A. Masson E. Ravel, S. Tar analysis in syngas from biomass gasification: comparison of different methods. In *18th European Biomass Conference and Exhibition*, pages 880–885, 2010.

[42] F. Defoort; S. Thiery; S. Ravel. A promising new on-line method of tar quantification by mass spectrometry during steam gasification of biomass. *Biomass and Bioenergy*, 65:64–71, 2014.

[43] D.L. Carpenter; S.P. Deutch; R.J. French. Quantitative Measurement of Biomass Gasifier Tars Using a Molecular-Beam Mass Spectrometer: Comparison with Traditional Impinger Sampling. *Energy and Fuel*, 21:3036–3043, 2007.

[44] B. Van de Belt M. Ahmadi; C Brage; K. Sjöström; K. Engvall; H. Knoef. Development of an on-line tar measurement method based on photo ionization technique. *Catalysis Today*, 176:250–252, 2011.

[45] M. Ahmadi; H. Knoef; B. Van de Belt; T. Liliedahl; K. Engvall. Development of a PID based on-line tar measurement method - Proof of concept. *Fuel*, 113:113–121, 2013.

[46] C. Baumhakl; S. Karellas. Tar analysis from biomass gasification by means of online fluorescence spectroscopy. *Optics and Lasers in Engineering*, 49:885–891, 2011.

[47] R. Sun; N. Zobel; Y. Neubauer; C. Cardenas Chavez; F. Behrendt. Analysis of gas-phase polycyclic aromatic hydrocarbon mixtures by laser-induced fluorescence. *Optics and Lasers in Engineering*, 48:1231–1237, 2010.

[48] A. Dieguez-Alonso; A. Anca-Couce; N. Zobel. On-line tar characterization from pyrolysis of wood particles in a technical-scale fixed-bed reactor by applying Laser-Induced Fluorescence (LIF). *Journal of Analytical and Applied Pyrolysis*, 102:33–46, 2013.

[49] D. Roveda; T. Kienberger; M. Grigiante; J. Karl. A tar online measurement system based on the absorption principle. In *20th European Biomass Conference and Exhibition*, pages 898–905, 2012.

[50] F.Patuzzi; D. Roveda; T. Mimmoa; J. Karl; M. Baratieri. A comparison between on-line and off-line tar analysis methods applied to common reed pyrolysis. *Fuel*, 111:689–695, 2013.

[51] R.G. Nielsen; P. Stoholm; M.B. Nielsen; J. Krogh; N. Noerholm; S. Antonsen; B. Sander; U. Henriksen; B. Qvale. The LT-CFB Gasifier - First Test Results From The 500 KW Test Plant. *unknown*, unknown.

[52] P. Stoholm; R.G. Nielsen; M.W. Flock; N. Jensen; B. Sander; L. Wolff; K. Richardt; U. Henriksen. The Low Temperature CFB Gasifier Latest 50 KW Test Results and New 500 KW Test Plant. *unknown*, unknown.

[53] L.S. Rothman; I.E. Gordon; et al. The HITRAN 2008 molecular spectroscopic database. *Journal of Quantitative Spectroscopy and Radiative Transfer*, 110:533–572, 2009.

[54] L.S. Rothman; I.E. Gordon; et al. The HITRAN 2012 molecular spectroscopic database. *Journal of Quantitative Spectroscopy and Radiative Transfer*, 130:4–50, 2013.

[55] L.S. Rothman; I.E. Gordon; R.J. Barber; H. Dothe; R.R. Gamache; A. Goldman; V.I. Perevalov; S.A. Tashkun; J. Tennyson. HITEMP, the high-temperature molecular spectroscopic database. *Journal of Quantitative Spectroscopy and Radiative Transfer*, 111:2139–2150, 2010.

[56] S.A. Tashkun; V.I. Perevalov; J.-L. Teffo. Remote sensing of the atmosphere for environmental security, 2006.

[57] S.A. Tashkuna; V.I. Perevalova; J-L. Teffo; A.D. Bykov; N.N. Lavrentieva. CDSD-1000, the high-temperature carbon dioxide spectroscopic databank. *Journal of Quantitative Spectroscopy and Radiative Transfer*, 82:165–196, 2003.

[58] L.S. Rothman; I.E. Gordon; S.A. Tashkun; S. Mikhailenko; Y. Babikov. HITRAN on the Web. website http://hitran.iao.ru/, accessed 17.10.2014.

[59] S.W. Sharpe; T.J. Johnson; R.L. Sams; P.M. Chu; G.C. Rhoderick; P.A. Johnson. Gas-Phase Databases for Quantitative Infrared Spectroscopy. *Applied Spectroscopy*, 58:1452–1461, 2004.

[60] I.V. Patroescu; I. Barnes; K.H. Becker; U. Platt T. Etzkorn; B. Klotz; S. Soerensen. Gas-phase absorption cross sections of 24 monocyclic aromatic hydrocarbons in the UV and IR spectral ranges. *Atmospheric Environment*, 33:525–540, 1999.

[61] U. Platt. Modern methods of the measurement of atmospheric trace gases. *Physical Chemistry Chemical Physics*, 1:5409–5415, 1999.

[62] Zsuzsa Sárossy. LT-CFB Sampling - Internal. Technical report, Technical University of Denmark, 2012.

[63] Thersites - the ECN tar dew point site. website http://www.thersites.nl/, accessed 28.11.2014.

Acknowledgements

At first, I would like to thank my supervisors Alexander and Sønnik Clausen, for giving me the chance to investigate a fascinating and complex topic. In addition, I want to thank the project for funding my PhD and making the work possible.

I also would like to thank my colleagues at the biomass gasification group at Campus Risø, especially, my colleagues Caspar and Karsten: thanks for the support, the open ear and the neverending jokes. It was a great time! I also want to thank all my other colleauges at BGG, you have always been there for fruitful discussions, helpful suggestions, a good laugh and interesting non-work related conversations. It was a pleasure to work and share my time with you.

Of course there are hundreds of people (friends, companions, students, teachers, role-models, inspirations, etc.) in my life that I would like to thank. I don't even try to acknowledge everyone, because I surely forget someone.

Nevertheless, there are a couple of people that have to be mentioned for their direct support during the last three years. First of all my girlfriend Julia, for the trust and the possibility to show every side of myself. To my BeSt friends with whom I walked through joy and sorrow. And of course, my family especially my parents, who guided me to find out for myself what is best for me.

So what did I learn? I learned that I can do what is necessary, that I can overcome my aversions and that stress is something you make yourself. I also learned that your plan is a good plan, if someone screws it up but you are still getting through in time - without additional stress.

Centre of Combustion and Harmful Emission Control
Department of Chemical and Biochemical Engineering
Technical University of Denmark

Søltofts Plads, Building 229
DK 2800 Kgs. Lyngby

Tlf. +45 4525 2800
Fax +45 4525 4588

www.chec.kt.dtu.dk

ISBN : 978-87-93054-71-4